SIMULATED TRANSPORT OF RADON IN SOIL GAS

A THESIS SUBMITTED TO THE GRADUATE DIVISION OF THE
UNIVERSITY OF HAWAII IN PARTIAL FULFILLMENT
OF THE REQUIREMENTS FOR THE DEGREE OF

MASTER OF SCIENCE

IN GEOLOGY AND GEOPHYSICS

AUGUST 1990

RETURN TO
HAWAII INSTITUTE OF GEOPHYSICS
LIBRARY ROOM

By

Jeff M. Cotter

Thesis Committee:

Donald Thomas, Chairman
Richard E. Green
Frank Peterson

We certify that we have read this thesis and that, in our opinion, it is satisfactory in scope and quality as a thesis for the degree of Master of Science in Geology and Geophysics.

THESIS COMMITTEE

Chairman

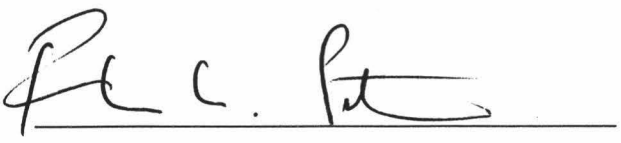

THIS THESIS IS DEDICATED,
WITH LOVE,
TO MY FATHER

ACKNOWLEDGEMENTS

This thesis could not have been completed without the assistance of many people and although they are too numerous to thank here, I will gratefully remember them all. First and foremost I would like to thank my thesis advisor Don Thomas, both for giving me the opportunity to work on this project and for patiently putting up with me as I learned (often the hard way) probably the most important lesson of my research; when faced with a seemingly insurmountable problem, you only need to do one thing: whatever is necessary. A warm mahalo also goes to Diana Holford who taught me how to use her radon transport model, RN3D, as well as some of the ins and outs of Unix, and also cheerfully helped debug my numerous error-ridden programs.

For assistance with the (sometimes) hard and dirty field effort associated with this project, grateful thanks goes to Don Thomas, Gary Delanoy, Robert Corral, Robert Miyahira and Mary Gaspari. Invaluable help with some of the laboratory analyses was provided by Howard West and Gary Delanoy. I would also like to thank Dick Green and the Department of Agronomy and Soils for providing the use of some key field equipment for this project as well as very useful advice on how to best use it.

I gratefully acknowledge Richard Nakano, David Santiago and the rest of the personnel at the UH Poamoho Experimental Station for providing access to the field site and indispensable support for the field effort. I also wish to thank my thesis committee Don Thomas, Dick Green and Frank Peterson for their suggestions and advice while reviewing this thesis. Finally, my heartfelt thanks goes to Robin Wong who has given her support, advice and help from the time a Masters degree was only a dream, up until its final completion.

ABSTRACT

A field monitoring study was undertaken to characterize the interaction between environmental factors such as rainfall, atmospheric pressure changes, wind-driven pressure changes and soil gas radon mobility. Two identical test and control arrays containing radon, soil moisture and differential pressure monitoring instruments were installed in central Oahu, Hawaii. Radon activities in soil gas were monitored using passive, electronic alpha particle detectors at depths of 0.8, 1.3 and 2.3 m; soil moisture and differential soil gas pressures were monitored at equivalent depths. After an evaluation period to confirm that the test and control arrays showed similar radon responses, the test array was covered with a plastic barrier to determine the significance of advective exchange of soil gas with atmospheric air.

The field results show radon concentrations in soil gas were found to be strongly dependent on depth in the soil profile: at 0.8 m the average soil gas radon concentration was 22,000 Bq/m^3; at 1.3 m it was 37,000 Bq/m^3; and at 2.3 m it averaged 48,000 Bq/m^3. Significant radon activity increases (30 to 120%) at 0.8 and 1.3 m depth were found to follow moderate to intense rainfall events. The activity changes are attributed to reduced advective and diffusive pathways for radon loss to the atmosphere and partitioning of radon into a smaller volume of soil gas due to increased soil saturation. Rainfall events show little effect on radon concentrations at 2.3 m. Radon concentrations at the shallow depths also exhibit a slow decline during extended dry periods due to increased advective and diffusive loss of radon through the drier soil; the deepest probe showed only minor changes in radon activity during the dry periods.

Radon activities also responded to synoptic and semi-diurnal atmospheric pressure changes at 0.8 m depth throughout the study. A similar response was observed at 1.3 m depth only when the soil was at its driest but no pressure response was observed at 2.3 m

depth at any time. Effects due to wind-driven pressure changes are inconclusive at present. Results from the advective barrier experiment strongly suggest that mixing of soil gas with atmospheric air causes a significant reduction in soil gas radon concentrations at depths of 0.8 and 1.3 m, but little effect at 2.3 m depth.

Computer simulation of the measured and observed data was performed using RN3D, a finite element, radon transport code. Simulated radon transport is by advection and diffusion in the gas phase and diffusion only in the liquid phase. The modeling effort was intended to calibrate RN3D, as well as reveal the relative sensitivity of radon behavior to soil physical properties.

RN3D was calibrated by conducting steady state simulations and adjusting soil diffusion coefficients to simulate the observed radon concentration profile. Transient, 1D model runs were then used to further adjust the diffusion coefficients and determine soil air permeabilities. Using field measured air permeabilities, RN3D was initially unable to simulate the observed variations in the radon time series; however, if air permeabilities were raised by a factor of 1000 above field values, RN3D was able to simulate the observed radon variations with respect to synoptic and diurnal pressure changes as well as radon activity increases due to rainfall events. This suggests that the technique used in this study to measure soil air permeability does not adequately account for preferential flow and large scale soil features which contribute to the true soil air permeability or that the transport equations used in RN3D do not realistically characterize the subsurface air flow in a highly saturated, low permeability soil. A sensitivity analysis performed with RN3D showed that soil diffusion is the most important parameter in determining radon concentrations in soil gas and radon flux from soil, followed by soil crack geometry and then by soil air permeability.

TABLE OF CONTENTS

TABLE OF CONTENTS (continued)

TABLE OF CONTENTS (continued)

LIST OF TABLES

LIST OF FIGURES

LIST OF FIGURES (continued)

LIST OF FIGURES (continued)

LIST OF FIGURES (continued)

CHAPTER 1

INTRODUCTION

Radon transport in soil gas and groundwater has been studied for many years in connection with uranium exploration, as a tracer for moving air and groundwater, and as a possible predictor of seismic activity. Nazaroff and Nero (1988), Tanner (1964, 1980) and Wilkening (1981) give comprehensive reviews of the extensive literature on the subject. The discovery in recent years of elevated levels of radon in the indoor environment has led to intensive investigation of the physical mechanisms which control the release and transport of radon through soils and into manmade structures. Nero (1988) has estimated that the radiation dose from inhaled decay products of radon is the major component of the natural radiation exposure of the general population. For the United States, the average lifetime risk of lung cancer caused by exposure to radon and its decay products is estimated to be 0.3%, causing an estimated 10,000 cases of lung cancer annually among the U.S. population of 235 million (Nero et al., 1986). The primary source of indoor radon has been recognized to be radon that has migrated from soil. An understanding of the mechanisms and processes governing radon transport is essential to identifying both the populations at risk, as well as effective mitigation methods for reducing radon exposure risks.

This thesis describes the application of computer simulation techniques to analyze data obtained from a field survey measuring soil gas radon activity and its correlation to changing soil and meteorological conditions. The field work was performed at the University of Hawaii's Poamoho Agricultural Experimental Station on Oahu, Hawaii. The work was carried out under grant number DE-FG03-88-ER60663 from the U. S. Department of Energy and is part of an ongoing study entitled "An Investigation of Radon Release and Mobility in the Subsurface Environment". Radon activities in soil gas were

monitored using passive electronic alpha particle detectors. Soil moisture, barometric pressure, and differential soil gas pressure data were also collected as part of the field survey. The modeling effort was conducted using RN3D, a finite element radon transport code (Holford et al., 1989).

A. The Problem

Because radon is chemically unreactive under normal conditions its concentration at a measurement point is a function of two primary factors: 1) The abundance and distribution of its parent radionuclide, radium, in the source material and 2) the efficiency of transport processes which bring about its release and movement from the source material.

Since ^{222}Radon occurs within the decay series of ^{238}Uranium and is the daughter of ^{226}Radium its concentration in soil gas is directly related to the abundance of these isotopes in the source material. However there is no strict correlation between radon levels in soil water and soil gas and radium content of rocks and soil. In fact, good correlation exists only for extreme cases: if the uranium and radium content of the parent material is very low or very high, then the soil gas radon content is likely to be very low or very high. However, for the vast majority of materials which contain only modest amounts of radium, the radon content in adjacent soil water and/or soil gas can vary over many orders of magnitude (Reimer and Gunderson, 1989; Sextro et al., 1987). This illustrates that transport processes are dominant in controlling radon concentrations in most soils which contain modest amounts of radium.

The transport mechanisms responsible for the release of radon from the solid matrix and for its further movement through the porous media, need to be fully understood in order to identify the significant factors affecting radon behavior in the subsurface environment. Environmental conditions, such as barometric pressure changes and rainfall

events, are the major controlling factors of radon activity and flux in the soil. The interaction between environmental conditions and soil characteristics affects the structure, moisture content and radon transport characteristics of the soil. The transport characteristics in turn affect the radon concentration and flux within and from the soil. The goal of this thesis research was to characterize the interplay between environmental factors and radon behavior in soil in order to identify the important physical mechanisms controlling radon release and transport in the soil.

B. Previous Work

Early studies of radon in soil (Kovach, 1945, 1946) found that mixing of radon poor atmospheric air with radon rich soil gas in the soil resulted in higher concentrations of radon in soil gas at depth and lower radon concentrations in near-surface soil gas. Kovach also found that barometric pressure changes caused an increase of radon content in soil gas with falling pressure and a decrease of radon content in soil gas with rising pressure. Rainfall and wind were also observed to have significant effects on radon in soil gas but changes in soil temperature were found to have no detectable effect on radon concentrations (Kovach, 1945). More recent studies (Clements and Wilkening, 1974; Duenas and Fernandez, 1988; Fleischer, 1983; Fukui, 1987; Guedalia et al, 1970; Holford et al, 1988, 1989; Schery et al, 1984; Singh et al, 1988; Tanner, 1964, 1980; Thomas and Cotter, 1988; Wilkening, 1981) have confirmed the importance of soil moisture and pressure changes in radon transport through the vadose zone. The role of soil temperature in radon transport is still the subject of debate among investigators; Mogro-Campero and Fleischer (1977) have proposed that thermally induced convection may be an important process for the transport of radon in soil, but Schery and Petschek (1983) have calculated that thermal gradients high enough to induce convective flow are unlikely and would produce soil gas movement too small to be detected if they did occur.

It has been well established that soil moisture content is the most critical controlling factor in radon release and migration: it influences radon emanation from solids; the permeability of soil to air; and the diffusive capabilities of soil. Researchers have known for some time that radon emanation is enhanced by moderate levels of soil moisture (Guedalia et al, 1970; Morozova and Mukhraneli, 1971; Rogers et al, 1980; Strong and Levins, 1982; Tanner, 1980). Strong and Levins (1982) measured radon emanation coefficients from uranium mill tailings at varying moisture contents and found that a sharp rise in emanation occurred from the absolutely dry state up to 2% water by weight. Above 2 wt% water the emanation increased only slightly up to the saturation limit of the soil sample being tested. Fleischer (1983) has shown, in a theoretical study, that radon emanation from the parent matrix is increased by moderate amounts of interstitial water due to dissipation of recoil energy.

Once radon has emanated into pore spaces its further movement is controlled by advection and diffusion. Changes in soil air pressure are universally accepted as the major cause of advective transport of soil gas. The two causes of soil air pressure changes are: 1) large scale fluctuations due to synoptic and diurnal barometric pressure variations; and 2) localized effects due to wind driven pressure changes. There have been numerous field and laboratory studies (Clements and Wilkening, 1974; Duenas and Fernandez, 1988; Fernandez et al, 1983; Megumi and Mamuro, 1973; Raghavayya et al, 1981; Schery et al, 1982, 1984; Singh et al, 1988; Thomas and Cotter, 1988) which invariably support the inverse relationship between radon exhalation and barometric pressure first discovered by Kovach (1945). Researchers have also found that soil gas flux is enhanced under windy conditions (Cohen, 1985, 1986; Woodcock and Friedman, 1979). This mechanism is still poorly understood; pressure differentials induced by winds can fluctuate very rapidly so it is essential to consider how fast pressure fluctuations are transmitted through the soil.

Fukuda (1955) has shown theoretically that for sands and gravels propagation times are on the order of minutes or less but for clays times can be from days to months.

Diffusive transport of radon has been intensely studied in recent years (Cohen et al, 1986; Kalkwarf et al, 1982; Nielson et al, 1984; Rogers et al, 1984; Silker and Kalkwarf, 1983; Sogaard-Hansen and Damkjaer, 1987). A model proposed by Nielson et al (1984) estimates the diffusion coefficient (D) from soil moisture content and pore size distribution. The model accounts for diffusion in gas filled pores, water filled pores and Knudsen diffusion in very small pores by statistically combining pore segments of different radii to produce all serial combinations of pore sizes. This method has been questioned by Collin and Rasmuson (1988) who contend that it is too dependent on the number of pore size classes used and will underestimate D at higher water contents. The diffusive capability of soil remains one of the more difficult parameters to measure accurately. Field measurements are difficult and expensive to conduct; measurements made in the laboratory are relatively easy to conduct but do not take into account the effects of rainfall, sun and wind. Sogaard-Hansen and Damkjaer (1987) show that soils measured in situ generally give lower diffusive lengths due to higher water contents than soils measured in the laboratory.

Some investigators have recently attempted to devise ranking schemes that will advise developers, builders, or health officials of the relative risk from radon on a site specific basis. Generally these schemes focus on the intrinsic ability of the soil to transmit radon into a structure. Eaton and Scott (1984) developed a radon index number which involves both soil and structure characteristics. Tanner (1988a) has defined a radon availability number (RAN) which is computed from measurements of soil radon, permeability, porosity, water content and diffusion constant. All of these measurements are subject to wide spatial variability at a particular site as well as being influenced by changing environmental conditions through time.

C. Objectives

Since the 1970s there have been numerous radon studies which have incorporated radon and environmental monitoring programs (Clements and Wilkening, 1974; Duenas and Fernandez, 1988; Guedalia et al, 1970; Fernandez et al, 1983; Megumi and Mamuro, 1973; Ragahavayya et al, 1981; Schery et al, 1984; Singh et al, 1988). Numerical and analytical modeling of radon transport through soil have also been conducted by several investigators (Clements and Wilkening, 1974; Rogers et al., 1989; Schery and Siegel, 1986). Holford et al. (1989) have successfully calibrated and used the radon transport code, RN3D, on dry, high permeability soils. RN3D has also been used in sensitivity analyses and on test cases on hypothetical soils (Holford et al., 1988, Owczarski et al., 1989). However, to date, there have been no investigations in which data from a comprehensive, experimental field study are analyzed using a dedicated radon transport model. This research combines long-term radon activity and environmental monitoring with a numerical modeling effort to identify the most important factors affecting subsurface radon release and migration.

D. Experimental Approach

1.) Radon and Environmental Monitoring

The field monitoring effort involved two separate but identical radon and soil monitoring arrays emplaced 20 m apart. Each array consisted of the following: 1) three passive, electronic alpha particle detectors; 2) three soil moisture detectors; and 3) two differential pressure probes. One of the above instruments was buried at each of the three depths : 0.8 m, 1.3 m and 2.3 m. The radon detectors recorded alpha decays integrated over 15 minute intervals. In addition, barometric pressure and daily rainfall data at the site were collected.

One array was chosen as a test array and the other was the control array. The two arrays were situated so as to be in similar if not identical soil profiles but separated by enough distance (20 m) to ensure that experimental conditions imposed on the test array would not affect the control array radon response. The initial radon monitoring involved comparison of the radon response from the two arrays under natural conditions to establish the variability between the two and to provide a baseline data set characterizing normal radon response. Artificial conditions were then imposed on the test array for comparison to the control array exposed to natural environmental conditions. The use of a separate experimental array and control array has a significant advantage over previous radon monitoring programs in that it allows the isolation and identification of the different factors affecting radon activity in soil.

The objective of the field work was the correlation of the various environmental parameters with radon activity to distinguish the effects of meteorologic and environmental changes on radon activity. The data set was then used in the evaluation and calibration of a radon transport model which was used to simulate radon transport and activity in the soil in response to changing meteorologic and soil conditions.

2.) Simulated Radon Transport

The finite element radon transport model RN3D (Holford et al., 1989) was chosen for the analysis and simulation of the radon monitoring data. The governing air flow equation assumes transient, compressible, ideal gas flow. The governing radon transport equation includes the effects of advection through air-filled pores, diffusion through air-filled and water-filled pores, radioactive decay and radon emanation from soil. The full development of these equations is given in Chapter 3.

Initial model runs were conducted to calibrate RN3D using data obtained from the radon monitoring effort. The calibration process involves the adjustment of model

parameters within their accepted ranges until the simulated results adequately match the field data. Once calibration was completed, model runs were conducted to better evaluate the field monitoring data by simulating the effects of changes in soil characteristics (water content, air permeability and diffusion coefficient) on radon activity throughout the soil profile.

3.) Parameter Measurement and Estimation

Input data and parameters needed for RN3D simulations and model calibration include barometric pressure data, soil saturation, soil bulk density, soil porosity, soil radium content, soil air permeability, soil emanation coefficient and soil diffusion coefficient.

Barometric pressure data were obtained from nearby weather stations and on-site instruments. Soil cores were taken at 0.5 m depth to measure soil bulk density, soil porosity and soil water content. Soil core data for greater depths (0.5 to 2.5 m) were obtained from Green et al. (1982) and Miller (1987). Additional laboratory work included measurement of soil radium content and soil emanation coefficient.

Two critical soil parameters needed for modeling are the soil air permeability and soil radon diffusion coefficient. Both of these parameters are a function of soil water content and were estimated using soil water characteristic models (references cited in Chapter 5). Soil air permeabilities were measured at the site using a permeameter constructed for this project.

CHAPTER 2

BASIC PRINCIPLES

A. Radioactive Decay

Radioactivity is defined as the spontaneous disintegration of unstable nuclei accompanied by the emission of: 1) alpha particles (α), weakly penetrating helium nuclei, 2) beta particles (β), more penetrating streams of electrons, or 3) gamma rays (γ), electromagnetic radiation capable of penetrating up to 100 mm of lead. The rate at which radionuclides decay is a random process and only the probability of a decay occurring in a certain time interval can be expressed. The number of disintegrations which occur per unit time is proportional to the number of atoms present at the beginning of that time interval:

$$\frac{dN_i}{dt} = \lambda_i N_i \tag{2.1}$$

where N_i = number of atoms of radionuclide i present
λ_i = decay constant of i (s^{-1})
t = time (s)

The solution of equation (2.1) is given by:

$$N_i = N_i^0 e^{-\lambda_i t} \tag{2.2}$$

where N_i^0 = number of atoms of i originally present at time t_0
N_i = number of atoms of i present at time t_i.

The term most commonly used to express the rate of decay of a radionuclide is the half life ($t_{1/2}$), or the amount of time required for the number of atoms to be halved through radioactive decay:

$$N_i = \frac{N_i^0}{2} \tag{2.3}$$

Substituting (2.3) into (2.2) gives the half life of radionuclide i:

$$t_{1/2} = \frac{\ln 2}{\lambda} = \frac{0.693}{\lambda} \tag{2.4}$$

The amount of a radionuclide present is often expressed by the observed disintegration rate or activity. This is the number of α, β, or γ rays emitted over a certain time interval. The SI unit of activity is the Becquerel (Bq) which is equivalent to 1 disintegration per second. The activity is related to the amount of radionuclide present by:

$$A_i = \lambda_i N_i \tag{2.5}$$

where A_i = activity of radionuclide i (Bq).

Radioactive decay can continue through a chain of radionuclides each decaying with a specific decay constant to form a new radionuclide, termed a daughter, until a stable nucleus is formed. Consider for example, a case where a radioactive species (N_1) decays to a second radioactive species (N_2). The second species is formed at the rate at which the first decays:

$$\frac{dN_2}{dt} = \lambda_1 N_1 - \lambda_2 N_2 \, . \tag{2.6}$$

Substituting equation (2.2) for species 1:

$$\frac{dN_2}{dt} + \lambda_2 N_2 - \lambda_1 N_1^0 e^{-\lambda_1 t} = 0. \tag{2.7}$$

The solution of equation (2.7) is:

$$N_2 = \frac{\lambda_1}{\lambda_2 - \lambda_1} N_1^0 (e^{-\lambda_1 t} - e^{-\lambda_2 t}) + N_2^0 e^{-\lambda_2 t} \tag{2.8}$$

If the parent (N_1) has a longer half life than the daughter (N_2) and $\lambda_1 < \lambda_2$ a state of radioactive equilibrium is reached where, after a certain time, the ratio of N_1 to N_2 becomes constant. In equation (2.8), when t becomes sufficiently large, $e^{-\lambda_2 t}$ becomes negligible compared to $e^{-\lambda_1 t}$ giving:

$$N_2 = \frac{\lambda_1}{\lambda_2 - \lambda_1} N_1^0 e^{-\lambda_1 t}, \tag{2.9}$$

but $N_1^0 e^{-\lambda_1 t} = N_1$ so:

$$\frac{N_1}{N_2} = \frac{\lambda_2 - \lambda_1}{\lambda_1}. \tag{2.10}$$

If the half life of the parent is much longer than that of the daughter and therefore $\lambda_2 >> \lambda_1$, equation (2.10) can be modified by the approximation $\lambda_2 - \lambda_1 \approx \lambda_2$. Now the ratio of parent to daughter can be given as:

$$\frac{N_1}{N_2} = \frac{\lambda_2}{\lambda_1} \tag{2.11}$$

$$\lambda_1 N_1 = \lambda_2 N_2 \tag{2.12}$$

$$A_1 = A_2. \tag{2.13}$$

This condition is termed secular equilibrium and is reached when the activity of the daughter is equal to that of the parent.

In a decay series consisting of a long lived parent and a series of short lived daughters secular equilibrium is propagated through the entire series such that:

$$\lambda_1 N_1 = \lambda_2 N_2 = \lambda_3 N_3 = \ldots \lambda_n N_n \text{ and,} \tag{2.14}$$

$$A_1 = A_2 = A_3 = \ldots A_n. \tag{2.15}$$

Secular equilibrium can be destroyed by any process which results in the removal of one or more daughters. In a "closed" system where no daughter radionuclides are lost the rate of approach to secular equilibrium is controlled by the daughter with the longest half life.

B. Radon

Radon, atomic number 86, is a slightly soluble, radioactive, inert gas. There are 20 unstable isotopes of radon known, (^{204}Rn to ^{224}Rn), most of which have very short half lives. ^{222}Rn ("radon"; $t_{1/2}$ = 3.825 day), ^{220}Rn ("thoron"; $t_{1/2}$ = 54.5 sec) and ^{219}Rn ("actinon"; $t_{1/2}$ = 4.0 sec) are the three most common isotopes of radon. These three radon isotopes are formed respectively by the decay of radium isotopes ^{226}Ra ($t_{1/2}$ = 1622 yr), ^{224}Ra ($t_{1/2}$ = 3.64 day) and ^{223}Ra ($t_{1/2}$ = 11.70 day) within the decay chains of ^{238}Uranium, ^{232}Thorium and ^{235}Uranium. Of the three radon isotopes, ^{222}Rn is the most common due to its longer half life and the abundance of its parent ^{238}Uranium. Table 1 lists the complete decay chain of ^{238}Uranium. Unless otherwise stated further references to radon will indicate ^{222}Rn.

The disintegration of radium and radon nuclides is almost wholly by alpha decay or the spontaneous emission of alpha particles from their nuclei. Alpha particles are composed of 2 protons and 2 neutrons with a charge of +2. The emission of an alpha particle from the nucleus reduces the atomic number by 2 and the mass number by 4 to produce a daughter isotope of a different element, for example:

$$^{226}\text{Ra} \rightarrow {}^{222}\text{Rn} + \alpha \quad \text{and,} \tag{2.16}$$

$$^{222}\text{Rn} \rightarrow {}^{218}\text{Po} + \alpha \tag{2.17}$$

When ^{226}Ra decays to ^{222}Rn it emits an alpha particle of 4.78 Mev (Table 1) and a radon atom. Conservation of momentum requires that, in the absence of external forces, the momentum of the system before alpha decay (radium atom) equals the momentum of

Table 1

^{238}Uranium Decay Series

Number	Element	Isotope	Half Life	Energy (Mev) α	β	γ
92	Uranium	^{238}U	4.51x10^{9}y	4.19	--	0.048
90	Thorium	^{234}Th	24.1 d	--	0.19	0.09
91	Protactinium	^{234}Pa	1.17 m	--	2.29	1.0
92	Uranium	^{234}U	2.48x10^{5}y	4.77	--	0.05
90	Thorium	^{230}Th	8.0x10^{4}y	4.68	--	0.068
88	Radium	^{226}Ra	1622 y	4.78	--	0.186
86	**Radon**	**^{222}Rn**	**3.825 d**	**5.49**	**--**	**0.51**
84	Polonium	^{218}Po	3.05 m	6.00	--	--
		β decay (0.02%) to ^{218}At $t_{1/2}$ = 1.3 s α decay (99.98%) to ^{214}Pb				
82	Lead	^{214}Pb	26.8 m	--	0.65	0.24
83	Bismuth	^{214}Bi	19.7 m	5.50	1.50	0.61
		α decay (0.04%) to ^{210}Tl $t_{1/2}$ = 1.3 s β decay (99.96%) to ^{214}Po				
84	Polonium	^{214}Po	1.6x10^{-4}s	7.80	--	0.80
82	Lead	^{210}Pb	22 y	--	0.016	0.046
83	Bismuth	^{210}Bi	5.0 d	--	1.16	--
84	Polonium	^{210}Po	138.4 d	5.30	--	0.80
82	Lead	^{206}Pb	stable			

(After Friedlander et. al., 1964)

the system (radon atom plus alpha particle) after decay. The significant mass of the alpha particle imparts an appreciable energy to the nucleus upon its ejection causing the daughter isotope to recoil in the opposite direction. This recoil creates a path of intense damage on an atomic scale within the mineral. Further movement of the radon atom is then by diffusion until it escapes from the solid or disintegrates.

C. Radon Release and Transport

The release and movement of radon in soil pores involves three mechanisms:

1) Liberation from the solid matrix in which it is formed. This is characterized by the emanation coefficient and diffusion coefficient of the solid.

2) Transport through the bulk medium (solid + liquid + air) in response to a concentration gradient. This is characterized by the bulk diffusion coefficient.

3) Advective transport of radon due to movement of subsurface fluids (liquid or gas) which carry the radon. This can be characterized by Darcys Law.

1.) Emanation

The transport of radon out of the solid matrix is called the emanation. The emanation coefficient for radon is defined as the ratio of the number of radon atoms which escape from the solid to the total number of radon atoms formed by decay of radium in the solid.

It is now generally accepted that radon can escape from a solid grain as a result of alpha recoil when its parent, ^{226}Ra, decays. If the recoil terminates outside the grain in an open pore the radon can then migrate freely. Figure 1 schematically illustrates the emanation by recoil process.

The three modes by which emanation of radon from a solid can occur are: 1) Direct-recoil, 2) Indirect-recoil and 3) Diffusion. When a radium atom decays to

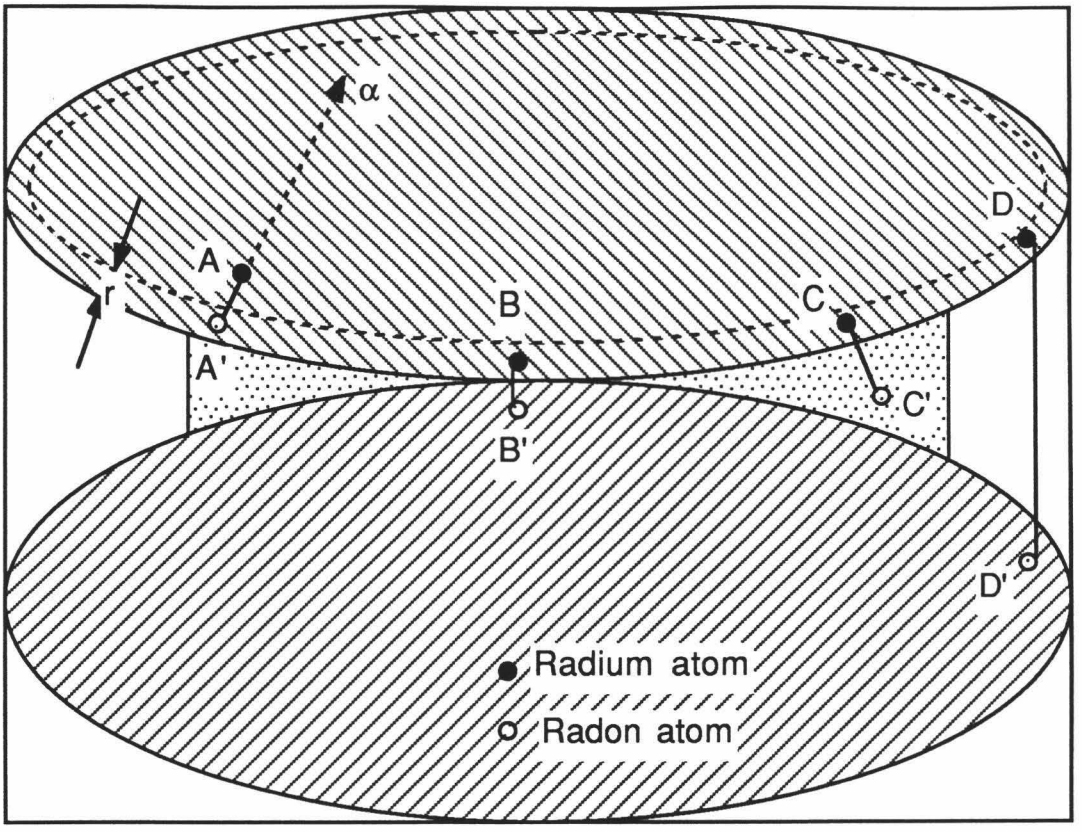

Figure 1. Schematic diagram of the emanation process. Two very fine grains are in contact near B. Water is present in the stippled zone of the pore space. The open zone is air filled; ^{226}Ra atoms A, B, C and D decay in the upper grain, each yielding an alpha particle (shown at A) and a ^{222}Rn atom A', B', C' and D'. Radium atom A lies deeper than the recoil range, r; recoil atom A' remains in the grain. Atom B' escapes but buries itself in the lower grain. Atom C' is free to diffuse through the pore due to its loss of recoil energy in the water. Atom D' loses little recoil energy in the air and buries itself in the lower grain. Atoms B' and D' still may escape their pockets by diffusion before the volatilized material condenses. The circles greatly exaggerate atomic dimensions.

radon, conservation of momentum requires that, the energy carried off by the alpha particle must equal the energy of the daughter radon atom. This results in its recoil within the solid (Figure 1). The radon atoms that end their recoil in a pore space are called the direct recoil fraction of the emanation coefficient. In most natural materials the recoil range is much smaller than the grain size, about 0.02 to 0.07 μm (Tanner, 1964), so that few recoil atoms are expected to escape from the grains in which they originate if the radium precursor is uniformly distributed (A - A' in Figure 1). If the intergranular distances are short, radon atoms resulting from surface deposits of radium will end their recoil in an adjacent grain (B - B' in Figure 1). For dry, compacted porous media the direct recoil fraction is less than 1% of the total emanating power (Tanner, 1980).

If the pores contain water, the range of the recoil atom is only about 0.1 μm (Tanner, 1964) and the probability that it will stop in the pore is greatly increased (C - C' in Figure 1). Thus the presence of liquid in the pore spaces increases the direct recoil fraction due to its shorter recoil range. Fleischer (1983) has shown that radon emanation from the parent matrix is increased by moderate amounts of interstitial water due to dissipation of recoil energy. Strong and Levins (1982) measured radon emanation coefficients from uranium mill tailings at varying moisture contents and found that a sharp rise in emanation occurred from the absolutely dry state up to 2% water by weight; above 2 wt%, emanation increased only slightly up to the saturation limit.

If the pores are gas filled, the recoil range in air is much greater than typical pore sizes, about 63 μm (Tanner, 1964), consequently the radon atom will traverse the pore and penetrate the adjacent solid grain to a depth equal to its recoil range in the solid material reduced by the amount of energy already expended in the pore space (D - D' in Figure 1). The energy absorbed is sufficient to melt or volatilize the material along the recoil path. The radon atom can then escape by diffusion back through the vaporized pocket before the material solidifies. This is called the indirect recoil fraction of the emanating power.

The molecular diffusion coefficient (D_m) of radon in solid and ionic crystals is widely given as 10^{-20} cm^2/s to 10^{-25} cm^2/s or less (Tanner, 1964). This yields a diffusion length (l), defined as $(D_m/\lambda)^{1/2}$, of only a few lattice constants during the mean life of radon. Hence, except for those radium atoms very close to the surface or in solid grains of appreciably smaller dimensions than the mean diffusion length of radon in the solid, the contribution to the emanating power by the diffusion fraction is very small. However most natural minerals and nearly all rocks and soils exhibit emanation coefficients greater than can be accounted for by recoil or by diffusion from mineral crystals that are structurally intact and in which the radium isotope parent is uniformly distributed. Tanner (1964, 1980) concludes that:

> "any appreciable emanations of radon-222 ... atoms come from radium isotopes distributed in shallow crusts or films or in the shallow surface layers (approximately as deep as the recoil range) of intact crystals of the host minerals. Radon isotopes in the deeper regions of the crystals are unavailable without the development of large internal surfaces, such as may result from chemical corrosion, weathering, or intensive fracturing on a microscopic scale... The principle mechanism by which the radon isotopes enter the pores, capillaries, or microfractures is radioactive recoil into liquid-containing spaces or diffusion from solid material appreciably smaller than the diffusion length of the most short-lived isotope observed."

2.) Diffusion

For a one dimensional system the diffusion coefficient is defined by Ficks law relating diffusional flux to the concentration gradient:

$$j = -D_m (\partial C/\partial z), \qquad (2.18)$$

where j = radon flux in open pore space (M/L^2T)
C = interstitial radon concentration (M/L^3)
D_m = molecular diffusion coefficient (L^2/T).

The negative sign before the diffusion coefficient indicates that radon moves toward the zone of lower concentration. Often the bulk diffusional flux per unit cross-sectional area of soil, J, is referred to because the flux from only the pore spaces, j, is not an easily measured quantity. The two are related by:

$$J = j\,n \text{ and} \tag{2.19}$$

$$J = -n\,D_m\,(\partial C/\partial z), \tag{2.20}$$

where n = soil porosity (L^3/L^3).

The use of equation (2.20) to relate the concentration gradient to the bulk flux is valid provided account is taken of the restricted nature of the channels through which diffusion occurs in soil. The two primary factors which reduce radon flux in porous media are the reduction in cross-sectional area for diffusion and the lengthened diffusion pathway due to the circuitous nature of the pores:

$$J = -\tau\,n\,D_m\,(\partial C/\partial z) \text{ and} \tag{2.21}$$

$$J = -D_e\,(\partial C/\partial z), \tag{2.22}$$

where τ = tortuosity $(L/L_e)^2$
L = bulk thickness (L)
L_e = diffusion path length (L)
D_e = effective diffusion coefficient for soil (L^2/T).

Radon diffusion in soils occurs through both the air filled and water filled regions of open pore space. The diffusion equations are similar for both phases and can be combined with the appropriate distribution coefficient to give an expression for diffusion

through the two phase soil system. Table 2 gives typical values for mean diffusion lengths and effective diffusion coefficients.

Table 2

Typical Mean Diffusion Lengths and Effective Diffusion Coefficients

Medium	Length (m)	Diffusion Coefficient (m^2/s)
Air	2.20	1×10^{-5}
Porous Soil	1.55	5×10^{-7}
Water	0.020	1×10^{-10}
Saturated Porous Soil	0.016	5×10^{-11}

(After Tanner, 1964 and Fleischer and Mogro-Campero, 1978)

3.) Advection

Fluids in the soil (liquid or gas) can migrate in response to a pressure driven gradient. These fluids can "carry" radon with them. For a one dimensional, homogenous and isotropic soil system, Darcys law can be written:

$$v = - \frac{k}{\mu} \left(\frac{\partial P}{\partial z} \right) \tag{2.23}$$

where v = Darcy velocity of soil gas (L/T)
k = soil intrinsic permeability to air (L^2)
μ = dynamic viscosity of air (M/LT)
$\partial P/\partial z$ = pressure gradient (M/L^2T^2).

The advective movement of soil gas is strongly dependent on the soil permeability to air which in turn varies due to soil type and water content. Pressure gradients in soil induced by barometric pressure changes and/or the effects of wind can range from about 1 to 10 Pa/m (Nazaroff et al., 1986) and drive the advective flow of soil gas.

Representative soil categories and their associated air permeabilities and darcy velocities for a typical pressure gradient of 5 Pa/m are given in Table 3.

Table 3

Typical Soil Permeabilities to Air and Darcy Velocities

Soil Type	Permeability (m^2)	Darcy Velocity (m/s)
Clay	1×10^{-16}	2.9×10^{-11}
Sandy Clay	5×10^{-15}	1.4×10^{-9}
Silt	5×10^{-14}	1.4×10^{-8}
Sandy Silt and Gravel	5×10^{-14}	1.4×10^{-8}
Fine Sand	5×10^{-12}	1.4×10^{-6}
Medium Sand	1×10^{-10}	2.9×10^{-5}
Coarse Sand	5×10^{-10}	1.4×10^{-4}
Gravel	1×10^{-8}	2.6×10^{-3}

$\mu = 17.5 \times 10^{-6}$ kg/m s; $\partial P/\partial z = 5$ Pa/m

(After Sextro et al, 1987; Nero, 1988)

CHAPTER 3

THE MODEL

A. Description

RN3D is a finite element radon transport model developed at Pacific Northwest Laboratory (Holford et al., 1989). Radon transport is two phase, by advection and diffusion in the gas phase and diffusion in the water phase. The fortran code is capable of simulating transport in one dimension (1-D) without soil cracks, two dimensions (2-D) with soil cracks and three dimensions (3-D) with cracks. Steady state or transient air flow is possible with homogenous isotropic or heterogenous anisotropic soil conditions. The model simulates pressure gradients in the soil caused by air pressure changes at the soil/air interface which drive the advective transport of radon in the gaseous phase. Diffusive transport of radon is simulated in both the gas phase and the liquid phase. The model runs conducted for this research are 1-D in steady state, as well as 1-D and 2-D with transient air flow. The discussion of the general governing equations given below follows the derivations given by Holford et al. (1989).

1.) Governing Equations

The concentration of radon gas in air (C) is defined as the mass of radon per unit volume of air. The porosity of a soil (n) is defined as the ratio of void space to total volume of soil. The concentration of radon gas per unit bulk volume of soil is therefore equal to nC. The mass of radon transported per unit time per unit bulk cross-sectional area of soil is called the flux density. The diffusive flux density (Fd) is defined by Ficks law for molecular diffusion in soil (Bear, 1979):

$$Fd_i = -D^*_{ij} \frac{\partial(nC)}{\partial x_j} \tag{3.1}$$

where x = spatial coordinate, where i, j indicate direction
D^*_{ij} = diffusion coefficient in soil (L^2/T).

The diffusion coefficient in soil is defined as (Bear, 1979):

$$D^*_{ij} = D_a \tau^*_{ij} \tag{3.2}$$

where D_a = diffusion coefficient in air
τ^*_{ij} = tortuosity coefficient of soil.

The advective flux density (Fa), or the mass of radon transported per unit time per unit bulk cross-sectional area of soil by gas flow, is defined as (Bear, 1979):

$$Fa_i = v_i C \tag{3.3}$$

where v_i = Darcy velocity of gas (L/T).

The Darcy velocity is defined as the volume of gas flowing per unit bulk cross-sectional area of soil per unit time.

Conservation of mass requires that the net mass transported into a unit volume of soil be equal to the change in the mass stored in the volume, minus the mass lost by radioactive decay, plus the mass of radon produced by the decay of radium in the soil. The resulting continuity equation for soil takes the form:

$$-\frac{\partial(nC)}{\partial t} = \frac{\partial F_i}{\partial x_i} + \lambda(nC) - n\phi \tag{3.4}$$

where $F_i = Fd_i + Fa_i$ = total flux density
λ = decay constant of ^{222}Rn (T^{-1})
ϕ = production rate of radon per unit volume of pore space (M/L^3T).

Substituting equations (3.1) and (3.3) into (3.4) and dividing through by porosity (n) gives the governing radon transport equation:

$$\frac{\partial C}{\partial t} = \frac{\partial}{\partial x_i}\left(D^*_{ij}\frac{\partial C}{\partial x_j}\right) - \frac{\partial}{\partial x_i}\left(\frac{v_i C}{n}\right) - \lambda C + \phi \tag{3.5}$$

For this research the soil was assumed to be isotropic with a scalar tortuosity (τ^*) which makes D^* a scalar.

The radon transport equation and the air flow equation are coupled by Darcys law (Bear, 1979):

$$v_i = - \frac{k_{ij}}{\mu} \left[\frac{\partial P}{\partial x_i} + \rho g \frac{\partial z}{\partial x_j} \right] \tag{3.6}$$

where v_i = Darcy velocity (L/T)
k = intrinsic permeability of soil to air (L^2)
μ = dynamic viscosity of air (M/LT)
P = absolute gas pressure (M/LT^2)
ρ = gas density (M/L^3)
g = gravitational acceleration (L/T^2).

Conservation of mass requires that the net rate of fluid flow into and out of a unit volume of soil be equal to the change of fluid mass stored within the volume. The continuity equation is then expressed (Bear, 1979):

$$- \frac{\partial (n\rho)}{\partial t} = \frac{\partial (\rho v_i)}{\partial x_i} . \tag{3.7}$$

Combining the continuity equation and Darcys law gives:

$$\frac{\partial (n\rho)}{\partial t} = \frac{\partial}{\partial x_i} \left[\frac{k_{ij}\, \rho}{\mu} \left(\frac{\partial P}{\partial x_j} + \rho g \frac{\partial z}{\partial x_j} \right) \right] . \tag{3.8}$$

For an ideal gas the equation of state is:

$$\rho = MP/RT \tag{3.9}$$

where M = molecular weight
R = universal gas constant
T = absolute temperature.

For isothermal flow, then:

$$\frac{\partial \rho}{\partial t} = \frac{M}{RT}\frac{\partial P}{\partial t} \tag{3.10}$$

and substituting equations (3.9) and (3.10) into (3.8) gives:

$$\frac{\partial (nP)}{\partial t} = \frac{\partial}{\partial x_i}\left[\frac{k_{ij}\,\rho}{\mu}\right] + \frac{\partial P}{\partial x_j}\left[\frac{\partial}{\partial x_i}(P\rho g k_{ij})\right]\left(\frac{\partial z}{\partial x_j}\right) \tag{3.11}$$

Because the density of air is so small the effects of gravity are assumed to be negligible. Also the soil is assumed to be homogenous, isotropic and incompressible therefore the porosity (n) is uniform in space and time. Using the foregoing assumptions equation (3.11) reduces to:

$$n\frac{\partial P}{\partial t} = \frac{\partial}{\partial x_i}\left(\frac{k_{ij}P}{\mu}\frac{\partial P}{\partial x_j}\right) \tag{3.12}$$

which, using the chain rule, can be rewritten for a partially saturated soil:

$$\left(\frac{n_a}{P}\right)\frac{\partial P^2}{\partial t} = \frac{\partial}{\partial x_i}\left(\frac{k_{ij}\partial P^2}{\mu\ \partial x_j}\right) \tag{3.13}$$

where n_a = air-filled porosity of soil.

Equation (3.13) is the governing equation for transient air flow.

2.) Finite Element Method

The radon transport equation (3.5) and the air flow equation (3.13) are solved using the Galerkin finite element method. Using this technique the governing equation for radon transport equation (3.5) and the governing air flow equation (3.13) may be rewritten, respectively:

$$L(C) = \frac{\partial C}{\partial t} - D^* \frac{\partial C}{\partial x^2} + \frac{\partial}{\partial x_i}\left(\frac{v_i}{n} C\right) + \lambda C - \phi = 0 \tag{3.14}$$

and,

$$L(P) = \frac{n_a}{P} \frac{\partial P^2}{\partial t} - \frac{\partial}{\partial x_i}\left(\frac{k_{ij}}{\mu} \frac{\partial P^2}{\partial x_i}\right) = 0 \tag{3.15}$$

where, L is the Laplacian operator.

The procedure used by the Galerkin finite element method is to introduce a trial solution $\hat{C}$ for the concentration C, or $\hat{P}$ for the pressure P, at each node:

$$\hat{C}(x_i,t) = \sum_{j=1}^{nn} N_j(x_i)\, C_j(t) \tag{3.16}$$

similarly,

$$\hat{P}(x_i,t) = \sum_{j=1}^{nn} N_j(x_i)\, P_j(t) \tag{3.17}$$

where, N = weighting function at each node j
nn = number of nodes in model region.

Because $\hat{C}$ and $\hat{P}$ are only approximations for C and P, the residual (or error) at each node in the problem domain is a measure of the degree to which the concentration or air flow at that node does not satisfy the governing equation. The Galerkin method requires that the weighted integral of the error summed over the entire solution region, R, equal zero, (Pinder and Gray, 1977). For the radon transport equation then:

$$\int_R N_I\, L(\hat{C})\, dR = 0. \tag{3.18}$$

This yields

$$\int_R N_I \left[\frac{\partial \hat{C}}{\partial t} - D^* \frac{\partial^2 \hat{C}}{\partial x^2} + \frac{\partial}{\partial x_i}\left(\frac{v_i}{n} \hat{C}\right) + \lambda \hat{C} - \phi\right] dR = 0. \tag{3.19}$$

Substituting equation (3.16) for $\hat{C}$ in equation (3.19) gives:

$$\int_R \left[\frac{\partial C_J}{\partial t} N_I N_J - D^* C_J \frac{\partial N_I}{\partial x_i}\frac{\partial N_J}{\partial x_i} + C_J N_I \frac{\partial}{\partial x_i}\left(\frac{v_i}{n} N_J\right) + \lambda C_J N_I N_J - \phi N_I\right] dR = 0. \quad (3.20)$$

The time integral is solved using a standard implicit, finite-difference approximation:

$$\frac{\partial C_J}{\partial t} = \frac{C_J(t_{m+1}) - C_J(t_m)}{t_{m+1} - t_m} = \frac{C_J^{m+1} - C_J^m}{\Delta t} \quad (3.21)$$

where, C^m = concentration at previous time step
C^{m+1} = concentration at current time step
Δt = time increment.

Substituting equation (3.21) into equation (3.20) yields:

$$\int_R \left[\frac{1}{\Delta t} N_I N_J + D^* \frac{\partial N_I}{\partial x_i}\frac{\partial N_J}{\partial x_i} + N_I \frac{\partial}{\partial x_i}\left(\frac{v_i}{n} N_J\right) + \lambda N_I N_J \left(C_J^{m+1}\right)\right] dR$$
$$= \int_R \left[\phi N_I + C_J^{m+1}\left(\frac{1}{\Delta t} N_I N_J\right)\right] dR. \quad (3.22)$$

A fully implicit time stepping scheme is used to ensure stability. The systems of linear equations are solved using Gaussian elimination in a sparse matrix package called SPARSPAK-A (Chu et al., 1984).

The solution of the flow equation by the Galerkin finite element method is similar to that for the transport equation, except that there are fewer terms in the flow equation and it is weakly non-linear. Applying the same techniques to the governing flow equation, (3.15), as in equations (3.18) and (3.19) gives:

$$\int_R \left(\frac{\partial P_J^2}{\partial t} N_I N_J + \frac{k_{ij}}{\mu} P^2 \frac{\partial N_I}{\partial x_i}\frac{\partial N_J}{\partial x_i}\right) dR = 0. \quad (3.23)$$

Equation (3.23) is solved in terms of P^2; the P in the coefficient of the nonlinear time term is treated as the average pressure for all the nodes in an element. Applying the implicit finite difference technique to the time derivative as was done in equation (3.22) yields:

$$\int_R \left[\frac{1}{\Delta t} \frac{n}{p^{m+1}} N_I N_J + \frac{k_{ij}}{\mu} \frac{\partial N_I}{\partial x_i} \frac{\partial N_J}{\partial x_i} \right] dR \left(P_J^{m+1}\right)^2 = \int_R \left[(P_J^m)^2 \frac{1}{\Delta t} \frac{n}{P^{m+1}} N_I N_J \right] dR. \tag{3.24}$$

During solution of equation (3.24) the pressure at the current time step, P^{m+1}, is an unknown and is a function of both the left and right hand side of the flow equation. Due to this nonlinearity in the flow equation, P^{m+1} must be solved for iteratively. This is done by setting P^{m+1} equal to P^m, the known pressure from the previous time step, for the first iteration and solving the equation iteratively until the difference between two successive iterations is less than some prescribed tolerance.

B. Assumptions and Boundary Conditions

As with all subsurface fluid transport models, certain simplifying assumptions must be made and boundary conditions explicitly stated to fully define the model region. Air flow in the soil is driven by air pressure changes at the surface which result in a complex and nonuniform flow field in the soil. Figure 2 is a schematic diagram of a 1-D soil model showing the boundary conditions and the various components affecting radon transport. For the 1-D case a boundary condition of $C = 0$ is imposed at the top of the soil because the concentration of radon in the free atmosphere is assumed to be zero. This boundary condition also requires that there is no advective flux across the top boundary ($v_a C = 0$). Only diffusive flux is assumed at the soil-air interface. The bottom boundary is represented by the water table (Figure 2) which is assumed to be an impermeable barrier

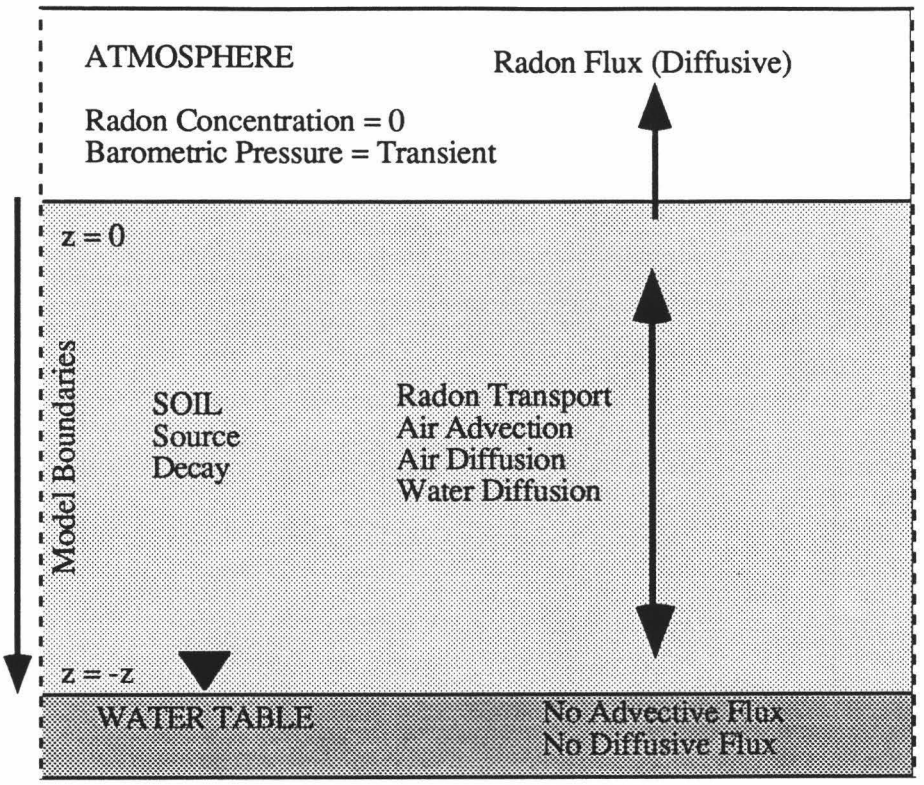

Figure 2. Schematic diagram of one dimensional soil model and boundary conditions. The effects of radioactive decay, the radon source term, soil bulk density , soil porosity, soil saturation and emanation are included. Molecular diffusion is assumed to be governed by Ficks law. The flow of gas is governed by Darcys law. ^{226}Ra is assumed to be evenly distributed throughout the soil. At the top of the soil a boundary condition of C = 0 is imposed because the concentration of radon in the free atmosphere is assumed to be zero. The bottom of the model region is the water table which is also assumed a no-flux, no-flow boundary. Transport within the soil is by advection and diffusion, flux at the soil/air interface is by diffusion.

to air flow ($v_a = 0$) and diffusive flux, therefore no radon transport by diffusion or advection occurs across this boundary.

Figure 3 is a schematic diagram of a 2-D cracked soil model showing the various components affecting radon transport. The boundary conditions for the 2-D radon transport and flow model are shown schematically in Figure 4. The bottom boundary conditions are the same as for the 1-D case. The side boundaries are also assumed to be no-flux, no-flow boundaries. At the top of the soil there is again no advective flux assumed, only diffusive flux. At the top of the crack it is assumed that advective flux dominates and is strong enough to cause concentrations to rise above zero directly above the crack. There is no diffusive flux modeled across this boundary $(\partial C/\partial x) = 0$. The sides and bottom of the crack are within the model region where transport is by advection and diffusion.

C. Required Input

RN3D requires several parameters for the soil and gas properties to be read as input data. Table 4 summarizes these parameters. The advective flow of soil gas is driven by barometric pressure changes at the surface. Pressure data are read by RN3D from a file specified by the user. With the exception of soil diffusion coefficient, all of the values for input parameters were measured directly in the field or the lab. Estimates of diffusion coefficients were derived from a soil water characteristic model called RETC (Van Genuchten 1980, 1985) which generates a pore size distribution consisting of all possible combinations of single and composite pores. Bulk diffusion coefficients for partially saturated soils were generated by the method of Neilson et al., (1984) which combines diffusion through both air and water filled pore spaces. Diffusion coefficients were also estimated from an empirical model proposed by Rogers et al. (1984).

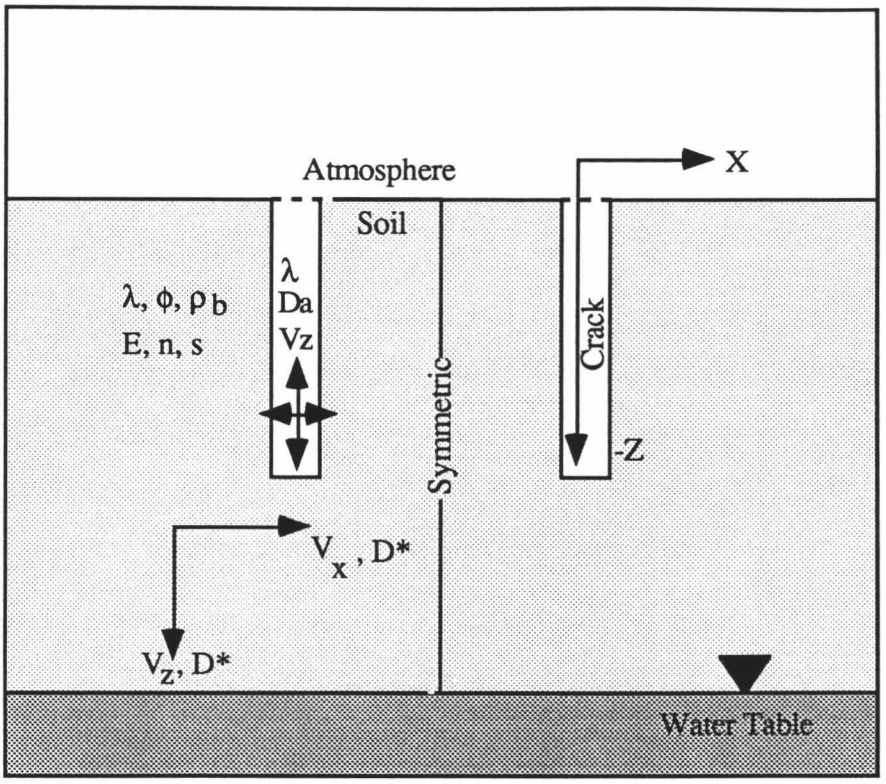

Figure 3. Schematic diagram of two dimensional cracked soil model. Flow and transport are two-dimensional in the soil, but effectively one-dimensional in the crack. The effects of radioactive decay (λ), the radon source term (ϕ), soil density (ρ), soil porosity (n), soil saturation (s) and emanation (E) are included. Because the crack is narrow and diffusion is strong it is assumed that radon is evenly mixed across the width of the crack. The coordinate system consists of the x-direction (parallel to the soil/air boundary) and the z-direction, negative downward (perpendicular to the soil/air boundary). Molecular diffusion (D^*) is assumed to be governed by Ficks law. The flow of gas (v) is governed by Darcys law. ^{226}Ra is assumed to be evenly distributed throughout the soil.

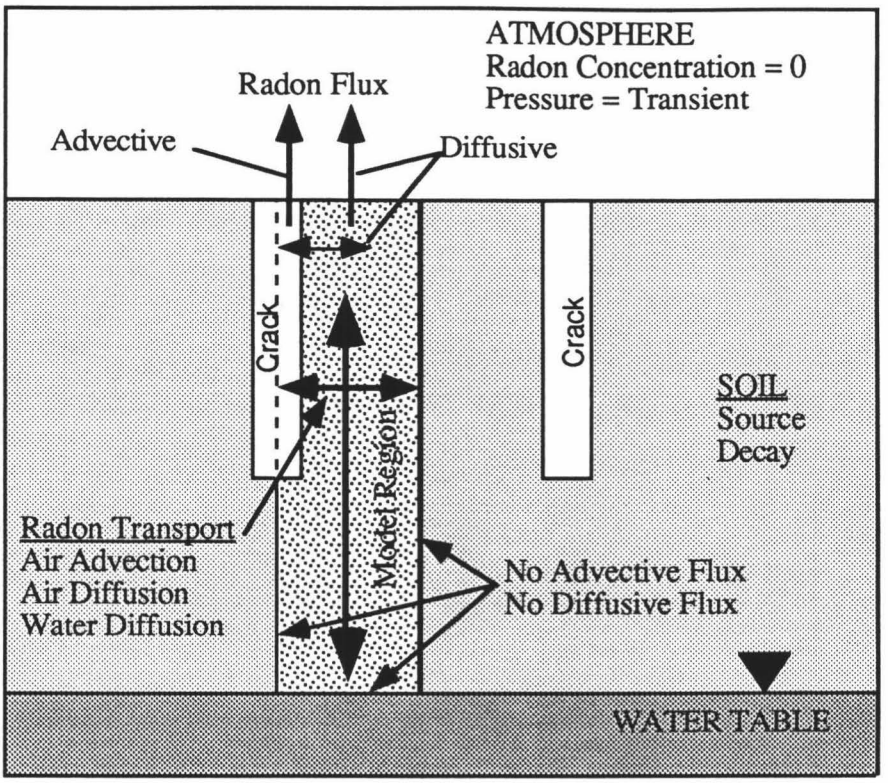

Figure 4. Boundary conditions for radon transport and gas flow equations in 2-D. At the top of the soil a boundary condition of $C = 0$ is imposed because the concentration of radon in the free atmosphere is assumed to be zero. This boundary condition further requires that there is no advective flux across the top boundary of the soil ($vC = 0$), only diffusive flux. At the top of the crack a boundary condition of $\partial C/\partial z = 0$ is imposed because advective transport dominates ($vC \neq 0$) and is strong enough to cause measurable radon concentrations directly above the crack. This boundary condition also implies that there is no diffusive flux across this boundary. The sides of the model region are given no-flux, no-flow boundaries and the bottom of the model region is the water table which is also assumed a no-flux, no-flow boundary.

Table 4

Summary of RN3D Input Parameters and Variables

Parameter/Variable (units)	Parameter/Variable (units)
Boundary and Initial Conditions	**Soil Properties**
top boundary concentration (M/L^3)	saturation (*)
initial condition pressure (M/LT^2)	crack permeability (L^2)
change in P(atm)/time (M/LT^3) or,	bulk density (M/L^3)
barometric pressure data vs time (M/LT^2)	intrinsic air permeability (L^2)
	diffusion coefficient (L^2/T)
	emanation coeff.-dry soil (*)
	emanation coeff.-sat. soil (*)
	radium activity (activity/M)
Model Geometry	**Gas Properties**
crack spacing (L)	dynamic viscosity of air (M/LT)
crack depth (L)	radon half life (T)
crack width (L)	Rn distribution coeff.-water/air (*)
crack length (L)	Rn diffusion coeff.-air (L^2/T)
depth to water table (L)	
total width of model (L)	
grid spacing (L)	
	(* = Dimensionless)

D. Modifications

In order to provide more realistic simulations of the field data obtained at the Poamoho site the model was modified to account for soil parameters which vary with depth. The code was modified to allow entry of bulk density, porosity, saturation, air permeability and diffusion coefficient for layers of user specified thickness. Figure 5 illustrates schematically how the layers are incorporated in the model.

Another modification which has been incorporated into the model is the ability to specify initial conditions which are not steady-state. RN3D, in its original form, starts all transient simulations from a steady-state condition ($\partial C/\partial t = 0$). This meant that consecutive simulations could not be performed realistically because the new simulation would always start at a different condition than where the previous run finished. The model has now been modified to allow initial conditions to be read from the final time step of a previous run. This allows simulation of rainfall events where the top layer becomes saturated and the downward movement of a wetting front can be modeled. This feature allows greater flexibility in the simulation of real environmental conditions.

E. Suitability of RN3D for This Study

RN3D was chosen for this research because it is the most sophisticated radon transport model, dealing with transport in naturally occurring soils, available at this time. Other models presently available are either tailored to simulate radon transport into manmade structures (DSMA ATCON, 1985), or simulate the flux of radon from uranium mill tailings, (Nielson and Rogers, 1989). Other available models do not take into account transport due to pressure perturbations, do not consider two-phase diffusive transport or are analytical solutions to the radon transport equations requiring serious limiting assumptions and greatly simplified geometries.This study is the first attempt to validate RN3D with real data on low permeability, high water content soils. It has previously been

validated by Holford et al. (1989), on dry, high permeability soils and it has been used in sensitivity analyses and on test cases of hypothetical soils (Holford et al., 1988, Owczarski et al., 1989).

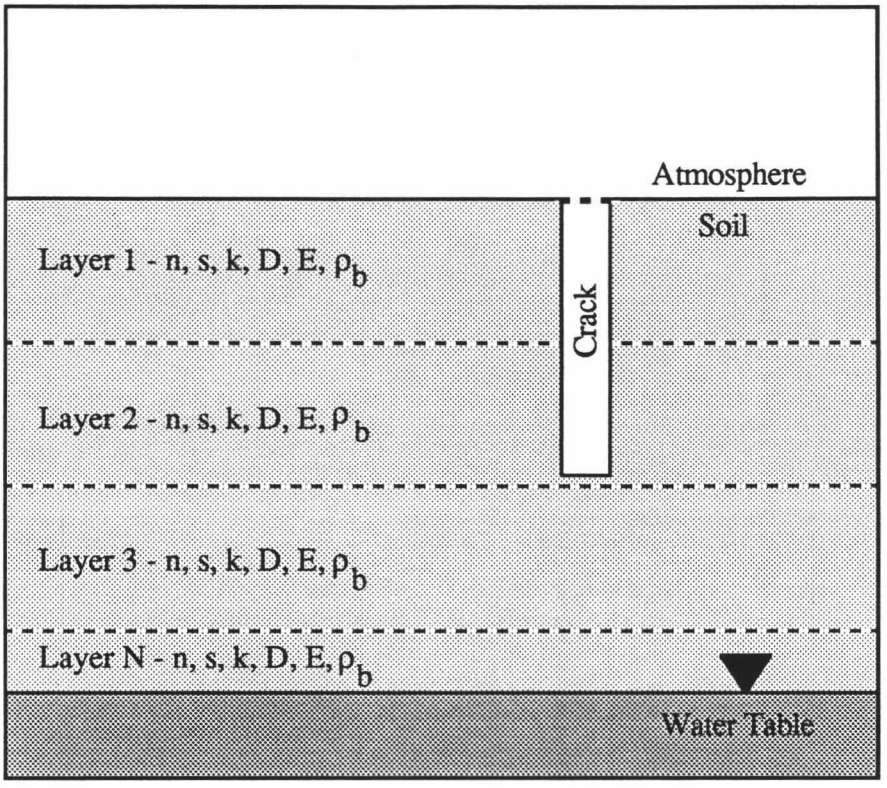

Figure 5. Schematic illustration of different layers exhibiting different soil properties. Different values for porosity (n), saturation (s), air permeability (k), diffusion coefficient (D), emanation (E) and bulk density (ρ) can be entered for up to ten different layers. Thickness of the layers is specified by the user.

CHAPTER 4

DATA COLLECTION AND EXPERIMENTAL METHODS

A. Radon and Environmental Monitoring

1.) Poamoho Site

The radon monitoring and data collection phase of this research program were carried out at the University of Hawaii Poamoho Agricultural Experimental Station (UHPAES). Figure 6 illustrates the location and topography of the area. Soil at the UHPAES has been classified as a member of the Wahiawa Series silty clay (Ikawa et al., 1985). Table 6 in Appendix A provides a description of a soil profile taken less than 100 m west of the radon monitoring site and Table 7 in Appendix A gives a laboratory analysis of soils from the UHPAES.

The Poamoho site, which lies at an elevation of 215 m on Oahu's central plain, was chosen for a number of reasons: 1) the geology and geochemistry are relatively uniform over several kilometers distance and to depths of tens to hundreds of meters (MacDonald et al., 1983), eliminating unknown effects on radon observations due to spatial variations in geology and geochemistry; 2) the soil characteristics and chemistry at this site have been well characterized by Green et al. (1982) and Ikawa et al. (1985); and 3) necessary support and facilities could be provided by UHPAES personnel.

During periods of sparse rainfall a network of surface cracks, some extending 0.5 m into the soil, was observed at the Poamoho site. The effect of these cracks on radon activities in the shallow soil environment is substantial and will be discussed in Chapter 5.

Research published subsequent to the selection of the Poamoho site revealed that there is an erosional surface or discontinuity present in soils of Oahu's central plain at a depth ranging from 0.5 m to 1.3 m. Soils below the discontinuity are derived from

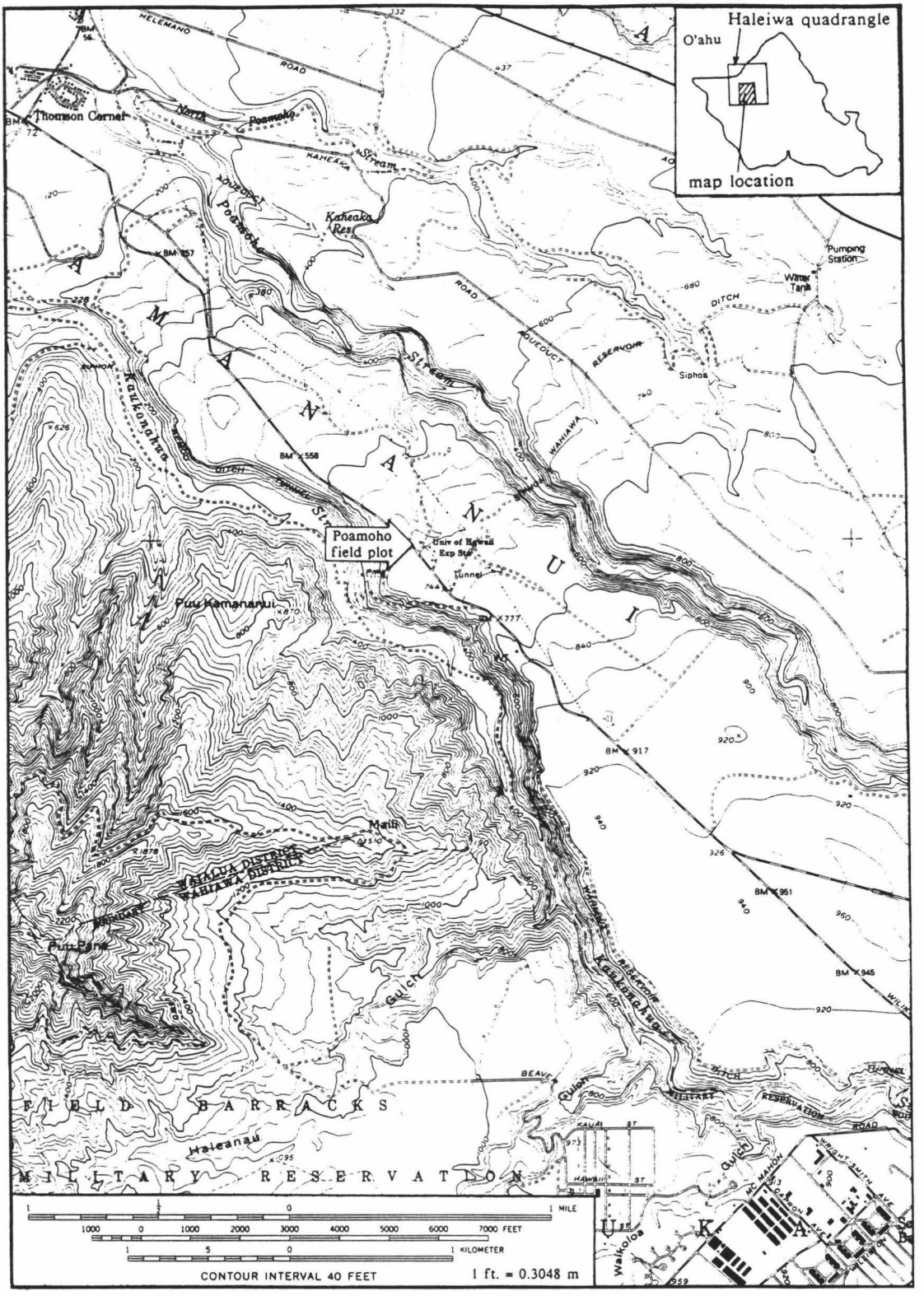

Figure 6. Topographic map of the Poamoho area (U.S. Geological Survey, 1983).

weathering of the Koolau and Waianae basalts. Above the discontinuity the soils are derived from a mixture of volcanic ash deposits and tropospheric dust (Gavenda, 1989). However soil characteristics pertinent to this study (porosity, bulk density, air permeability) show little variation between the two horizons and the effect of the discontinuity on the radon response in the soil was judged to be negligible.

As mentioned in Chapter 1, the work described in this thesis is a portion of an ongoing investigation; as the project is still continuing, new instrumentation and experimental configurations are being installed. Figure 7 shows a plan view of the full monitoring array at the Poamoho site as it existed at the completion of this thesis research and Figure 8 shows a schematic cross section of one of the monitoring arrays. The full experimental and control monitoring array was installed as the monitoring instruments became available. What follows is a description of the various instrumentation used and a chronological account of their installation.

2.) Meteorological Monitoring

Meteorological data on barometric pressure and rainfall were essential for this study. Hourly barometric pressure data were obtained from the National Weather Service. These data were recorded at the Honolulu Airport, about 30 km from the Poamoho site. Daily rainfall data for the Poamoho site were obtained from a rain gauge monitored by UHPAES personnel.

3.) Radon Monitoring

The detection of radon in soil gas was carried out using the Alphanuclear Model 611 alphaLOGGER™, a passive, electronic detector which counts and records alpha particle radiation. The unit is cylindrical in shape, 51 mm in diameter by 350 mm long and constructed of stainless steel. A 400 mm^2, solid state, silicon alpha detector is housed

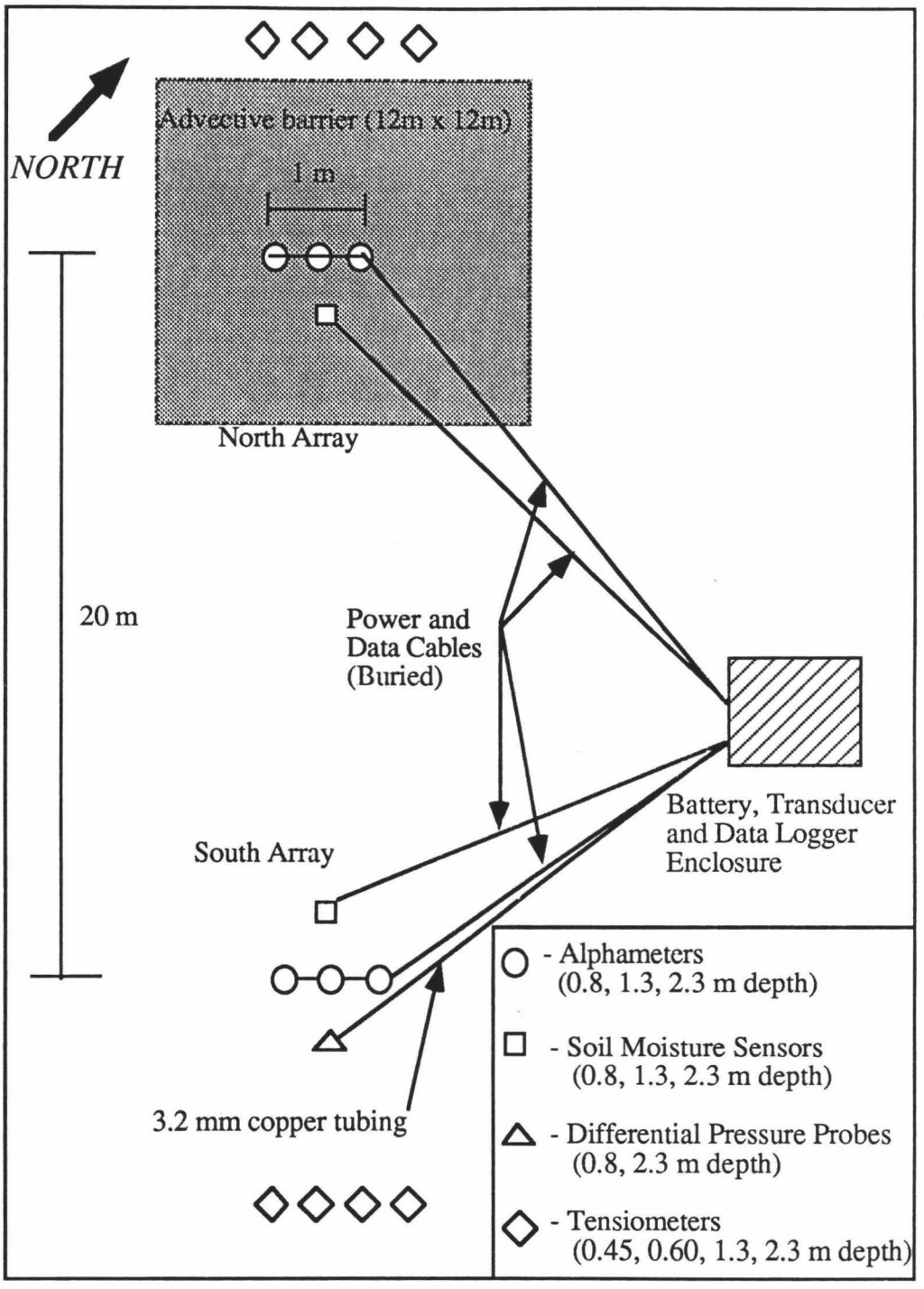

Figure 7. Plan view of the radon and soil monitoring array at the UHPAES. Shown are the alphameters, soil moisture probes, differential pressure probes, tensiometers and advective barrier.

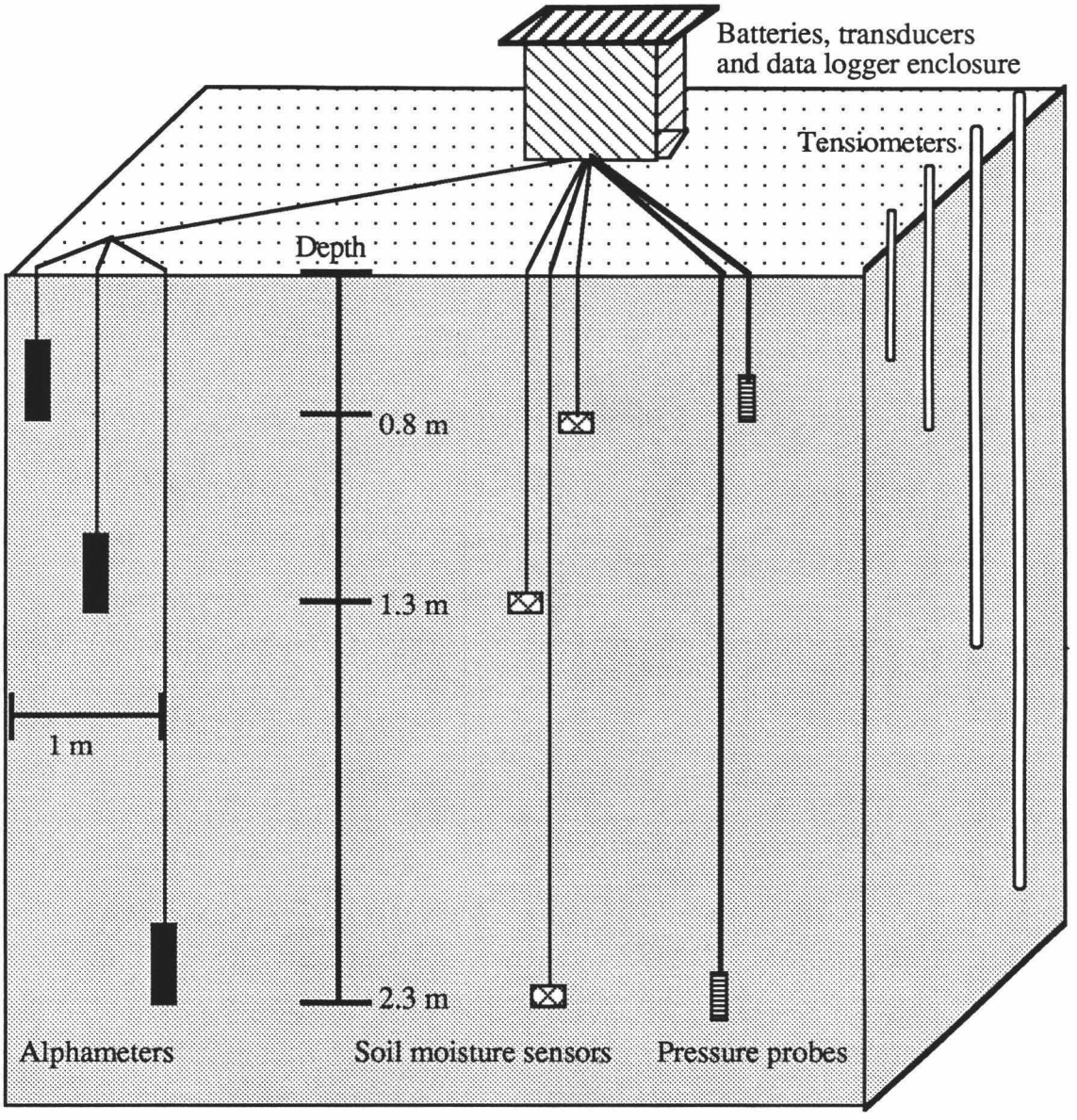

Figure 8. Schematic cross-sectional view of a monitoring array. Shown are the alphameters, soil moisture sensors, differential pressure probes and tensiometers.

behind an aluminized mylar membrane which excludes ambient light and moisture while still allowing the passage of alpha particles through to the detector. A distance of 64 mm separates the silicon detector from the soil ensuring that only alpha particles from radon in soil gas within the sample volume are detected; any alpha particles originating from Uranium or Radium in the soil would be attenuated by the 64 mm distance. Alpha particle counting data are integrated over 15 minute time intervals and stored in an internal memory buffer until retrieval by a laptop computer over an RS-232 serial data link.

a.) Initial Alpha Detector Installation

As mentioned in Chapter 1, the radon monitoring effort consisted of two radon detection arrays, the experimental array and the control array, with three alpha detectors in each. However, due to a significant delay in delivery of the six alpha detectors from the supplier, a single alpha detector was installed in August 1988 followed by a second alpha detector in December 1988. The first two detectors were separated by 15 m horizontal distance.

The purpose of the first two detectors was to provide initial data on the amount of radon present and to test different deployment protocols. The first detector was installed, as shown in Figure 9a, in a PVC-encased well approximately 1.5 m deep. The hole was bored by a hand operated, 0.1 m diameter bucket auger. A shielded power/data cable extended to the surface. Power was supplied by an 18 volt DC gel cell battery.

The deployment method used for the first alpha detector resulted in artificially induced perturbations in the data (discussed in Chapter 5), and for this reason, the second detector and all subsequent detectors were installed, as shown in Figure 9b and described below, to minimize these effects.

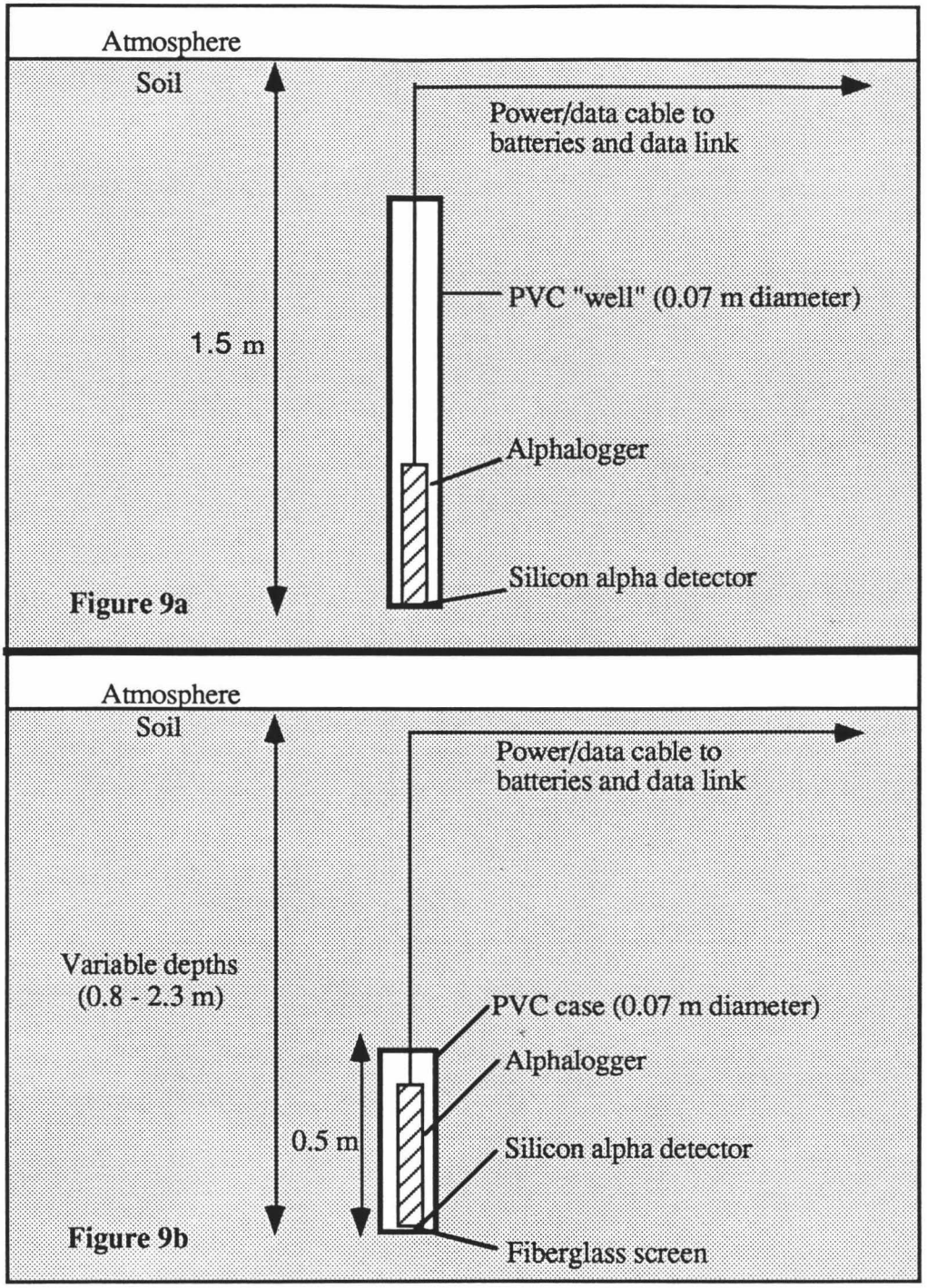

Figure 9. Illustration of alphameter deployment. Figure 9a shows the initial deployment method and Figure 9b the final deployment scheme used for all the alphameters.

b.) Alpha Detector Array Installation

In March, 1989 the six radon monitoring alphameters were deployed. The two arrays were installed identically and separated by a distance of 20 m (Figure 7). Each alphalogger was wrapped on the top and sides, leaving the sample volume unobstructed, with self-vulcanizing rubber tape and housed in a PVC case, open on the bottom, to protect against pressure from soil, rocks and water damage to the unit during the two to three years the meters are expected to remain in place (Figure 9b).

It was found after retrieval of the initial alphalogger (Figure 9a), that soil had clogged the sample volume resulting in substantially less than 64 mm separating the soil from the detector surface. To alleviate this problem a fiberglass screen was stretched across the base of the PVC casing allowing soil gas to pass easily through the screen but preventing entry of soil. Each radon detection meter was fully buried in its own hole, 0.5 m, 1.3 m and 2.3 m deep respectively. The holes were hand-augered and placed approximately 0.5 m apart (Figures 7 and 8). Every attempt was made to back fill the hole to its original compaction to minimize disturbance to the natural soil profile and minimize channelling effects through the disturbed soil. Only the power/data cable of each detector led to the surface of the hole. All six alphaloggers were powered by an 18 volt lead-acid battery.

4.) Soil Moisture Detection

The amount of water present in the open pore spaces of the soil is the most important factor influencing radon release and transport in the subsurface. Emanation, diffusion and air permeability of the soil are all controlled by soil moisture content. For this reason monitoring of soil moisture on a time scale consistent with the radon monitoring was imperative to this investigation. A porous, ceramic soil moisture sensor connected to an automatic data logging network was chosen to obtain these data.

a.) Soil Sampling

Due to repeated delays in obtaining the soil moisture sensors and data loggers from the suppliers, soil samples were taken whenever possible to determine soil gravimetric moisture content (ratio of soil moisture mass to dry soil mass). Soil samples were taken from hand augured holes at the depths of 0.8 m, 1.3 m and 2.3 m and placed in watertight cans. The gravimetric soil moisture content was calculated by weighing the sample at field conditions, then oven-drying at 105 C for at least 24 hours before reweighing to determine the dry soil weight. The soil moisture parameter of interest in soil gas transport is the degree of saturation (ratio of soil moisture volume to total pore volume). Once the gravimetric moisture content is known the saturation (S) can be readily obtained from the relation:

$$S = \frac{\theta_g \rho_b}{n \rho_m} \tag{4.1}$$

where, θ_g = gravimetric moisture content (M/M)
ρ_b = soil bulk density (M/L^3)
ρ_m = soil moisture density (assumed to be 1 g/cc)
n = soil porosity (L^3/L^3).

Average values for soil bulk density and porosity were taken from studies of the Poamoho soils by Green et al. (1982), Ikawa et al. (1985), Miller (1987) and from soil cores collected at 0.5 m depth.

b.) Soil Moisture/Temperature Sensors

In June, 1989 the soil moisture detectors and data logging array were received and installed. The moisture probes are Agwa II™ soil matric potential sensors manufactured by Agwatronics Inc. Soil matric potential is a measure of the energy opposing moisture transfer from the soil to plant roots due to soil capillary tension, in negative bars. The

sensor measures heat dissipation in a porous ceramic medium. The heat dissipated by the ceramic is directly proportional to the amount of water contained in the void spaces of the ceramic. The sensor contains a small heater and temperature sensor. When a moisture measurement is taken, two temperature readings are made: the first measures the soil's ambient temperature and the data logger records this value; the heater then turns on and after sixty seconds a second temperature reading is made. The soil matric potential is then calculated as a function of the difference between these two temperature measurements and recorded by the data logger. The data were stored by the logger until down-loading to a laptop computer via an RS-232 serial data link. The loggers and moisture/temperature sensors were powered by a 12 volt gel cell battery.

The matric potential calculated by the soil moisture sensors was converted to soil volumetric moisture content (ratio of soil moisture volume to soil pore volume) by means of soil water characteristic and retention data compiled for the Poamoho soils by Green et al. (1982) (for depths less than 2 m) and by Miller (1987) (for depths greater than 2 m). These data are shown in Figure 59 (Appendix A) along with smooth power functions that have been fitted through the data sets. Once the volumetric water content (θ_v) was computed for a given tension, the saturation (S) was calculated by the relation:

$$S = \frac{\theta_v}{n}. \tag{4.2}$$

The soil moisture/temperature array was installed as shown in Figures 7 and 8. A single hole was hand-augured to 2.3 m and a sensor was buried at each measurement depth, 0.8 m, 1.3 m and 2.3 m. A power/data cable connected each sensor to the data logging system. Only a single hole was bored for the three sensors to minimize disturbance to the nearby radon monitoring array.

It was discovered after several heavy rainfall events that the moisture readings being delivered by the soil moisture monitoring system were too low. Calibration of the soil moisture system against measurements by porous cup tensiometer was undertaken and is described in the next section (Field and Laboratory Measurements).

5.) Soil Differential Pressure Monitoring

Pressure differences between the atmosphere just above the soil surface and the soil gas within the soil column drive the advective transport of soil gas. Synoptic and diurnal barometric pressure changes, having periods from several hours to several days can change soil gas radon concentrations by as much as 20 percent (Cotter and Thomas, 1989). Wind induced pressure differentials have time constants from seconds to minutes and can change radon concentrations in soil as well, although this mechanism is poorly understood. The observation of these changes in pressure is necessary to understanding the behavior of radon activity and its transport in shallow soil gas.

Monitoring of differential pressures in soil was accomplished by means of highly sensitive differential pressure transducers attached to hollow probes buried at depths of 0.8 m and 2.3 m in the soil (Figure 10). The probes were placed in close proximity to the radon monitoring array (Figures 7 and 8). The hollow probes are copper tubing, 25 mm in diameter by 150 mm long, which reduce to 3.2 mm diameter copper tubing that runs to the surface and is connected to one port of a Setra Systems Model 264 differential pressure transducer. The other port on the transducer is connected to 3.2 mm copper tubing on the surface (Figure 10). The transducer measures pressure differences between soil gas at depth and pressure at the surface every 15 minutes and the reading is recorded by an automatic data logger. The transducers are powered by an 18 volt lead-acid battery.

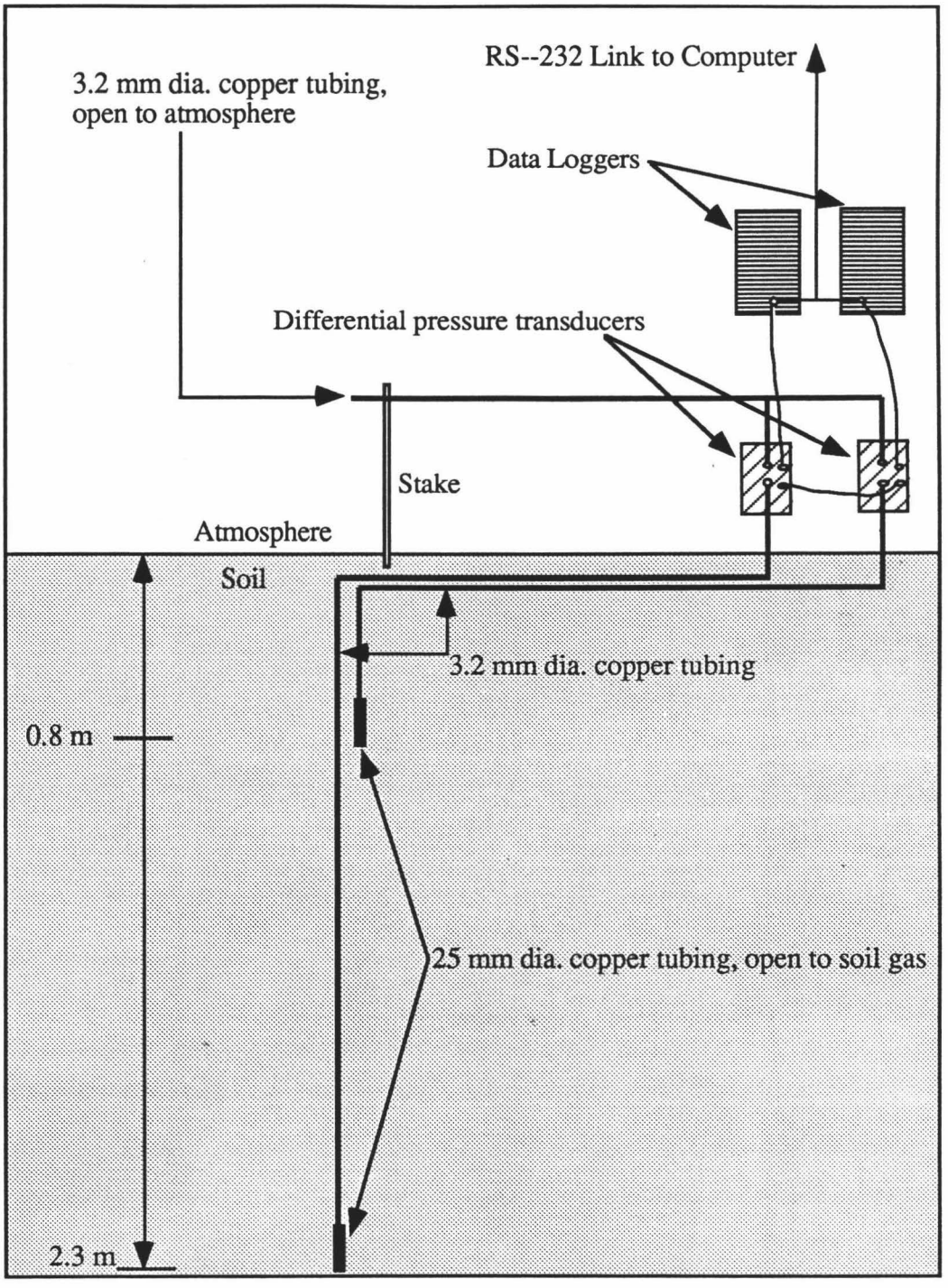

Figure 10. Schematic diagram of differential pressure monitoring system. Shown are the soil probes, surface tube, transducers and data loggers.

B. Field and Laboratory Measurements

As listed in Table 4, soil parameters needed for input into the radon transport model include: soil bulk density, soil porosity, soil air permeability, soil radium content and soil emanation. Techniques used for the measurement of these parameters are described below.

1.) Soil Air Permeability

A portable soil air permeameter was constructed for this project utilizing a design proposed by Reimer (written communication, 1988). The permeameter is schematically illustrated in Figure 11. A measurement is taken by driving a hollow steel probe into the soil to the desired depth (up to 1 m) by means of the slide hammer. The probe is then attached to the permeameter by the flexible rubber tubing. The absolute atmospheric pressure is recorded and the pump is turned on, drawing air from the soil through the pressure and flow transducers. The rate of air flow and accompanying pressure are recorded. By varying the flow rate with the control valve, a range of different flow rates and pressures can be recorded to calculate the best average permeability.

The permeability was then calculated by an equation proposed by Tanner (1988b):

$$k = \frac{4.8 \times 10^{-9} Q_v}{r \Delta P} \qquad (4.3)$$

where k = soil air permeability (m^2)
Q_v = volumetric flow rate (l/min)
ΔP = difference between atmospheric and sample pressure (Pa)
r = radius of influence of air flow in soil (assumed 10 cm).

As air permeability of soil is a function of soil moisture content, gravimetric soil samples were collected to determine moisture content each time permeability measurements were made. Table 8 of Appendix B lists soil air permeabilities measured at the Poamoho site.

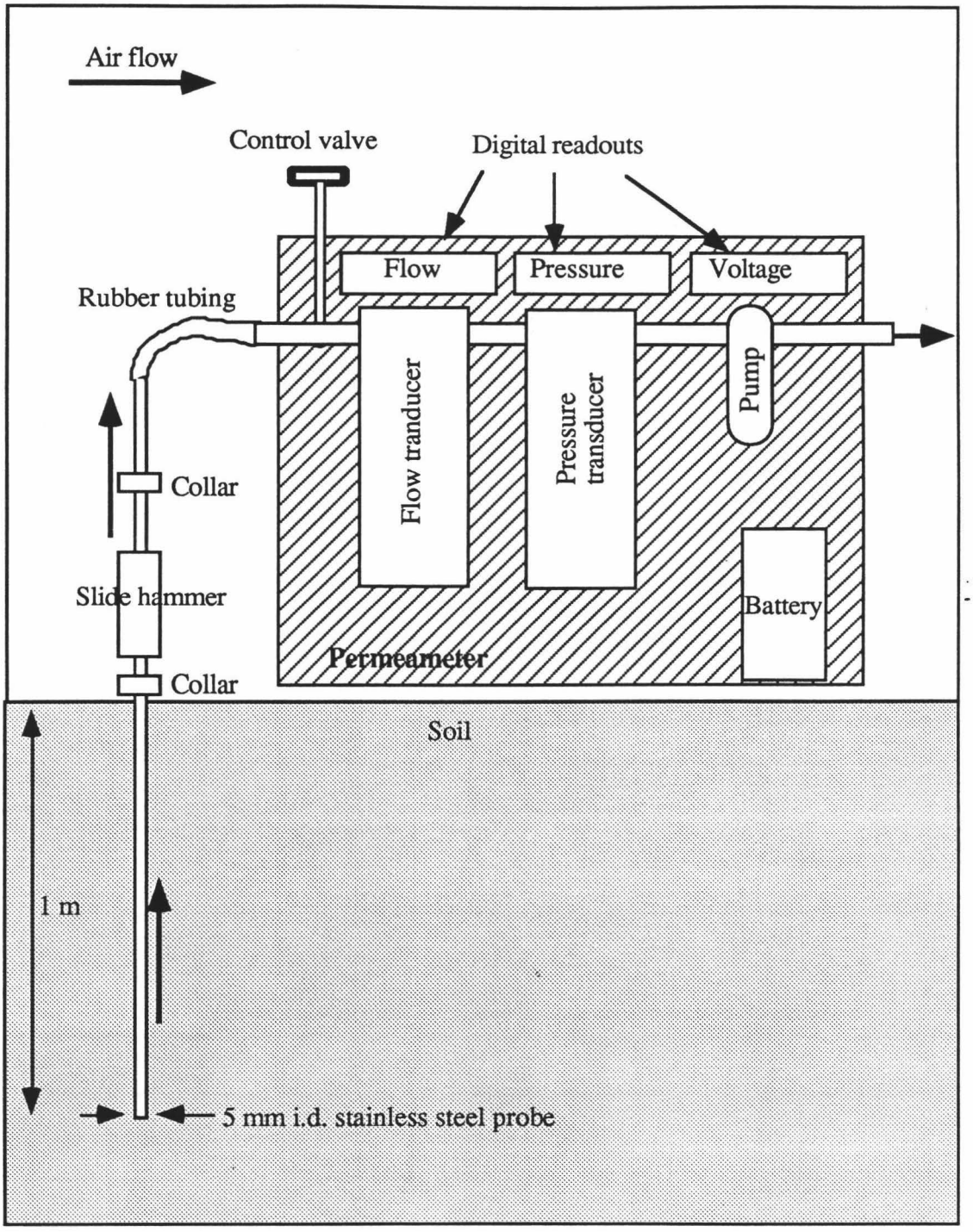

Figure 11. Schematic diagram of measurement apparatus for soil air permeability. Shown are the steel measurement probe, and permeameter with flow and pressure transducers.

2.) Soil Radium Content

Soil samples were collected at depths of 0.8, 1.3 and 2.3 m to determine radium content of the Poamoho soil. This was done by dissolving approximately 1 gram of each soil sample in a 3:1 mixture of hydrofluoric and nitric acid to remove any organic compounds and to completely dissolve the sample. The resulting solution was evaporated to dryness on a hot plate then redissolved in about 50 ml of 2 M hydrochloric acid and sealed in stoppered glass bottles. The radium content of each dissolved soil sample was then determined by allowing the radium and radon in the soil/acid solution to come to secular equilibrium (five ^{222}Rn half lives) and then analyzing the sample for radon content using a radon stripping system (Mathieu, 1977). Assuming that the radon and radium contained in the sample are in secular equilibrium, the amount of radon present in the soil/acid solution will approximately equal the radium content of the soil.

The method of Mathieu (1977), circulates helium gas through the soil/acid solution. The helium acts as a "carrier" for the radon which is stripped from the helium in a liquid nitrogen bath (b.p. 77 K), containing a "trap" which freezes the radon gas (m.p. 202 K) within the trap. Helium is circulated through the solution for about 30 minutes to ensure that at least 95% of the radon is removed from the sample and frozen in the trap. The liquid nitrogen bath is removed and the trap is warmed, returning the radon to a gaseous state. The radon and helium carrier are then swept into an evacuated scintillation cell (Lucas cell). After waiting two hours to allow radon to come to equilibrium with its daughters the alpha activity in the Lucas cell is counted in a photomultiplier tube and the radon content of the sample is calculated.

As a check on the results obtained by this technique, a separate analysis of soil radium content was performed at Pacific Northwest Laboratory using gamma emission analysis. The results obtained by both methods are presented in Table 9 of Appendix B.

3.) Soil Core Analysis

Four soil cores were collected at 0.5 m depth to measure soil bulk density, soil porosity and radon emanation. The procedure involved the insertion of brass cylinders (0.076 m x 0.076 m diameter) into the soil to collect an undisturbed volume of soil.

a.) Soil Emanation

Radon emanation (ratio of radon emitted from soil to total radium present in soil) is a critical parameter in understanding subsurface radon behavior. Commonly, radon emanation is measured from crushed soil samples or slurries (Rogers et al., 1980; Strong and Levins, 1982). For this research, it was decided to attempt to measure emanation from undisturbed soil samples (soil cores) to get a measure of the emanation from the Poamoho soil in an in situ state. This was done by subjecting the four soil cores collected at Poamoho to different levels of saturation and sealing them in airtight containers to trap all emanated radon. Waiting 4 weeks to allow the radon to come to complete equilibrium with its radium parent, the cores were then analyzed for radon content by the method of Mathieu (1977) described earlier in this chapter. Using the radium content calculated for the soil at the same depth (0.5 m) gives the emanation. Figure 60 of Appendix B gives the emanation versus saturation curve for the Poamoho soil.

b.) Bulk Density and Porosity

Once the emanation analysis had been performed on the cores the soil bulk density (ratio of dry soil mass to soil bulk volume) was determined by oven drying the core samples at 110 C for 24 hours and finding the dry soil mass. Once the bulk density (ρ_b) is known the soil porosity (n) can be calculated by the relationship:

$$n = 1 - \frac{\rho_b}{\rho_s} \qquad (4.4)$$

where ρ_s = soil particle density (2.85 g/cc assumed).

Table B.4 of Appendix B gives the values of bulk density and porosity calculated for the four sample cores along with bulk density and porosity data from previous studies (Green et al., 1982; Ikawa et al., 1985).

C. Instrument Calibration

1.) Alphameter Calibration

In order to determine the absolute concentration of radon in soil gas the alpha decay count data supplied by the alpha meters needed to be calibrated against a known radon concentration. The apparatus constructed for this purpose is shown schematically in Figure 12. Air is pumped through the soil sample at field condition and into the gas sample bag to ensure homogenous mixing of the soil gas. The alphameter sealed into the gas sample bag was monitored for 2 weeks to ensure that the radon had reached an equilibrium state within the sample bag. This was determined when the alpha count had reached a constant value. At that point a sample of soil gas was taken through the sample port and analyzed for radon content with the apparatus described earlier. The absolute radon content of soil gas was then compared to the alpha count data to give the counting efficiency of the alphameter. A counting efficiency for each alphameter was determined using counting data supplied by the manufacturer. The calibration constants are listed in Table 11 of Appendix C.

2.) Soil Moisture Probe Calibration

To calibrate the soil moisture array, porous cup tensiometers were installed near both the control and test arrays (Figures 7 and 8). The tensiometers were deployed and

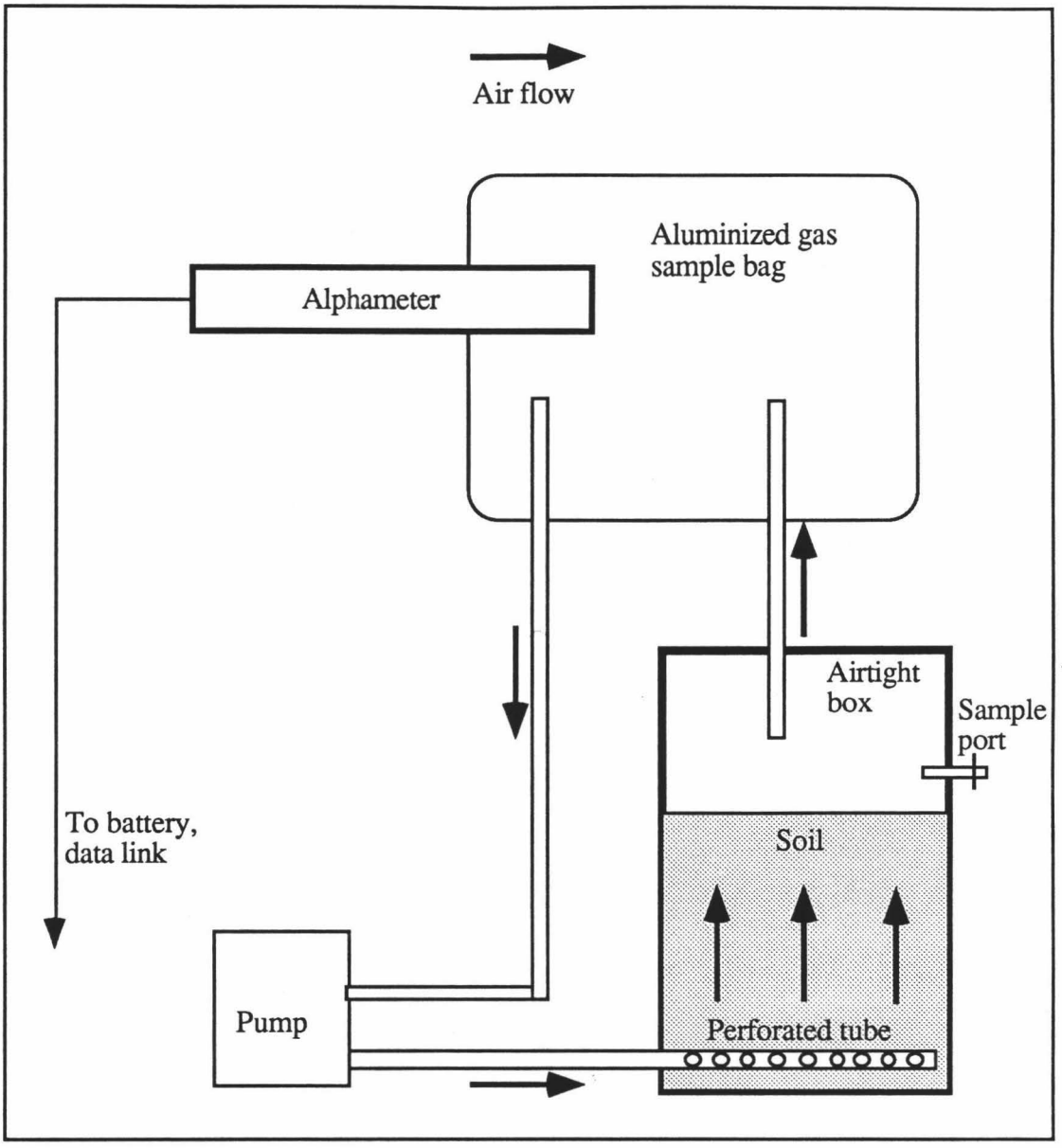

Figure 12. Alphameter calibration system. Shown are soil sample box, circulation system, gas sample bag and alphameter.

maintained as described in Cassel and Klute (1986). The readings taken from the tensiometers were assumed to reflect the true soil water pressure and the soil moisture probe array was adjusted to give readings which agreed with the tensiometers. The calibration equations are listed in Table 12 of Appendix C.

D. Advective Barrier Experiment

After a monitoring period of 7 months, during which it was confirmed that the radon response of the two monitoring arrays was very similar, a horizontal barrier was installed over the north array (Figure 7). The 12 m by 12 m plastic tarp was weighted around the edges and in the center to prevent disturbance by the wind and rain.

The purpose of the barrier is to severely limit the advective mixing of atmospheric air with soil gas while still allowing some diffusional loss of radon through the plastic membrane. By comparing the radon response data from the control array to the data from the experimental array the effects of short term (several hours) to long term (several days) barometric pressure changes on radon activity in soil gas can be identified, as well as the effects of short duration rainfall events. The results of this experiment are discussed in Chapter 5.

CHAPTER 5

RESULTS AND DISCUSSION

The data collected from the radon and environmental monitoring program are presented and discussed in the first part of this chapter. Modeling of the field data is discussed in the second part of this chapter. The primary objective of the radon field study was to identify how soil physical properties interact with environmental factors, such as rainfall, barometric pressure and wind, to enhance or diminish radon movement in the soil under natural and artificially induced conditions. Modeling of the field data provided a more complete understanding of how soil physical properties influence radon behavior.

A. Field Monitoring Results and Analysis

1.) Soil Moisture Effects

The degree to which the open pore space in the soil is filled with water has a profound influence on radon release and soil gas transport within and from the soil. As discussed in Chapter 2, soil moisture content influences the emanation of radon from the soil matrix, as well as soil permeability and soil diffusive capabilities. The effect of increasing and decreasing soil moisture contents on radon activities in soil gas is discussed below.

a.) Initial Alphameter Deployment

In July, 1988 the first alphameter was installed at the Poamoho site at a depth of about 1.5 m as described in Chapter 4 and illustrated in Figure 9a. Radon activity data obtained from this instrument for a 10 day period are presented in Figure 13. The radon data are plotted as alpha particle counts integrated over 15 minute counting intervals and as a 4 point (hourly) moving average. Field calibration of the alphameter indicated that 1

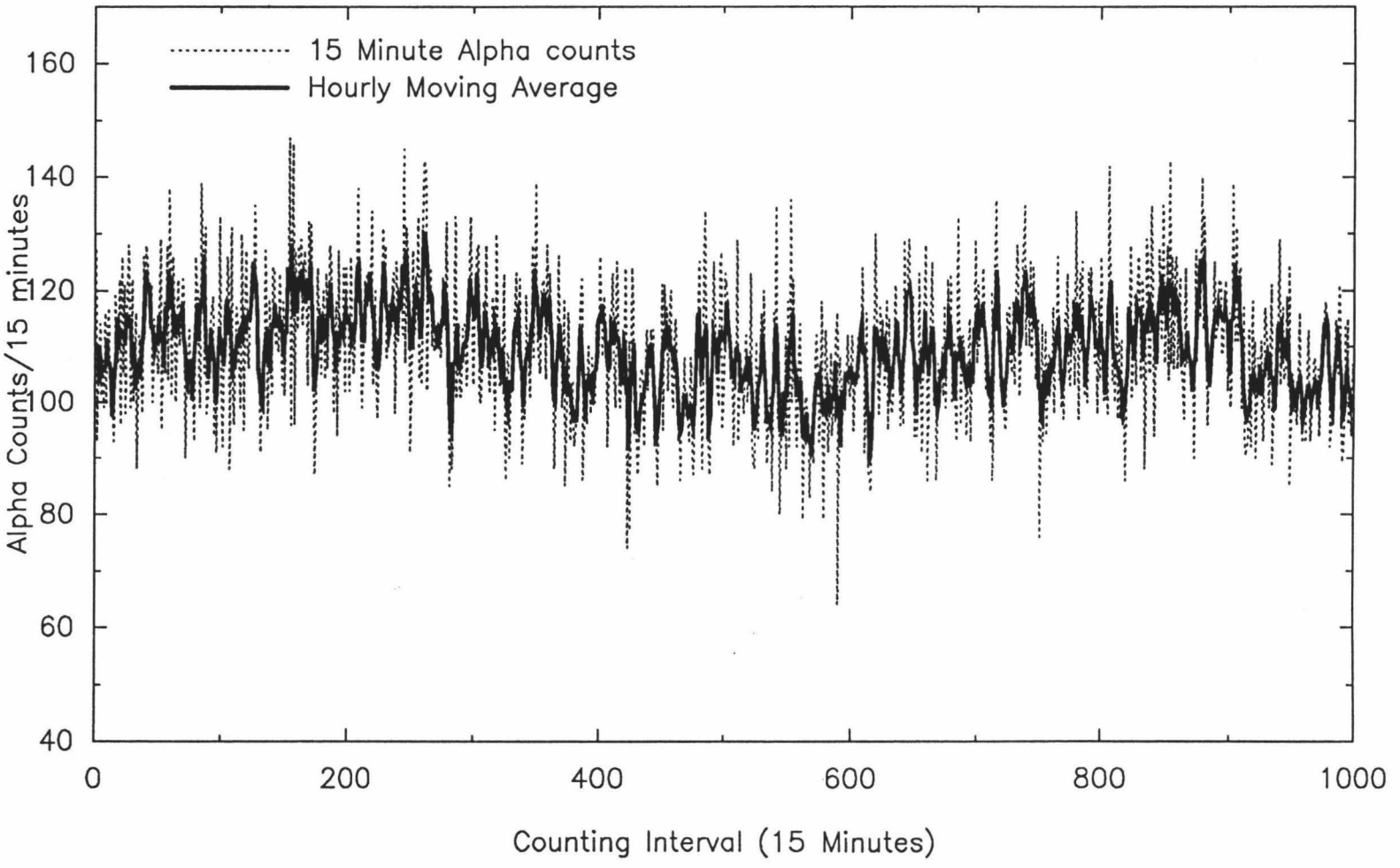

Figure 13. Radon activity time series from the initial alphameter. The data are 15 minute integrated alpha counts and an hourly moving average plotted for a 10 day period. One day is equivalent to about 100 counting intervals.

count per minute (CPM) was equal to a radon concentration in soil gas of approximately 3.5 Bq/l.

The radon data in Figure 13 show three important features: 1) in the 15 minute alpha count data there are very high frequency variations in alpha activity, from one 15 minute counting interval to the next, of about 25% of the mean count rate; 2) in the 15 minute data and the hourly data there are longer term variations in alpha activity having a magnitude of about 10% of the mean count rate and having periods on the order of several hours; and 3) a very long term variation in alpha activity apparent in both plots having a magnitude of about 5% of the mean and a period of about 5 days.

There are two explanations for the observed variations in radon activity. The first is the statistical error inherent in the counting of the alpha particles. Because radon decay is a random process, the standard deviation associated with each counting interval will approximately equal the square root of the integrated number of counts in each interval (Friedlander et al., 1964). However, this random error cannot account for the longer term (hours to days) variations seen in the radon data in Figure 13 because, as the number of counts increases, the percentage of the total count attributable to random error decreases substantially. In Figure 13 the average alpha count per 15 minute interval is about 110. Hence, the standard deviation of the unsmoothed data are about 10% of the mean of the 15 minute count ($(110)^{1/2}/110=0.10$), but only about 5% of the mean of the 1 hour count ($(440)^{1/2}/440=0.05$). Integrating the radon count data over longer intervals and smoothing by means of moving averages will tend to reduce the high frequency variation caused by random and semi-random processes such as counting error and wind driven pressure fluctuations (discussed in part 2, section d of this chapter), while bringing out the longer term systematic and environmentally induced variations in the radon response. Unless otherwise noted, further plots of radon activity data will be smoothed over at least 4 counting intervals (1 hour) to reduce random variation in the data.

The source of the longer term (hours to days) variation in radon activity in Figure 13 is the pressure-driven exchange of radon-poor atmospheric air with radon-rich soil gas. Figure 14 shows smoothed radon activity data obtained from the initial alphameter and hourly barometric pressure observations. The barometric pressure data contain semi-diurnal and synoptic variations characteristic of sub-tropical latitudes (reference given in part 2, section c of this chapter). It is apparent from Figure 14 that increasing barometric pressure correlates with lowered radon activities and decreasing barometric pressure correlates with increased radon activities. This is due to a combination of mechanisms: 1) advective mixing of radon-rich soil gas with radon-poor atmospheric air in the shallow soil; and 2) the advective and diffusive movement of radon within the soil profile in response to changing pressure and concentration gradients in the shallow soil.

Under conditions of increasing atmospheric pressure a certain amount of radon-poor atmospheric air is forced into the shallow soil. This, to a certain extent, lowers the amount of radon contained within the sample volume detected by the alphameter as well as displacing the existing radon-rich soil gas to a greater depth in the soil profile, causing an apparent drop in shallow soil radon concentration. As atmospheric pressure decreases, the reverse occurs: advective radon flux at the soil/air interface is enhanced due to increasing gas pressure gradients and high radon concentration soil gas from deeper levels moves up through the soil profile by advection as well as diffusion in response to the increased concentration gradient, causing an apparent increase in shallow soil radon concentration.

These particular data (Figure 14) suggest that the rate of exchange of soil gas with atmospheric air is fairly high, even though the magnitude of barometric pressure changes is quite small: the semi-diurnal pressure changes are normally of a magnitude of about 1 to 3 millibars and the synoptic pressure changes rarely exceed 5 millibars. However there is evidence that the method in which the initial alphameter was installed (Figure 9a) may have induced enhanced exchange of atmospheric air within the vicinity of the alphameter probe.

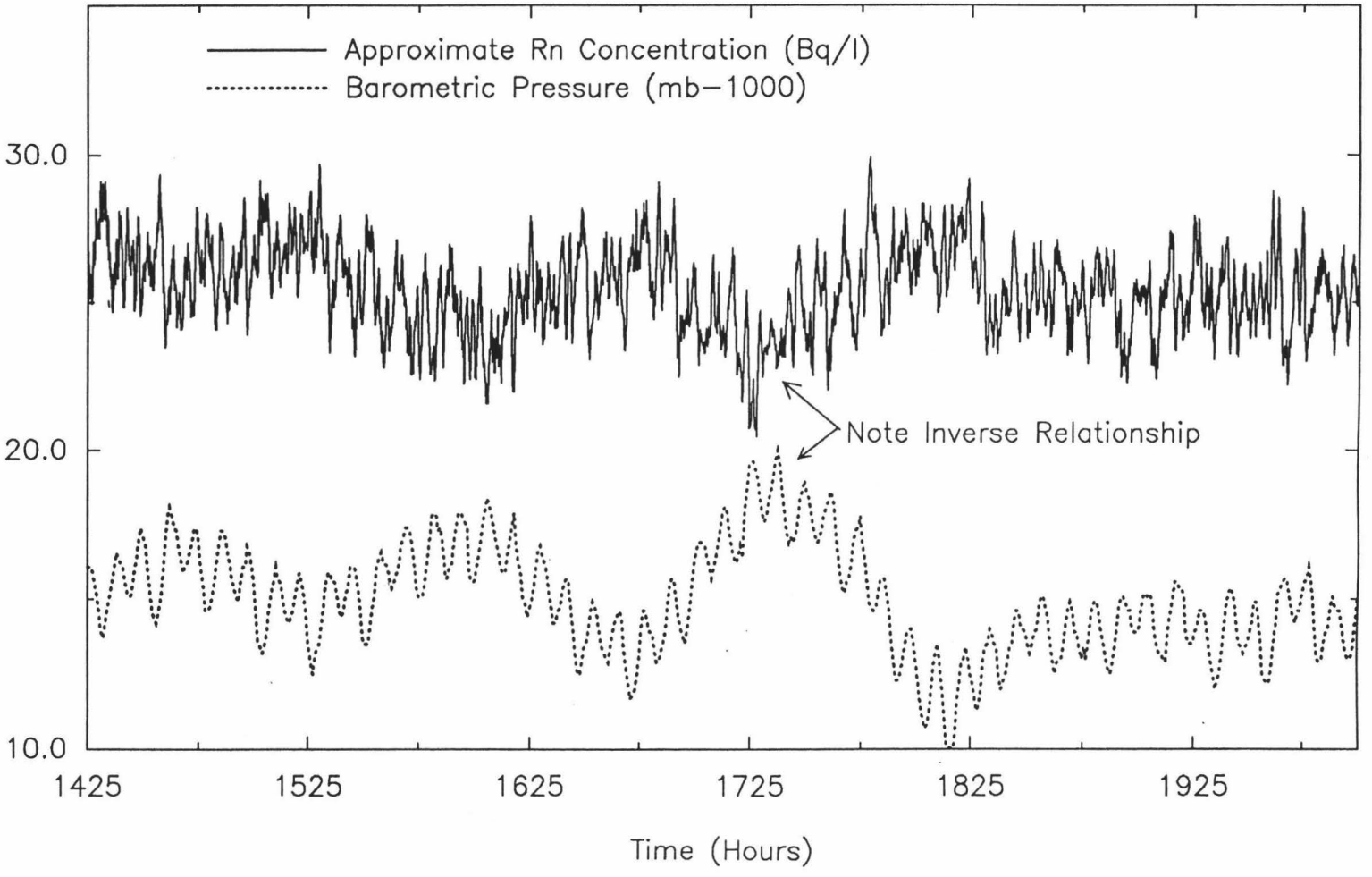

Figure 14. Radon and barometric pressure data time series. Radon data show an inverse relationship to atmospheric pressure changes.

The biggest perturbation in the radon data from the initial alphameter is the approximately 30% increase accompanying the large rainfall event at about hour 950 shown in Figure 15. There are three mechanisms related to increased soil moisture which could account for the large increase in radon concentration: 1) Increased radon emanation due to the increase in soil moisture. This is probably not a factor because the degree of soil saturation is always greater than 20% (discussed below), and as Figure 60 (Appendix B) shows, radon emanation in the Poamoho soil actually decreases as soil saturation goes above 20%. 2) Displacement of radon into a smaller gas volume due to near saturation of the soil and the low partitioning coefficient of radon into liquid water (Rn(l)/Rn(g)~0.25), thereby increasing its apparent concentration. 3) Increased saturation of the interconnected pore volume in the shallow soil reduces the advective and diffusive loss of soil gas radon to the atmosphere leading to a rise in radon concentration.

Although partitioning effects cannot be completely ruled out, subsequent examination of the data from the full radon monitoring array (discussed in the next section) suggests that the latter mechanism (3) is most likely to account for the observed radon activity increase in Figure 15. It would be expected then, given the decreased soil air permeability following an increase in soil saturation, that there would be a corresponding decrease in the magnitude of radon activity variations due to changes in atmospheric pressure variations. But a close look at the radon activity data following the rainfall event (hours 950 to 1820 in Figure 15) shows that the magnitude of the pressure-driven radon variations has actually increased over the amplitude of variations seen before the rainfall event.

The interpretation of this apparent anomaly in the radon response to decreased soil air permeability is that the installation of the radon monitoring probe has disturbed the normal radon response to barometric pressure changes at higher degrees of soil saturation. Although the "well" containing the radon monitoring probe has been back-filled at the top

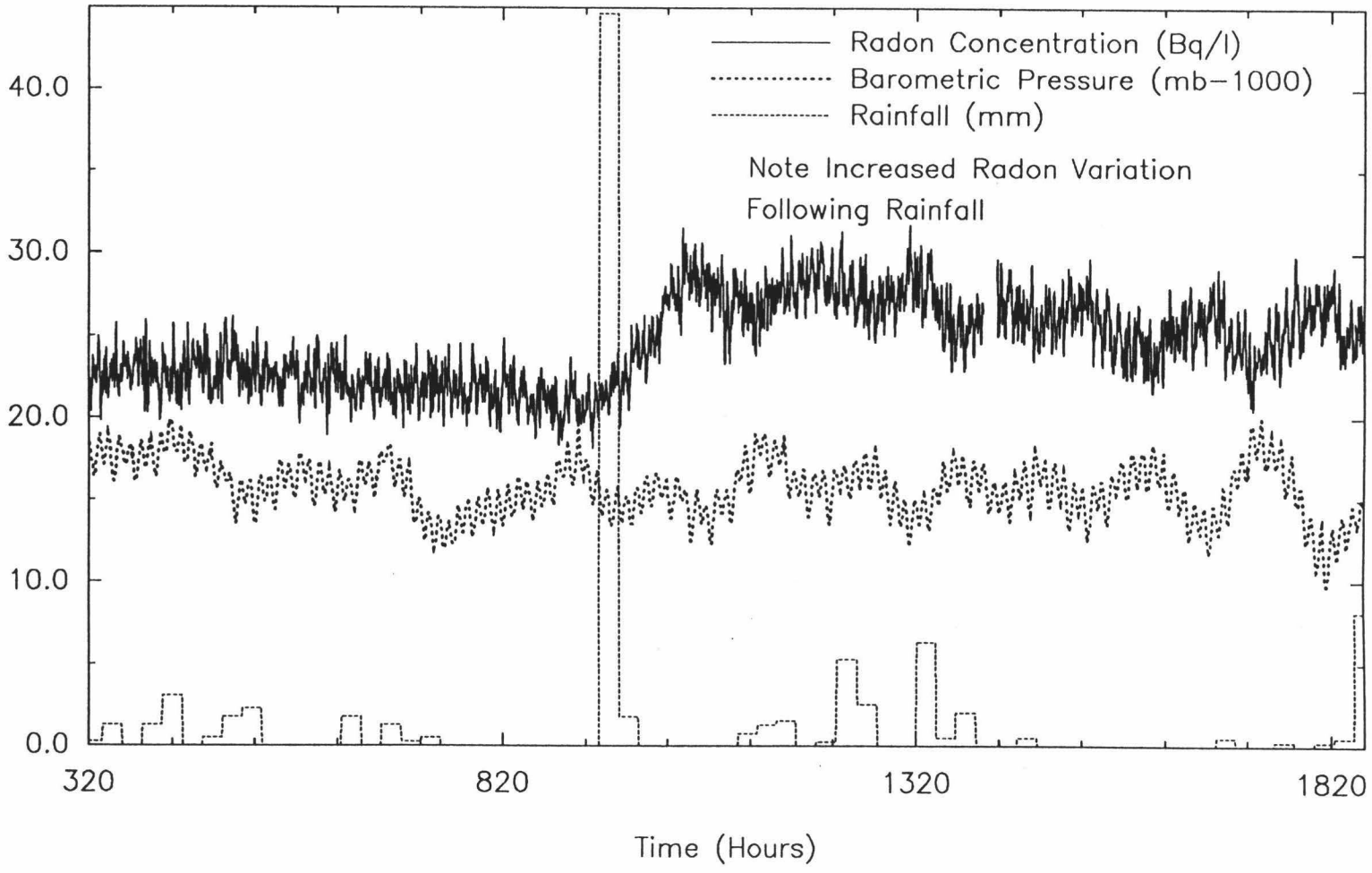

Figure 15. Radon and meteorologic data time series. Radon data are from initial alphameter and show increased response to atmospheric pressure changes following rainfall event at hour 930.

(Figure 9a), it has apparently provided a channel of substantially higher permeability than the surrounding soil. Under dry conditions the permeability contrast between the probe well and the surrounding soil is relatively low. At higher soil saturation following the rainfall event, the probe well would likely have a higher permeability than the surrounding soil, thus becoming a conduit for enhanced exchange of soil gas/atmospheric air driven by diurnal and synoptic pressure changes.

This suggested mechanism is significant in that it illustrates that permeability discontinuities and/or channels in the soil resulting from manmade disturbances or natural structuring of soils might have a profound effect on radon activity within the soil. The rate of exchange of soil gas with atmospheric air and the depth to which atmospheric pressure changes can be transmitted through the soil column are indicated to be highly dependent on preferential flow within the soil column, especially at higher soil moisture contents. A second important result of the initial alphameter study is that the deployment protocol of the monitoring instruments themselves can have a substantial impact on the character of the data, and care must be taken to ensure that spurious results are not inadvertently introduced by the monitoring instruments themselves. As a result of these findings, all subsequent alphameters were installed according to the protocol shown in Figure 9b. Although it is impossible to eliminate effects of the access hole on the radon response, the intent with the new deployment configuration was to minimize the effect of experimentally induced soil channelling. Analysis of radon data obtained from the new installation scheme to pressure-driven variations (section 2, part c, this chapter) indicates that the new deployment effort was successful in minimizing artificially induced channelling.

b.) General Soil Moisture Effects

The complete radon monitoring array was installed in March, 1989 as shown in Figures 7 and 8, by the method illustrated in Figure 9b. With the full radon monitoring array in place, data were collected showing how radon activity varies with depth in the soil column and how radon in soil gas at different depths responds to meterological perturbations. Figures 16 and 17 show the time series of radon at the three depths for the north and south monitoring arrays for the time period from installation in March 1989 to December 1989 along with barometric pressure changes and rainfall at the site for the same time period.

As can be seen by comparing the radon monitoring data in Figures 16 and 17, the radon response at the north and south arrays is quite similar. Once a similar radon response for the two arrays had been established, the advective barrier over the north array was installed (hour 5500, Figure 16). Results and observations of the advective barrier experiment are discussed later in this chapter (section 3).

The three most striking features in Figures 16 and 17 are: 1) the strong dependence of the radon concentrations on depth; 2) the sudden, large increases in shallow soil (1.3 m or less) radon concentrations following the rainfall events at hours 3500, 5000, 6000 and 6700; and 3) the gradual decline in radon concentrations in the periods between the rainfall events. The radon concentration gradient-depth relationship is examined in section 2 (part a), of this chapter; the soil moisture effects are addressed below. The soil moisture monitoring array was installed, as shown in Figure 8, on June 1, 1989. Data obtained from the soil moisture probes were calibrated against porous cup tensiometers. Figures 18, 19 and 20 show the radon activities, rainfall and percent soil saturation for 0.8 m, 1.3 m and 2.3 m depths, respectively, from June to December, 1989.

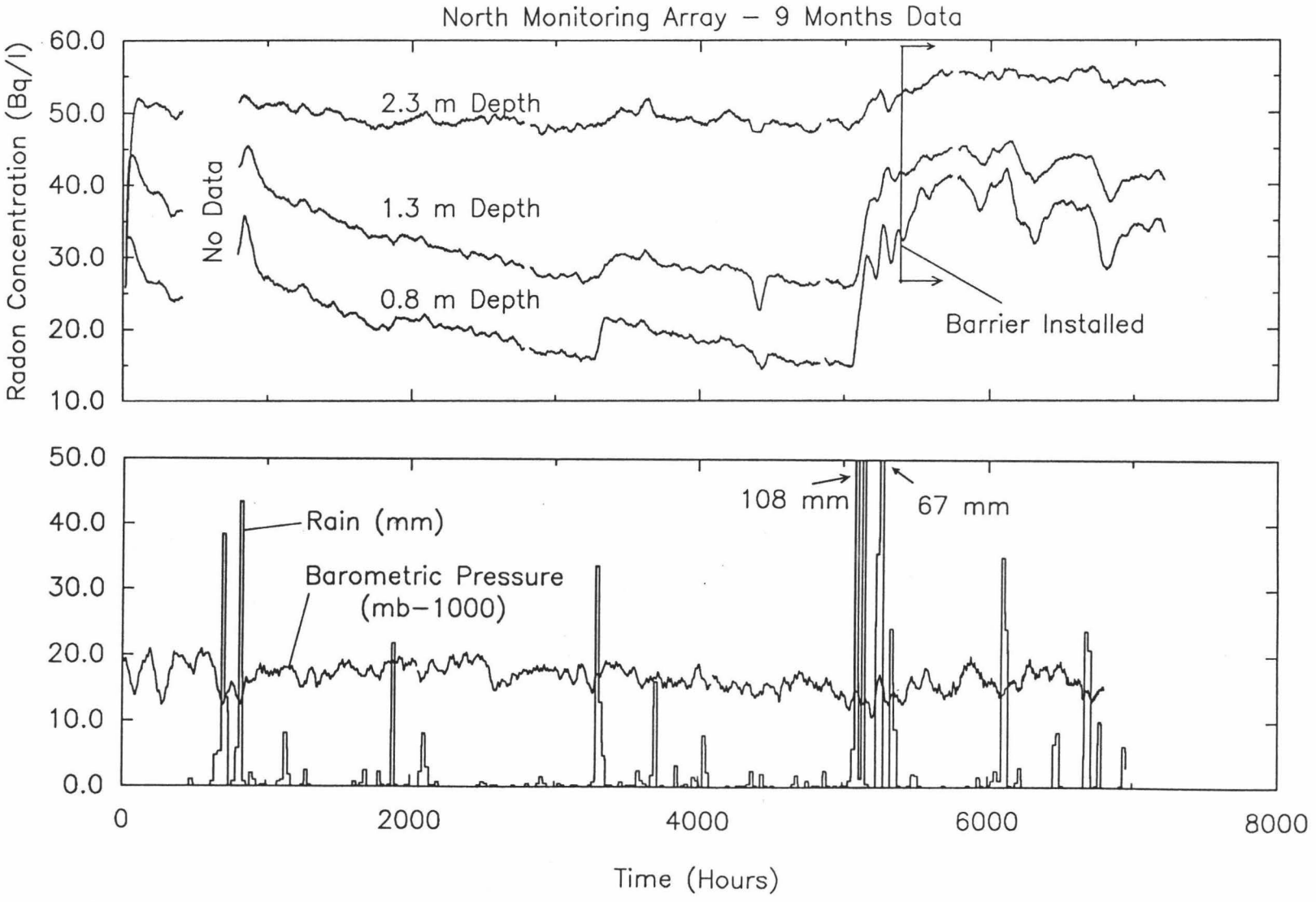

Figure 16. Radon and meteorologic time series for 9 month period. Radon data from north monitoring array.

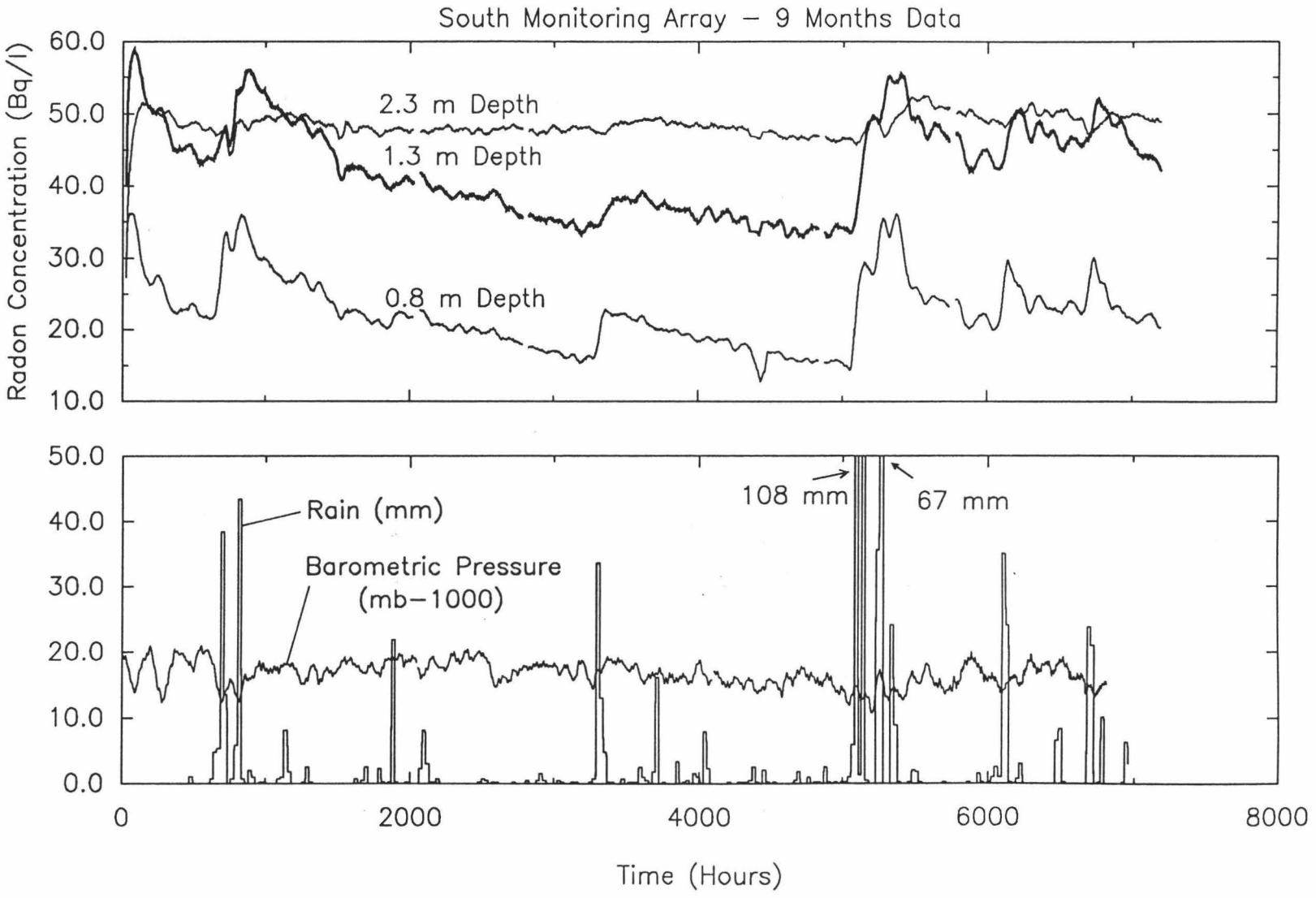

Figure 17. Radon and meteorologic time series for 9 month period. Radon data from south monitoring array.

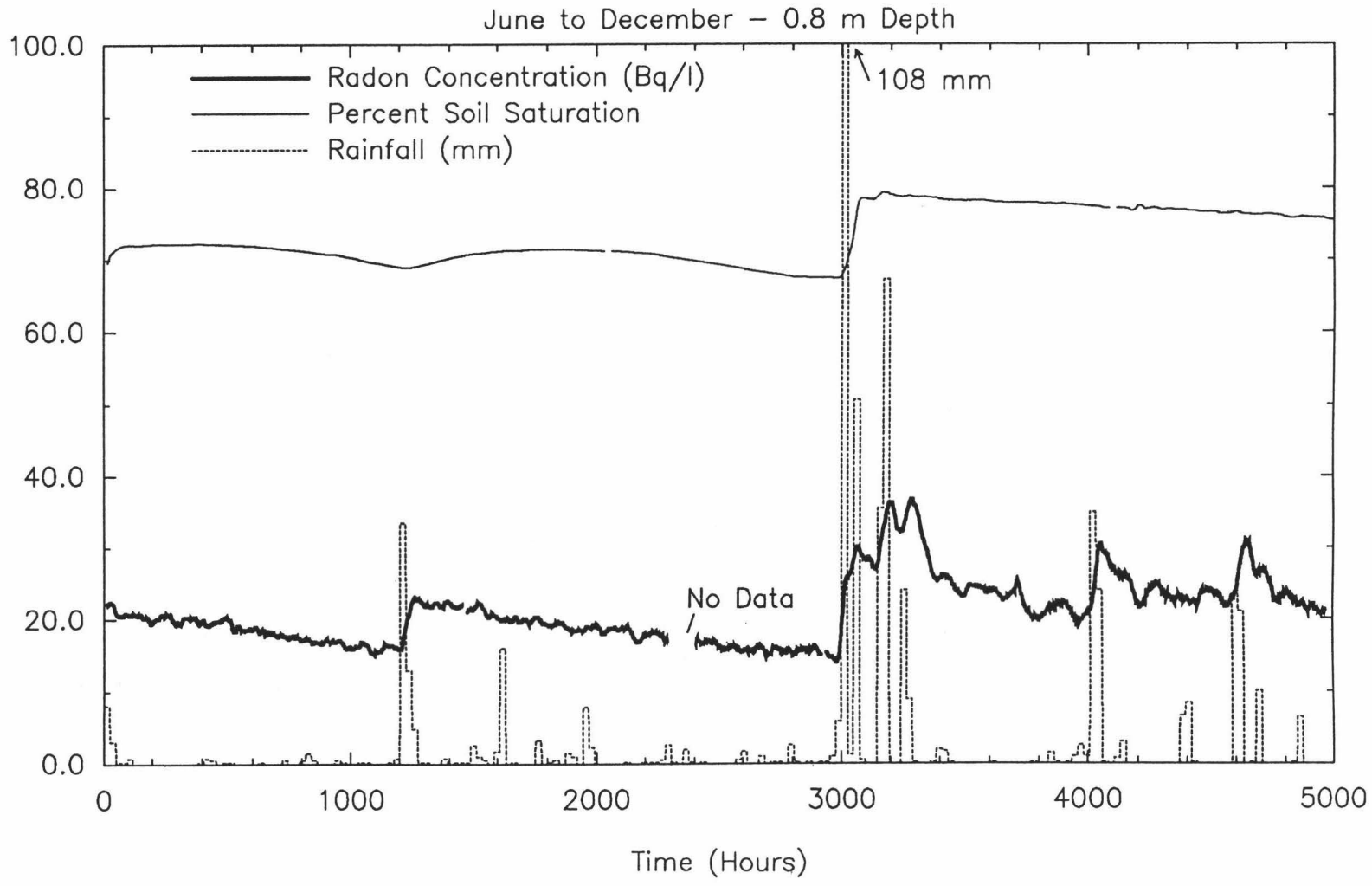

Figure 18. Radon, rainfall and soil saturation time series for June to December, 1989 at 0.8 m depth.

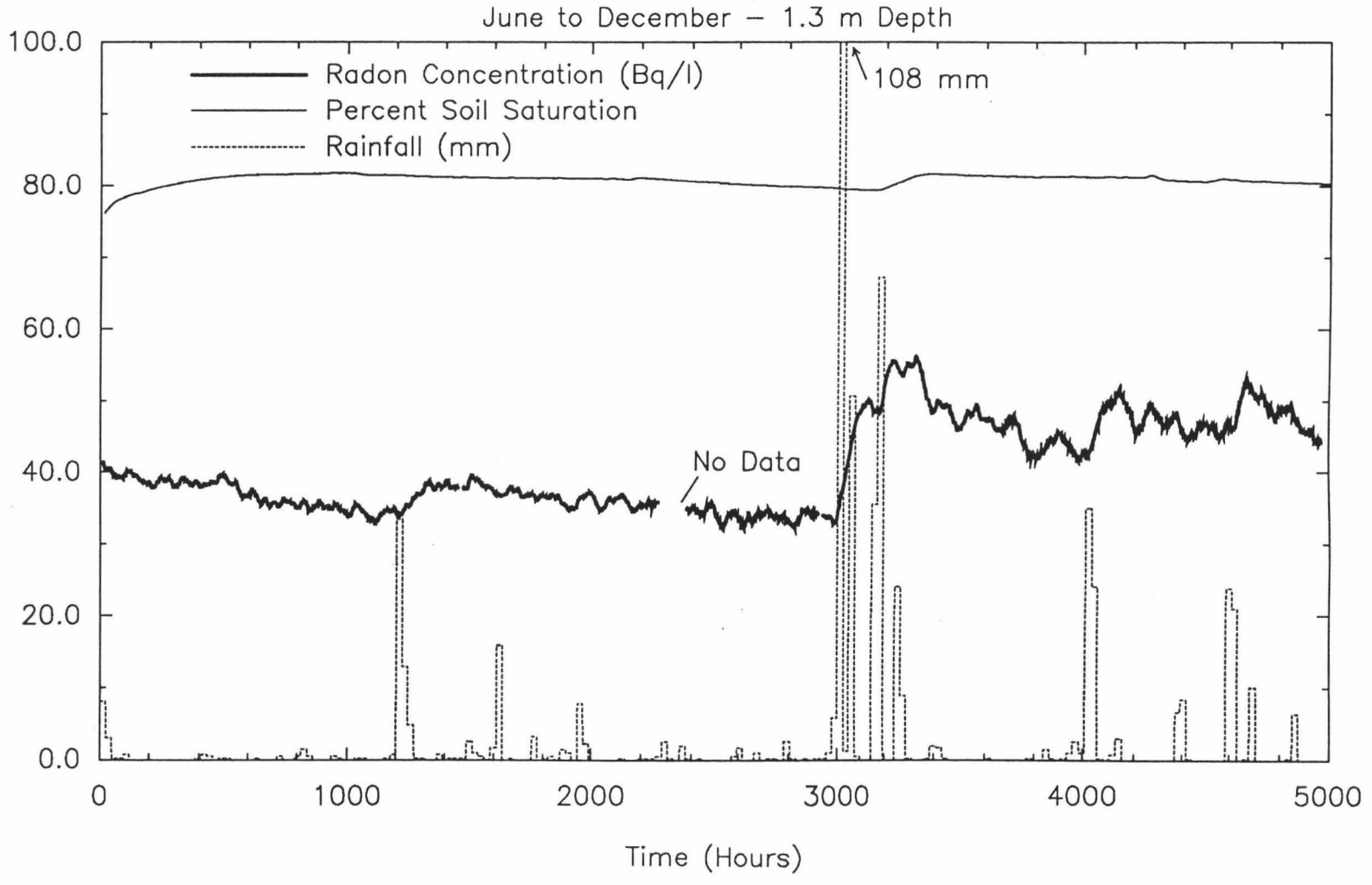

Figure 19. Radon, rainfall and soil saturation time series for June to December, 1989 at 1.3 m depth.

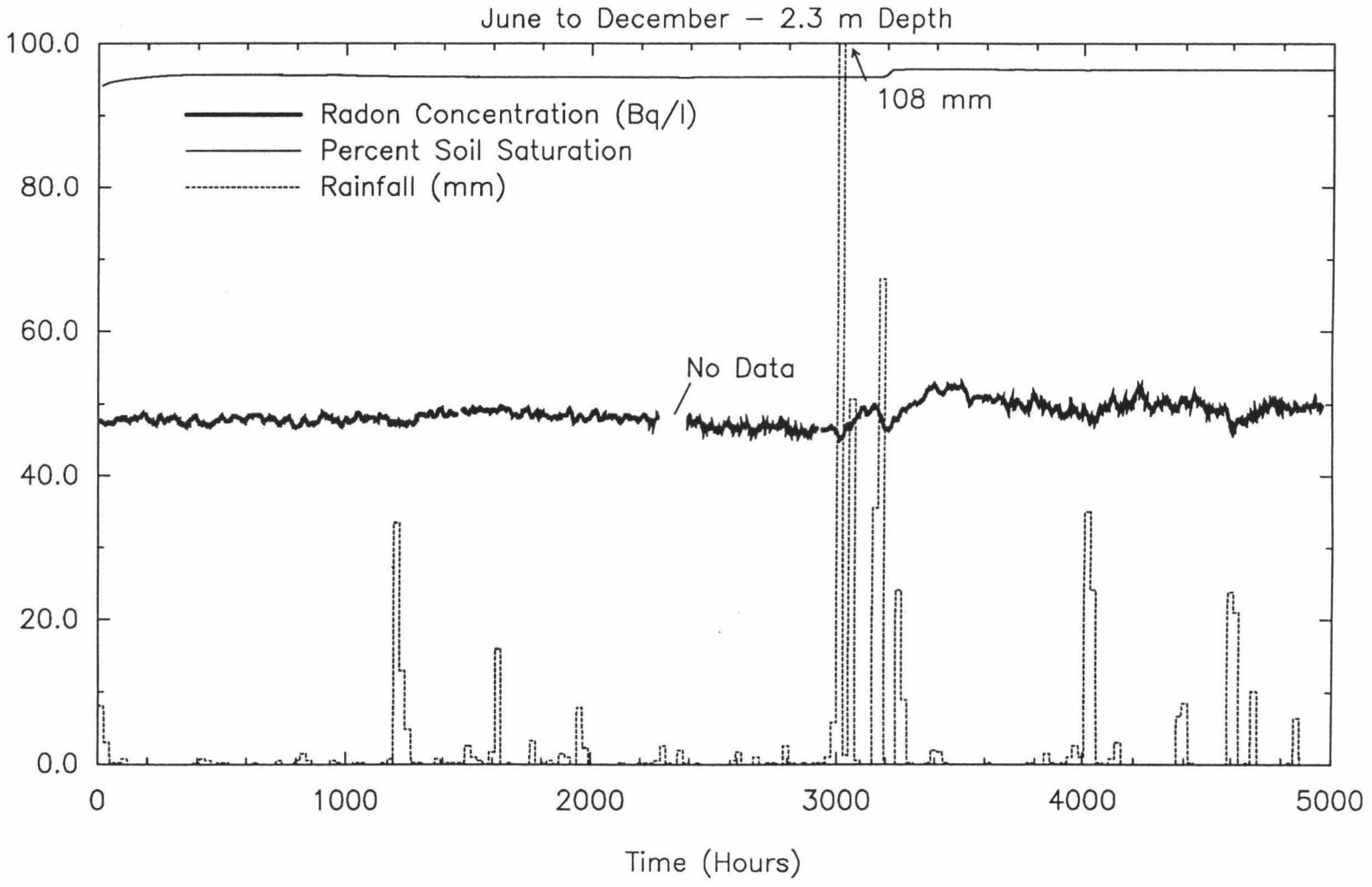

Figure 20. Radon, rainfall and soil saturation time series for June to December, 1989 at 2.3 m depth.

The information presented in Figures 18, 19 and 20 show that radon concentrations in soil gas are intimately tied to soil moisture contents and the occurrence, or absence, of rainfall events. The large increases in radon concentrations in the 0.8 m and 1.3 m probes are the most significant fluctuations present in the data. The soil saturation values in Figures 18 and 19 indicate that soil moisture contents decline slightly during the periods between rainfall events (hours 0 to 1000 and hours 1200 to 3000) and rise slightly subsequent to the rainfall. The soil saturation at a depth of 2.3 m (Figure 20) remains essentially constant at about 95 percent throughout the monitoring period. The apparent lag of soil moisture response behind radon response to the 1200 and 3000 hour rainfalls in Figure 19 is discussed below.

The gradual decline of soil saturations seen before and after the rainfall event at hour 1200 in Figure 18 and 19 are mirrored in the decline of the shallow soil gas radon concentrations. This reflects the drying of the surface soil (down to 1.3 m) and the accompanying elevation of soil air permeability and diffusion coefficient as well as the formation of surface cracks which enhance soil ventilation. This allows increased diffusional loss of radon as well as the enhanced advective exchange of atmospheric air with soil gas, resulting in a decrease of the soil gas radon content. The soil gas radon concentrations at 2.3 m (Figure 20) show no clearly discernible decline during the dry periods, duplicating the constancy of the soil moisture levels at that depth.

c.) Moderate Rainfall Effects

Figure 21 shows a more detailed view of the effect of the moderate (~55 mm) rainfall event at hour 1200 on soil moisture and radon concentrations at the three depths. At 0.8 m depth the soil saturation increases only slightly, from 70 to 74% over a period of about a week while radon levels at the same depth undergo a 25 percent increase immediately. At 1.3 m depth, soil saturation shows no discernible increase while radon

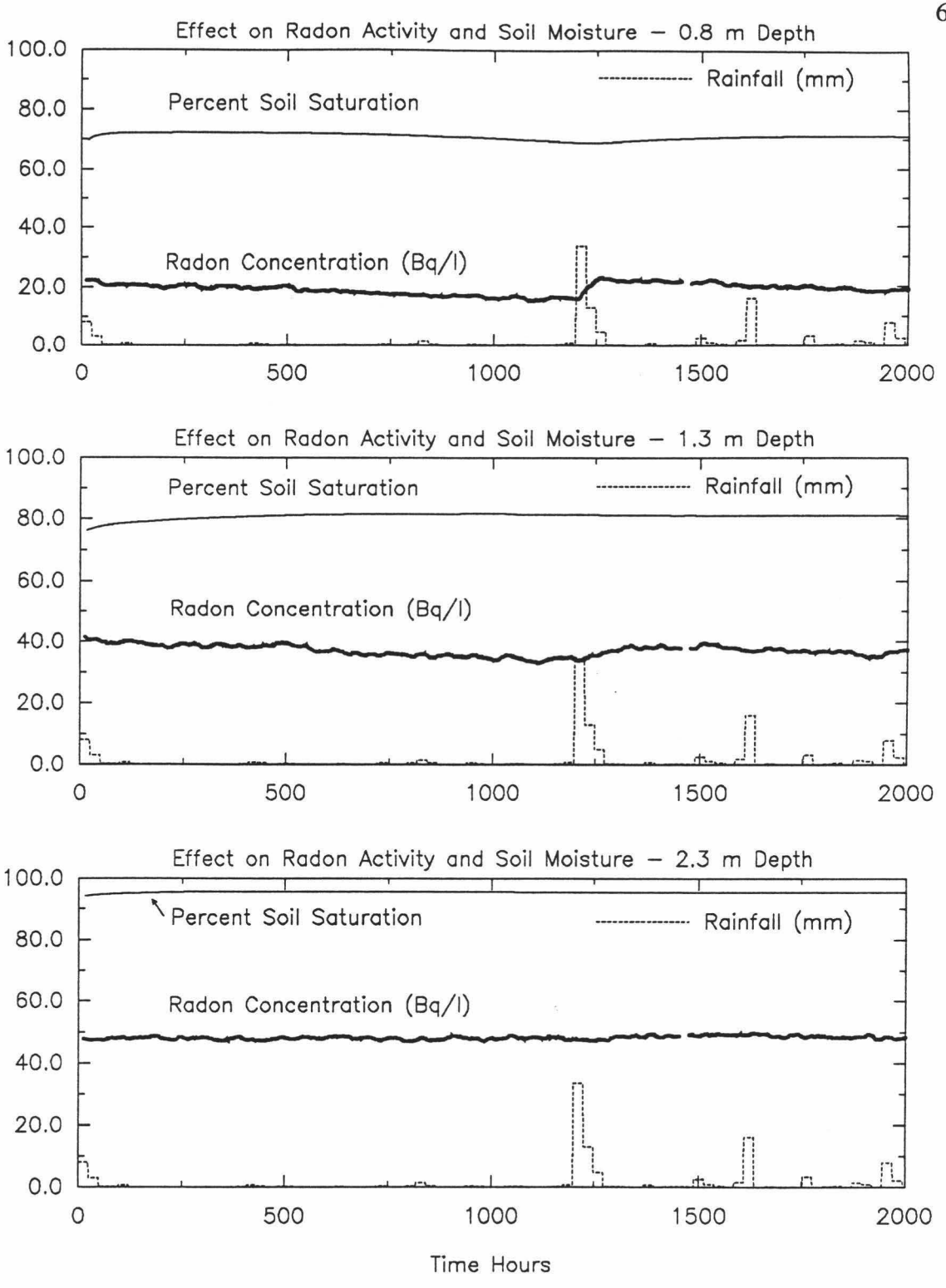

Figure 21. Radon and soil saturation response at the three monitored depths to a moderate rainfall event at hour 1200.

concentrations rise approximately 10 percent over about a weeks time. The saturation and radon concentration at 2.3 m depth show no apparent effect from the moderate rainfall event.

From a qualitative standpoint, it seems clear that raising the saturation of the soil causes: 1) partitioning of existing radon into a smaller gas volume; and 2) blockage of the continuous pore spaces which permit the exchange of atmospheric air and soil gas. Hence, the alphameters will detect a higher radon concentration and the soil is not as well ventilated so the radon accumulates to higher levels. In addition, the lower diffusion coefficient of water relative to air (Table 2) means that less soil gas radon will be lost to due to diffusion. The effect of the moderate rainfall event on soil moisture content and radon concentration appears to be attenuated with depth, having little effect on the deep radon concentration.

The radon response to the moderate rainfall event at 1.3 m is interesting as the soil saturation at 1.3 m shows no appreciable change, yet radon levels rise about 10%. This suggests that blockage of the shallow soil advective and diffusive pathways by soil water is very effective in raising radon concentrations. The wetting front from this rainfall apparently did not reach 1.3 m yet radon levels at that depth rose in response to increased soil water in the shallower layers indicating that a shallow soil "capping" effect can occur with even moderate rainfall.

d.) Intense Rainfall Effects

The effect of an extended period of heavy rain is shown in Figure 22. At hour 3000, approximately 170 mm of rain fell over a 4 day period, followed three days later by ~110 mm of rain, and followed two days later by ~60 mm of rain. As illustrated in Figure 22, soil moisture contents at 0.8 m experienced an increase from 67 to 77% saturation while radon concentrations at that depth showed a 120 percent increase over the duration of the rainy period. At 1.3 m the soil saturation increased only 5 percent but radon

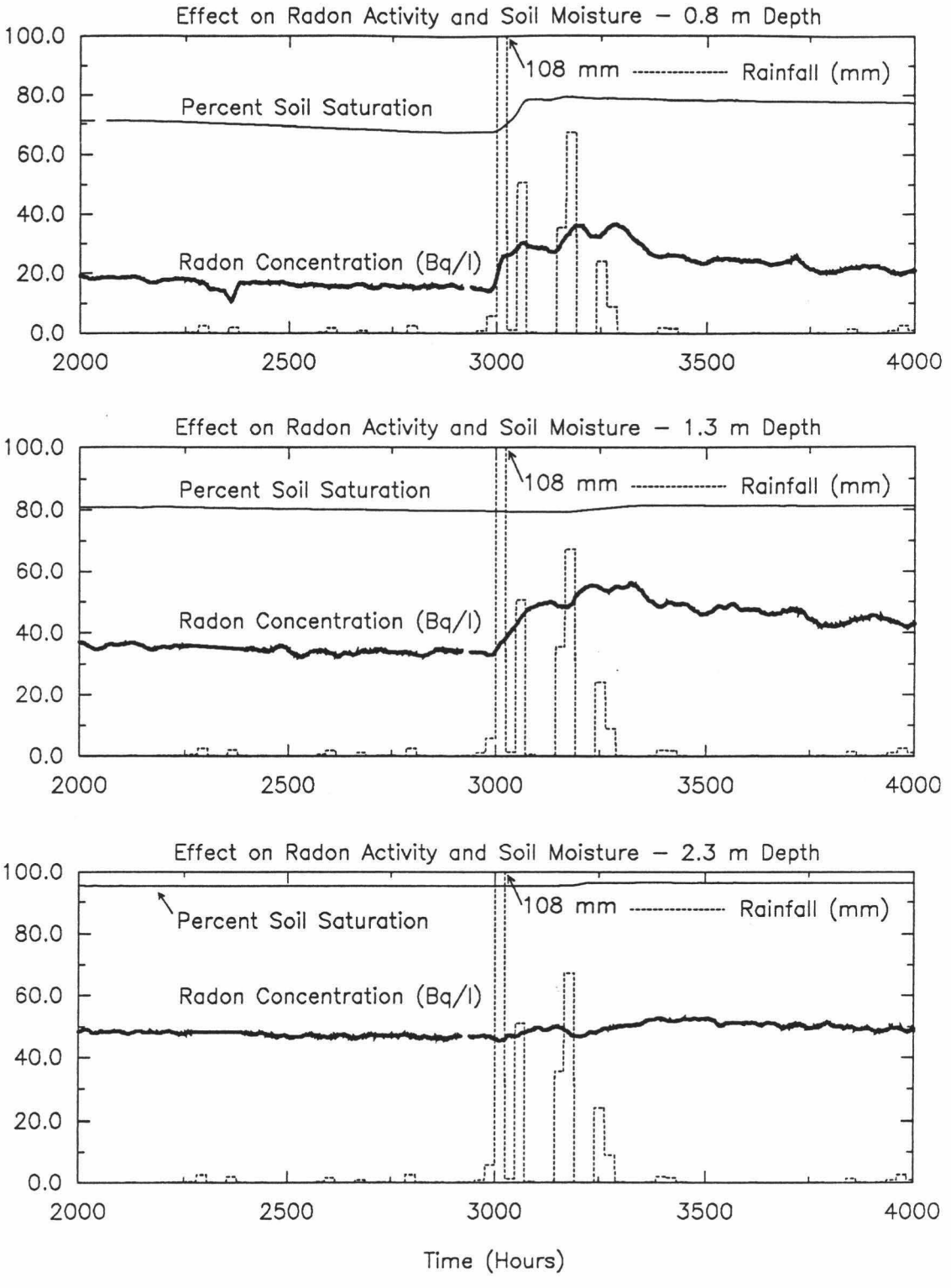

Figure 22. Radon and soil saturation response at the three monitored depths to an intense rainfall event beginning at hour 3000.

concentrations increased about 90 percent. Even at 2.3 m the soil moisture increased slightly and radon concentrations rose about 15 percent.

There are two interesting characteristics of the radon response to the heavy rainfall event shown in Figure 22. The first is the nearly instantaneous reaction of the radon at 0.8 m to each rainfall episode compared to the slightly delayed reaction of the radon at 1.3 m and the much attenuated, further delayed radon reaction at 2.3 m. The rapid rise and fall of radon concentrations at 0.8 and 1.3 m after each rainfall event suggest that preferential flow of water quickly fills the shallow soil, cutting off advective mixing of soil gas with atmospheric air and decreasing diffusional radon loss, thus causing the rapid rise in radon concentrations at 0.8 and 1.3 m seen in Figure 22. When the rain stops, the structured soil quickly drains, allowing shallow soil ventilation and diffusion to resume with the resultant rapid recovery of normal radon activities in a well-drained soil. Miyahira (1990) found, in a study of solute transport at the same location, that preferential flow caused increased and unpredictable mobility of solutes through the unsaturated zone.

The second interesting feature in Figure 22 is the substantial increase in radon concentrations at 1.3 m and 2.3 m corresponding to the very small, and significantly delayed, increase in soil saturation at those depths. This suggests that blockage of shallow soil advective and diffusive pathways for radon loss is more effective than partitioning effects in raising radon concentrations. In fact, radon levels at 1.3 and 2.3 m start to increase prior to the arrival of the wetting front (Figure 22) at those levels, indicating that "capping" of the shallow layers by increased soil moisture has influenced deeper radon activities. In addition, radon concentrations at 0.8 m depth, where advective and diffusive loss of radon would be the greatest, shows the largest increase, whereas radon activities at deeper depths, where smaller pore volumes would be quickly saturated by increasing soil moisture, shows the smallest radon activity increase (Figure 22).

The results of the initial alphameter deployment and the effect of increases in moisture content on radon activities in shallow soil gas clearly suggest that soil structuring and preferential flow are significant factors in the movement and behavior of radon in soil gas. The importance of soil cracks, flow channels and permeability discontinuities are magnified when the soils are highly saturated and the permeability contrast between the bulk soil and the open channels is most pronounced.

2.) Advective Mixing and Pressure Effects

Synoptic pressure changes due to passing weather systems and diurnal cycles in barometric pressure have been reported to have a profound effect both on radon activities and radon flux within and from the soil (Kovach, 1945, 1946; Clements and Wilkening, 1974; Fukui, 1987; Guedalia et al, 1970; Holford et al, 1988, 1989; Thomas and Cotter, 1988, 1989). One of the most important questions addressed by this thesis is whether changes in atmospheric pressure affect the movement of soil gas within and from the soil, as well as whether the presence of natural or artificial channels in the soil can provide conduits which enhance pressure driven flow and exchange of soil gases.

a.) Concentration Gradient

As mentioned in the previous section, one of the most obvious features in Figures 16 and 17 is the strong dependence of radon concentration in soil gas on depth in the soil. Figure 23 shows the average concentration profile for the same nine month period. This gradient reflects diffusional loss of radon from the soil along with advective exchange of soil gas with the atmosphere and dilution of radon concentrations at depths less than 2 m. Average concentration gradients calculated from the data in Figure 23 are 30 Bq l^{-1} m^{-1} to a depth of 1.3 m and 10 Bq l^{-1} m^{-1} from 1.3 m to 2.3 m depth.

The high concentration gradient from the soil surface to 1.3 m indicates that this is the predominant zone of soil gas/atmospheric mixing and diffusional radon loss. The

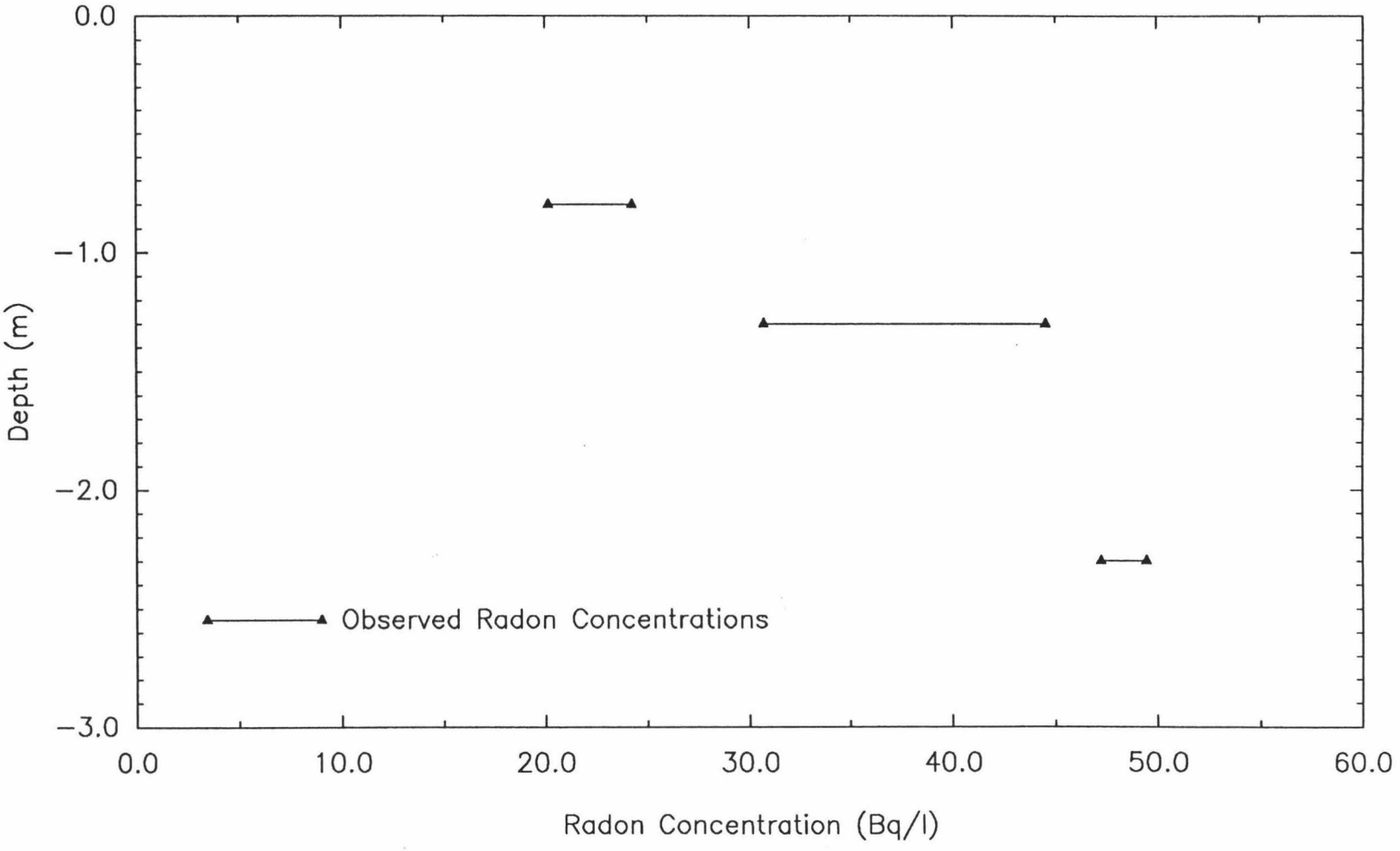

Figure 23. Average radon concentration profile for nine month monitoring period.

mixing in this zone is probably enhanced by the presence of cracks, root channels and macropores. The relatively low gradient below 1.3 m indicates that little mixing or diffusional loss is taking place at that depth and that radon concentrations in soil gas are approaching equilibrium where the amount of radon produced from the decay of radium is balanced by the amount of radon lost to decay.

b.) Synoptic Pressure Effects

The effect of long term, synoptic barometric pressure changes has previously been discussed in relation to the effect on the radon response of the initial alphameter deployment scheme. Installation of the second monitoring array allowed improved isolation of the effects of the synoptic pressure variations on the radon data by reducing the effect of artificial channelling.

To examine the effect of low frequency (periods of 24 to 72 hours) barometric pressure changes on the radon response, the barometric pressure and radon data were smoothed by a very long moving average scheme that acts as a low-pass filter to remove high frequency variations, leaving behind only the lower frequency fluctuations. The analysis presented here is strictly qualitative, involving the graphical comparison of trends in the data.

Figure 24 presents a plot of smoothed radon activities at the three soil depths, smoothed barometric pressure and rainfall for a 2 1/2 month time period. This time period was chosen because it contains substantial synoptic pressure changes but has relatively few rainfall events to interfere with and mask the effects of the synoptic fluctuations on the radon response.

It is apparent from Figure 24 that synoptic pressure variations have a marked effect on radon activities in the shallow soil (1.3 m or less), and negligible effect on the deeper radon activities. Between hours 750 to 800 in Figure 24 there is a 3 mb drop in barometric

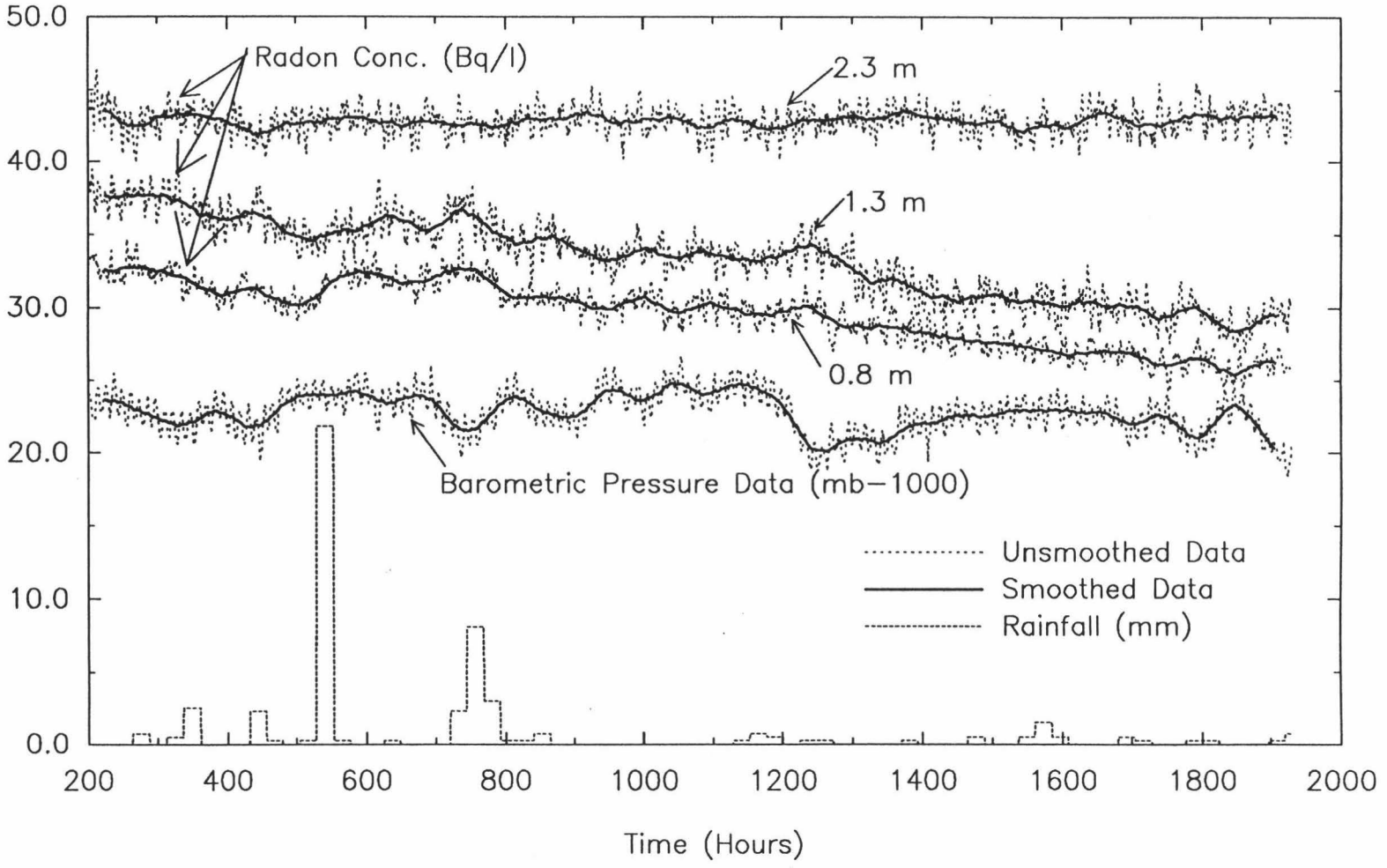

Figure 24. Smoothed and unsmoothed radon and barometric pressure time series showing effect of synoptic pressure changes on radon activities at three depths.

pressure accompanied by a small increase in radon concentration, however direct correlation is difficult due to the 10 to 12 mm rainfall event which also occurred at this time and could be the cause of the increase in radon concentration. A much better inference can be drawn for the time period from 900 hours to 1400 hours (Figure 24) where several increases and decreases in barometric pressure are mirrored by corresponding decreases and increases in radon concentration in the shallower probes, particularly at 1200 hours where a 5 mb drop in pressure results in an increase in radon concentrations at 0.8 m and 1.3 m depth.

Following the pressure drop at 1200 hours (Figure 24), there is a gradual increase in pressure accompanied by a gradual decrease in radon concentrations in the shallow soil to hour 1700. However, the gradual concentration decrease is likely due to drying and cracking of the soil, allowing for increased soil ventilation rather than a consequence of the pressure increase. Finally, beginning at hour 1650, there is a sequence of pressure variations which are well reflected in the shallow radon data due to the soil being relatively dry at this time.

Examination of the effect of synoptic pressure changes on radon concentration has provided evidence that radon flux and activities in the shallow soil (1.3 m or less) are influenced by long term barometric pressure changes. The effect is the most pronounced when the shallow soil is the driest. The inverse correlation between synoptic barometric pressure fluctuations and shallow soil gas radon activity is supported by the data presented in Figure 24. However, it must be noted that the disturbance in the soil column due to the radon monitoring instrument may be enhancing the apparent radon response. This effect is likely to be most pronounced in the shallower probes. The synoptic pressure variations do not appear to be transmitted to 2.3 m, even when the shallow soil is very dry. The constant high level of saturation at this depth (Figure 20) probably prevents transmittal of atmospheric pressure changes to this level in the soil.

c.) Diurnal Pressure Effects

Higher frequency diurnal and semi-diurnal pressure changes were next investigated to determine whether there is an identifiable response in the radon data to pressure variations with periods of 12 to 24 hours. The semi-diurnal S-2 pressure wave is a persistent characteristic of sub-tropical climates (Atkinson, 1971). The wave has its primary maxima at 1000 hours and its primary minima at 1600 hours with a secondary maxima and minima at 2200 and 0400 hours respectively. The magnitudes of these variations are typically on the order of 2 to 3 mb and often are of greater magnitude than the typical synoptic changes in barometric pressure. Analysis of the radon monitoring data was conducted to determine if there is a clear radon response to the S-2 pressure wave.

Figures 25 and 26 are plots of the radon and environmental monitoring data for the months of June and August, 1989, respectively. These two months were chosen for the investigation of diurnal and semi-diurnal pressure effects because they had the smallest synoptic pressure changes and the least rainfall of the 9 month monitoring period (Figures 16 and 17), and thus variation in radon activity would be due primarily to diurnal and semi-diurnal pressure changes.

The month of June (Figure 25) has a total of about 15 mm rainfall and all synoptic barometric pressure changes are 3 mb or less. The radon concentration data for the month shows a steady decline of about 10% in the shallow soil (1.3 m or less) with concentrations in the deeper soil (2.3 m) remaining constant in both the north and south monitoring arrays. This was due to the progressive drying of the shallow soil (hours 0 to 750, Figures 18 and 19) and resultant increased air permeability and diffusion coefficient which allows increased advective and diffusional loss of radon to the atmosphere. The deeper soil, being insulated from drying by 2 m of overburden, shows little change in mean soil gas radon concentration (Figure 20). The month of August (Figure 26) has intermittent, light rainfall

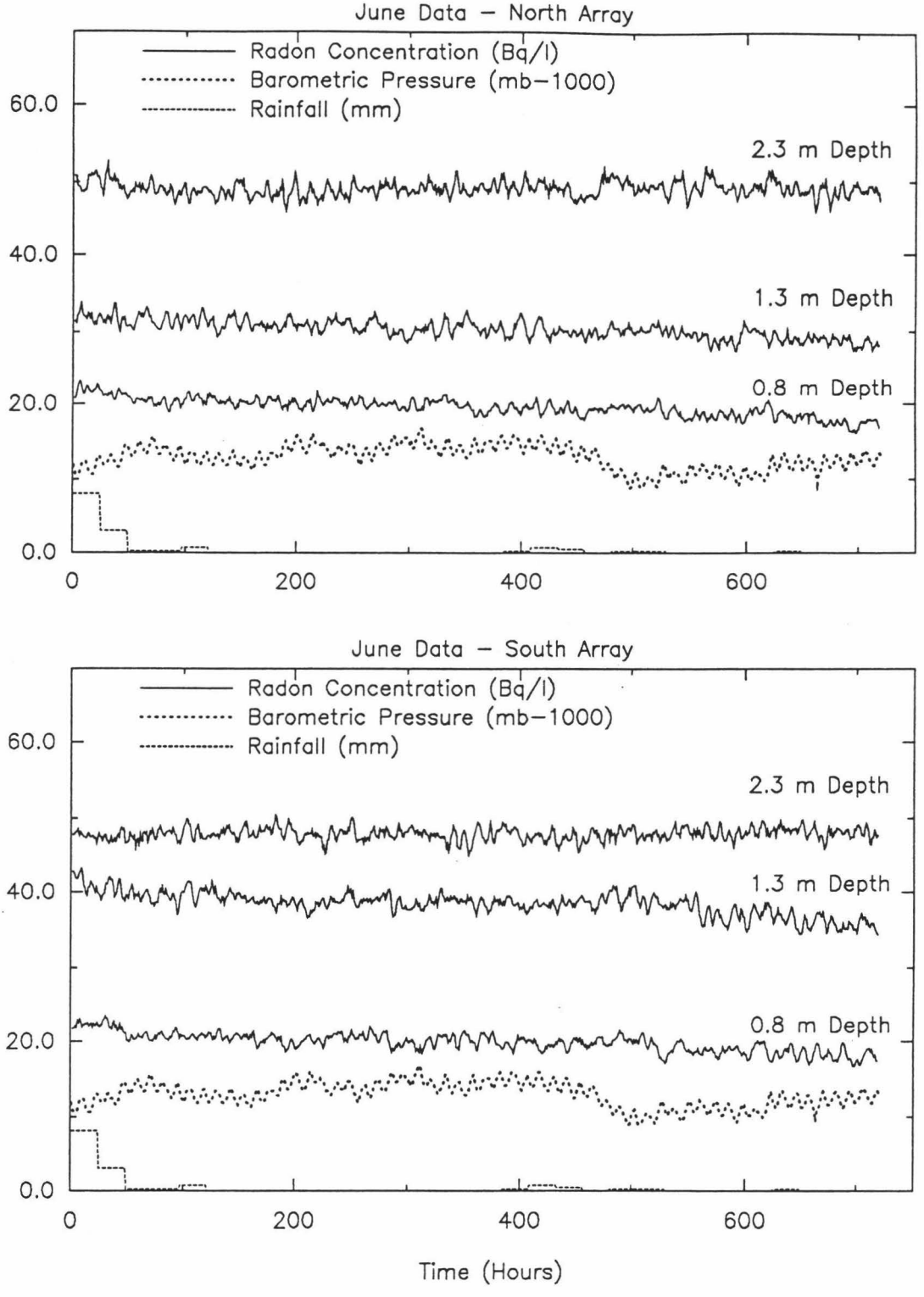

Figure 25. Radon, barometric pressure and rainfall time series at the north and south monitoring arrays for the month of June, 1989.

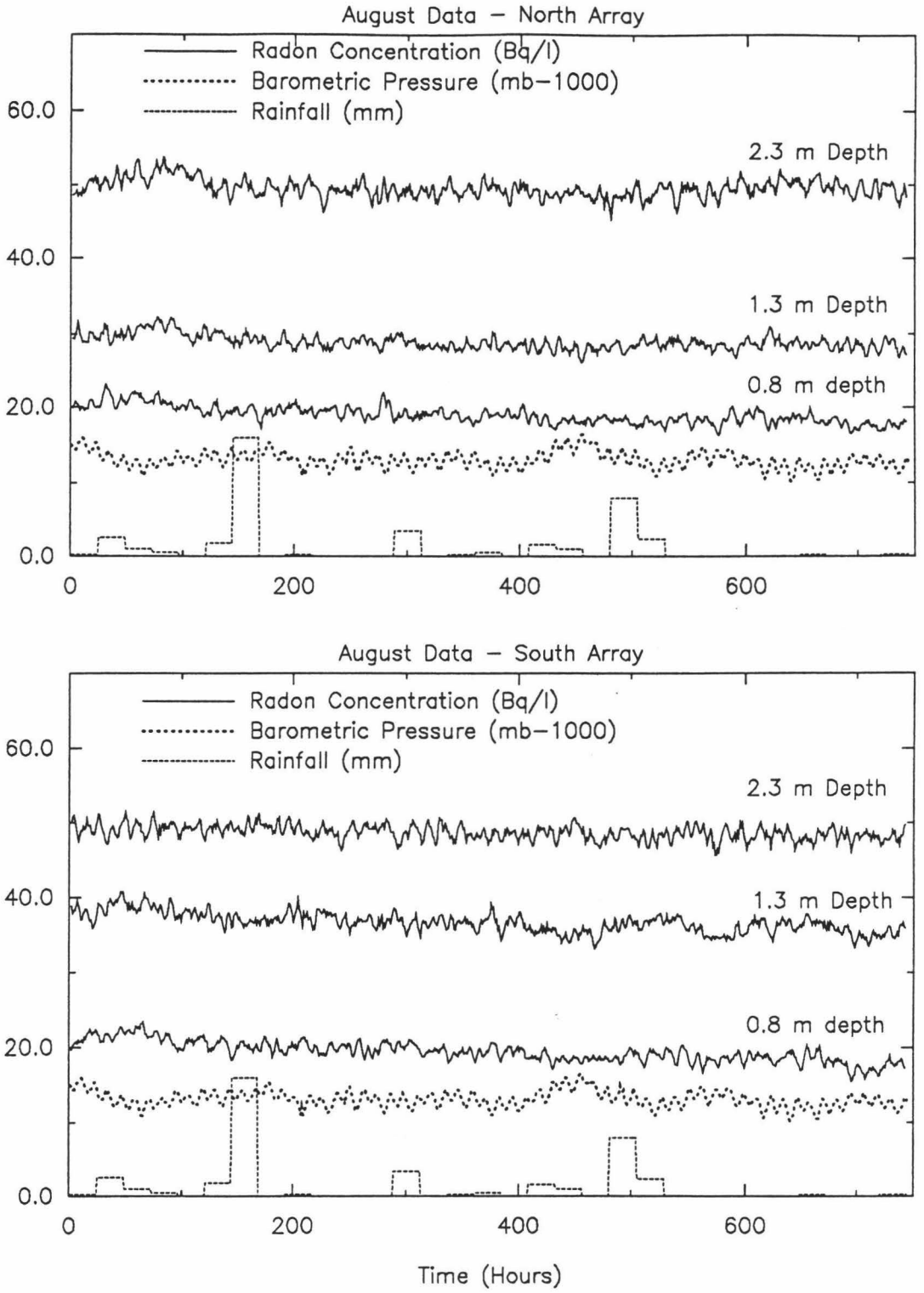

Figure 26. Radon, barometric pressure and rainfall time series at the north and south monitoring arrays for the month of August, 1989.

events and synoptic pressure changes of 3 mb or less. The radon concentration data for August show a decline of about 5% in the shallow soil with the concentration at deeper levels remaining nearly constant.

To analyze the time series data for periodicities caused by diurnal and semi-diurnal barometric pressure changes, harmonic analysis of the radon and barometric pressure data was conducted. Harmonic analysis involves decomposing the time series into its constituent parts by transforming the data from the time domain to the frequency domain. This is done by a discrete Fourier transform. The Fourier theorem holds that a time series, no matter how complex, can be regarded as the sum of a number of sinusoidal waves, or harmonics. The variance of the time series then, must also be composed of the sum of the variances of these same harmonics. A plot of the Fourier transform of the time series results in a periodogram, which is the power, or variance (s^2) versus the harmonic number (k).

Periodograms have associated with them very large standard errors which cannot be reduced by increasing the number of observations. Part of this error is due to aliasing, or the incorporation of irresolvable high frequencies into lower frequencies. Any high frequency component of the time series whose wavelength is less than twice the spacing between sample points cannot be detected. The highest frequency that can be resolved is the Nyquist frequency, whose wavelength is exactly 2Δ, where Δ is the distance between successive observations. Due to aliasing, the high frequency portion of a time series will be incorporated into lower frequencies. For a time series with an equally spaced number of observations (n), taken Δt time units apart, the frequency of each harmonic can be expressed (Haan, 1977):

$$f_k = \frac{k\, f_N}{m} \qquad (5.1)$$

where, f_k = frequency of harmonic k (T^{-1})
m = n/2 (n=even) or $\frac{n-1}{2}$ (n=odd)
f_N = Nyquist frequency = $1/2\Delta t$ (T^{-1}).

The period (P) of a particular harmonic is then:

$$P_k = 1/f_k. \tag{5.2}$$

Figures 27 and 28 are Fourier transforms of the barometric pressure and radon data for the months of June and August plotted as frequency versus variance. As can be seen in Figure 27, the barometric pressure data contains a strong spectral peak at a period of 12 hours corresponding to the S-2 pressure wave. In Figure 27 (June) the radon data at 0.8 and 1.3 m depth exhibit smaller peaks at a period of 12 hours. The 2.3 m data for June contains no discernible 12 hour peak and is typical of a purely random "noise" spectrum. In the August data (Figure 28), the barometric pressure data contains a strong 12 hour component and a lesser peak at a period of 24 hours. The radon data for August shows that at the 0.8 m depth, there are slight peaks at 12 and 24 hours. The response at the 1.3 and 2.3 m depths shows no discernible periodicities.

The source of the large peaks apparent in the periodograms at very low frequencies (Figures 27 and 28) is not entirely clear. To determine if these signals are derived from the effects of aliasing or are true signals from low frequency synoptic pressure changes, Fourier transforms of shorter time periods (3 days to 2 weeks) were performed. The shorter-term periodograms were also found to contain similar peaks at very low frequencies indicating that the apparent low frequency signals are derived primarily from aliasing although the apparent signal may also contain a small component from synoptic pressure changes.

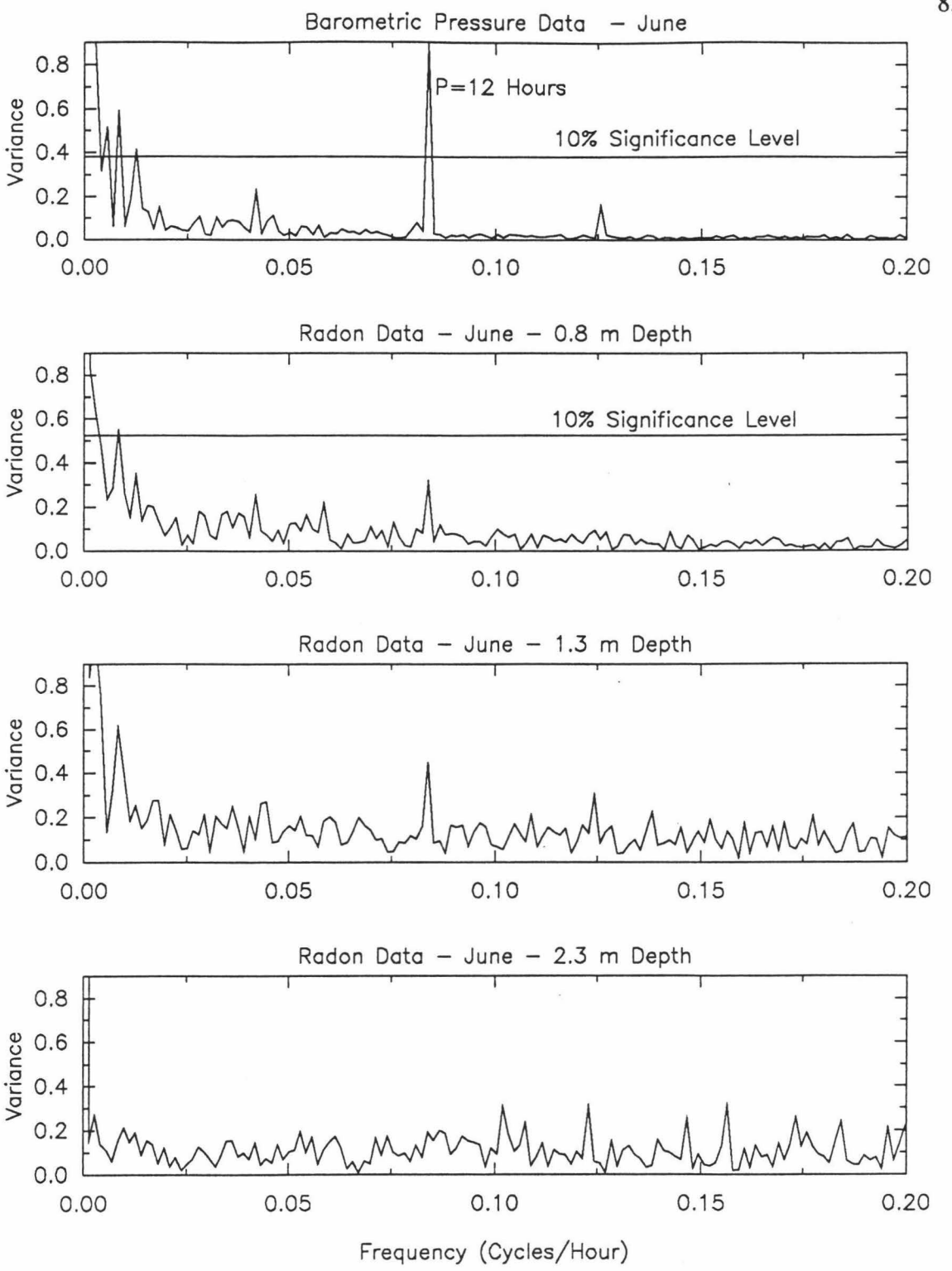

Figure 27. Fourier transforms of barometric pressure and radon data for month of June, 1989 showing a spectral peak at 12 h in shallow radon data due to the S-2 pressure wave.

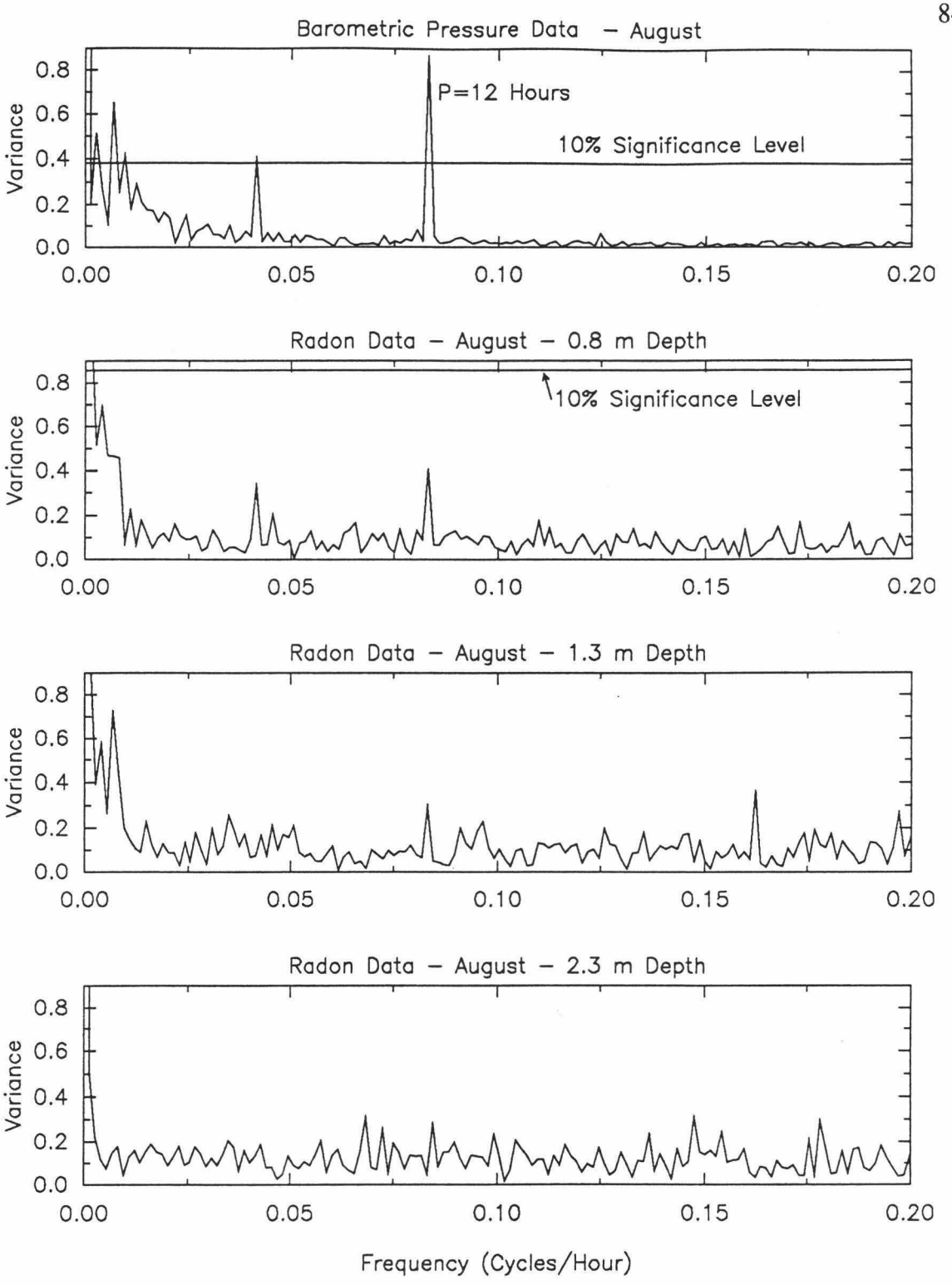

Figure 28. Fourier transforms of barometric pressure and radon data for month of August, 1989 showing a spectral peak at 12 h in shallow radon data due to the S-2 pressure wave.

The observed peaks in the Fourier transforms of the barometric pressure and radon time series do not automatically indicate a periodic component. The statistical test for the existence of a significant periodic component of the periodogram is called the Fisher test (Fisher, 1929) and requires comparison of the test statistic $\hat{g}$, against a critical value of g for a specified level of significance (α), (Davis, 1986):

$$\hat{g} = \frac{s^2_{max}}{2s^2} \tag{5.3}$$

where, s^2_{max} = variance of maximum peak

s^2 = total variance of time series.

and

$$g = 1\text{-}\exp\left(\frac{\ln \alpha - \ln m}{m\text{-}1}\right). \tag{5.4}$$

Testing the significance by this method involves constructing a null hypothesis which states: the time series is a purely random stochastic process. The alternative hypothesis is then: the time series is a random stochastic process with a superimposed periodic component. If the test statistic $\hat{g}$ exceeds the critical value of g, the periodic component may be presumed to exist and the null hypothesis is rejected within the level of significance set by (α). If the test value does not exceed the critical value the null hypothesis cannot be rejected and the observed spectral peak, s^2_{max} could have arisen by random chance due to sampling fluctuations.

The periodograms in Figures 27 and 28 show that the barometric pressure data contains a highly significant 12 hour period at a significance level of 0.1, (i.e. the probability of rejecting a correct hypothesis is 10%). The 12 hour spectral peaks in the radon data at 0.8 m and 1.3 m depth, however, do not achieve significance by this test.

Failure to reject the null hypothesis of a purely random stochastic process does not necessarily indicate that the S-2 pressure wave has no effect on the radon response in the shallow probes. Periodogram tests are most satisfactorily suited to time series data which

are composed of discrete spectra, such as the hourly barometric pressure observations. The radon data presented here represent a continuous record of alpha decay integrated over 1 hour counting intervals. Thus, the radon data contain discrete and continuous spectra made up of both a random noise component and a signal component. The noise component is responsible for a large amount of variance, resulting in the suppression of the signal component. Nonetheless, it is evident that the shallow radon data are composed of a small, 12 hour, periodic signal superimposed on a residual process consisting of random, high frequency noise and longer term variations.

Figure 29 illustrates the 12 and 24 hour radon response at 0.8 m depth for the months of April, May, September and October. The 12 hour response observed in the radon data for the months shown in Figure 29 is again, far below the 0.1 significance level due to a large amount of variance in the data resulting from large synoptic pressure changes and from moderate to intense rainfall events during the months plotted. The 1.3 m radon data only contains a 12 hour response in the very dry months of June and August, (Figures 25 and 26) due to heightened soil air permeability and the presence of surface cracks which can transmit pressure changes deeper into the soil profile. A 12 hour signal could not be identified in any of the deep, 2.3 m radon data.

The weakness of the 12 hour signal in the shallow radon data is probably due to several factors. The first is the small signal to noise ratio of the data due to the random nature of radioactive decay and the counting errors associated with the radon monitoring instruments. The second is the attenuation of the pressure wave at depth in the soil due to the very low air permeability of the soil and the very small (2 to 3 mb) pressure changes. The third factor is the interference of the longer term synoptic pressure changes adding another source of irregularity in the data which increases the overall variance and masks the shorter term diurnal signal.

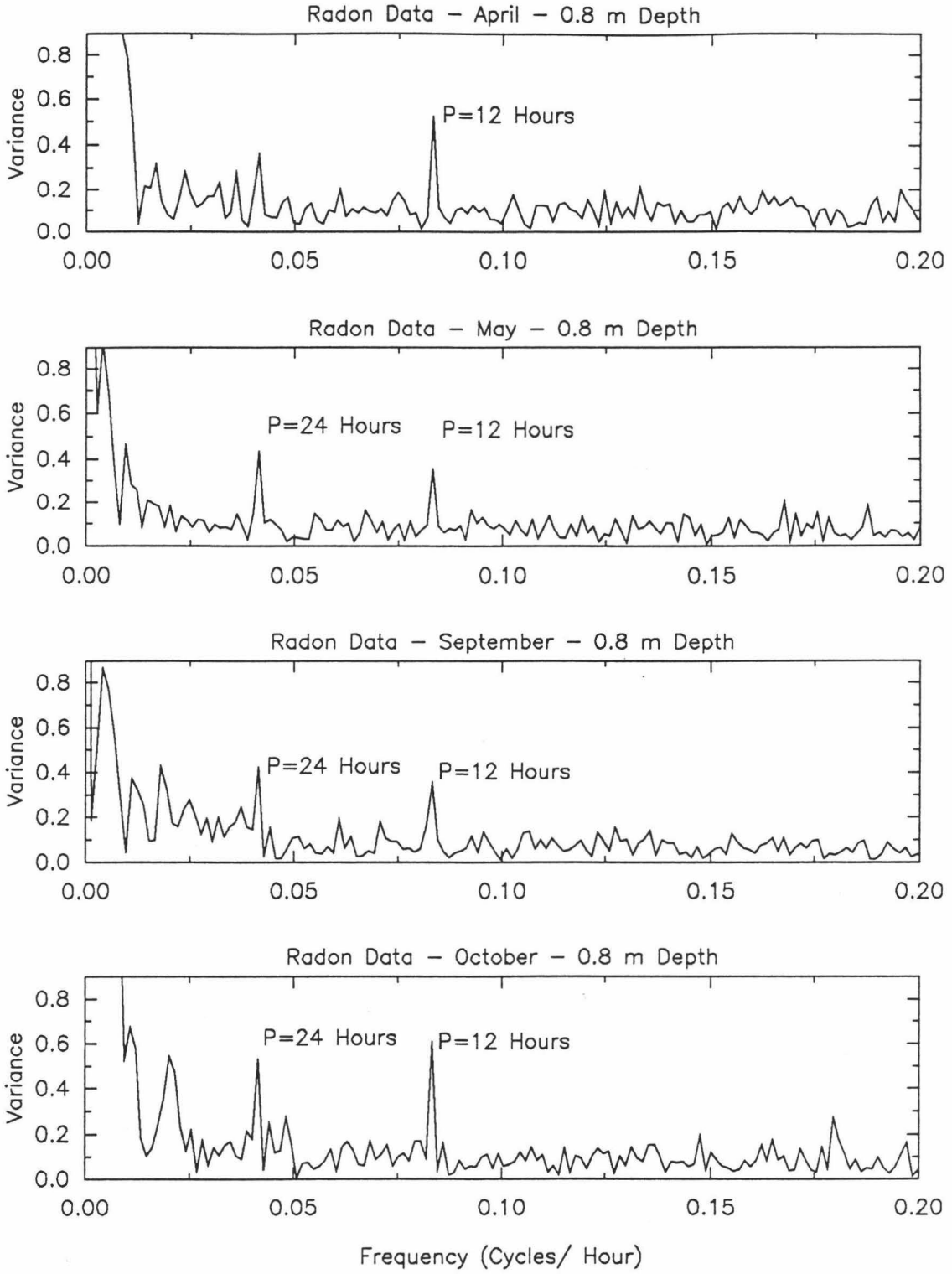

Figure 29. Fourier transforms of radon data for four months showing consistent spectral peaks at 12 and 24 h in 0.8 m depth radon data due to the S-2 pressure wave.

Bearing in mind the uncertainties introduced by the soil disturbance and installation of the alphameters, there appears to be substantial evidence for radon response to the 12 hour pressure wave. Harmonic analysis of the effect of the S-2 pressure wave has revealed that a consistent, 12 hour perturbation is introduced to the shallow soil radon activity. The higher frequency diurnal perturbation is superimposed on the lower frequency synoptic variation discussed previously. The diurnal effect is the strongest when the soil is very dry, due to increased soil air permeability and the presence of cracks which facilitate preferential flow of soil gas. These short term pressure changes do not extend down to 2.3 m, even under the driest conditions experienced during the study period because of the low air permeability of the deeper soil due to the consistently very high saturation, the absence of soil cracks at that depth and the attenuation of the pressure changes with depth.

d.) Wind Induced Pressure Effects

The last analysis of pressure effects is concerned with very high frequency pressure changes caused by wind gustiness. This was studied by examining the 15 minute interval radon data along with data obtained from differential pressure transducers in the soil. The differential pressure transducers were described in chapter 4 and illustrated in Figure 10. Data are currently being compiled for the complete analysis of wind driven pressure changes and their effect on soil gas as part of the ongoing radon investigation, but a very preliminary interpretation is presented here.

Figure 30 shows two plots of radon concentrations and differential pressures at 0.8 m and 1.3 m depth. The differential pressure transducers generate a voltage that is proportional to the differential pressure between the surface probe and the soil probe. The radon activity data shown in Figure 30 have been transformed to be on a similar scale with the output voltage of the transducers. The plots of the differential pressure data for the 0.8 m and 1.3 m probe are quite similar, with both exhibiting what appears to be a very

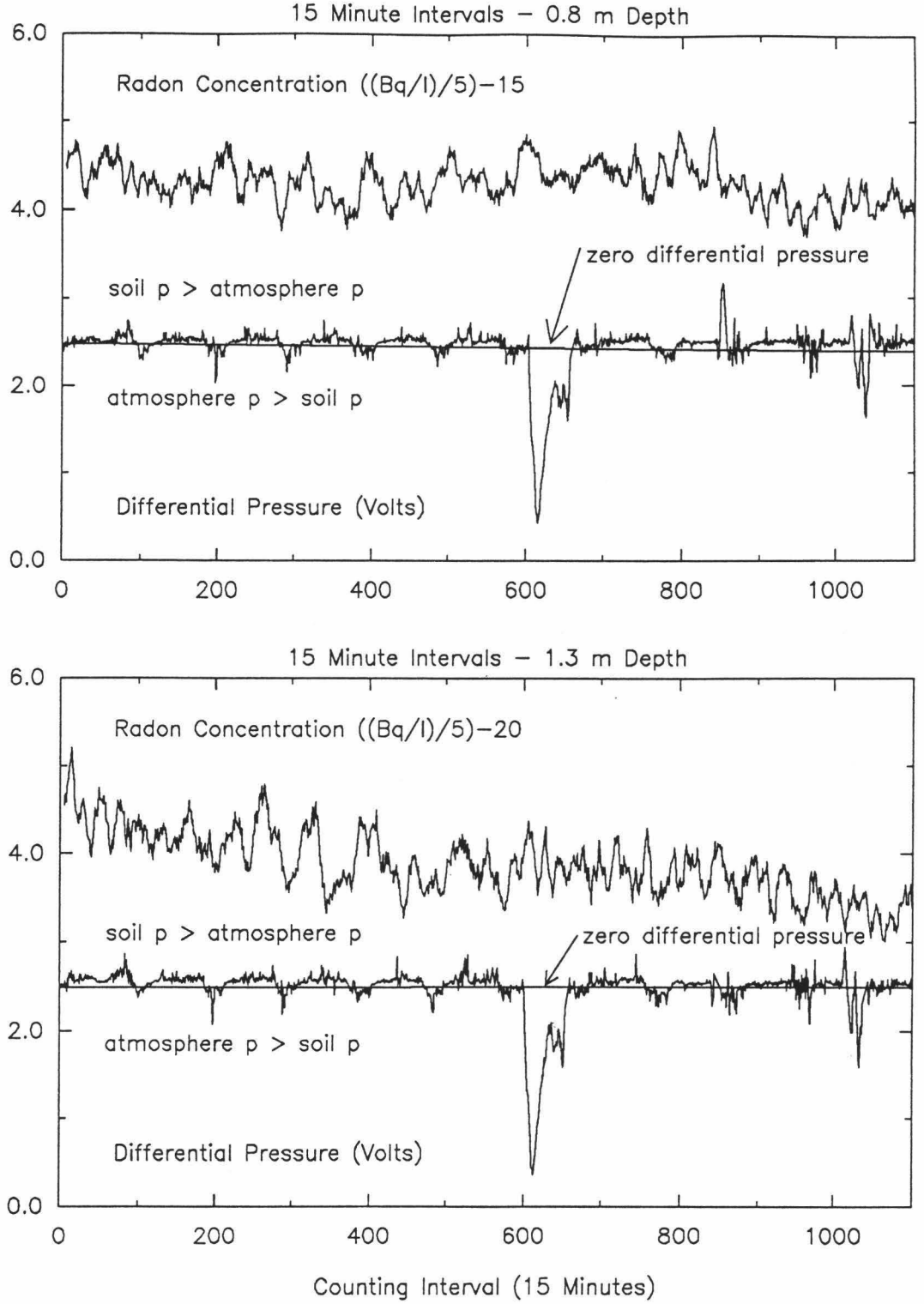

Figure 30. Fifteen minute interval radon activity data and differential pressure data at 0.8 and 1.3 m depths showing zero differential pressure line. Radon activities have been transformed to be on a similar scale with the differential pressures.

persistent, daily periodicity (96 fifteen minute intervals) about the "zero" differential pressure line. This would be consistent with a periodicity introduced by the normal tradewind regime experienced at the site during this time period: the tradewinds typically reach their maximum velocity once a day, from 10 to 2 pm. The period during the day when the wind is the strongest is when the differential pressure will be the greatest with the soil pressure being greater than the surface pressure. However, there may also be an unknown effect due to heating of the soil and the environment immediately above the surface during the day. The large perturbation present in the differential pressure data at hour 600 is of unknown origin but may be due to an electronic malfunction as the winds were quite light on that particular day.

Casual examination of the radon activity data in Figure 30 discloses no periodicities or perturbations that may be related to the apparent daily period of the differential pressure data. Figure 31 presents Fourier transforms of the radon and differential pressure data from Figure 30. The 0.8 m radon data shows the 12 hour peak due to the S-2 wave discussed in the previous section along with a very high frequency peak which is probably due to aliasing, while the 1.3 m radon data displays no identifiable periodicities. The differential pressure probe data seem to fail to detect the S-2 pressure wave and appear to lack the 24 hour signal which appears significant in the raw data. Indeed, the Fourier transforms of the differential pressure data seem to consist of only random noise but with some possible peaks apparent at very high frequencies that are likely also due to aliasing.

The sampling period of 15 minutes for the radon and differential pressure data may be too long to detect the effects of wind driven pressure changes as the shortest wavelength that can be detected is 30 minutes, as dictated by the Nyquist frequency. It is likely that the effects of wind gustiness operate at much shorter time intervals of about 10 to 30 seconds. Fukuda (1955) has shown theoretically and experimentally that the depth to which pressure changes resulting from wind gustiness is only about 5 mm below the surface for a

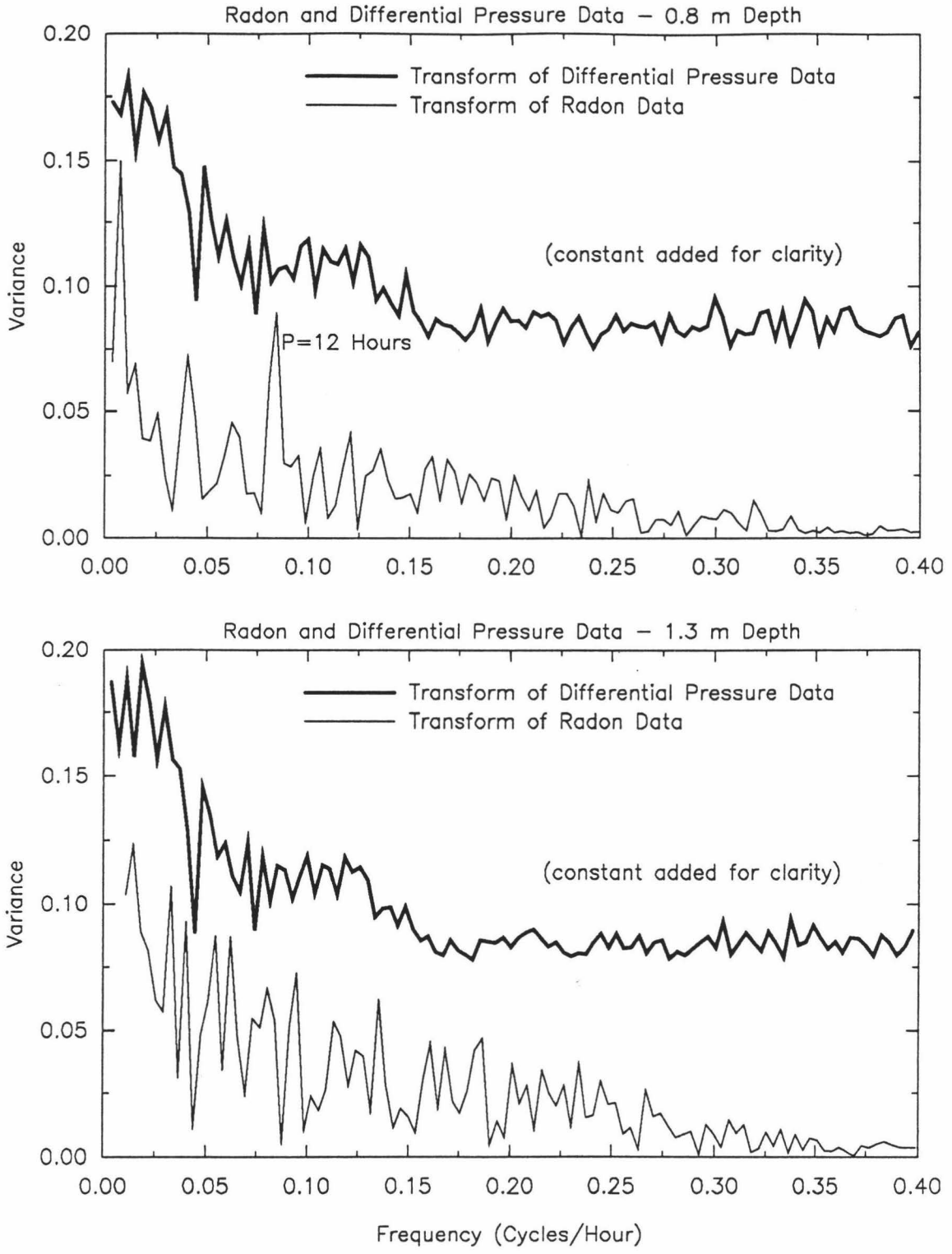

Figure 31. Fourier transforms of radon and differential pressure data at 0.8 and 1.3 m depths showing 12 h spectral peak in 0.8 m radon data.

homogenous, sandy soil. This work however, did not include the effect of cracks and structural discontinuities. Data are still being collected as part of the ongoing project and as additional information becomes available a more thorough analysis of the differential pressure data and the effect of wind driven pressure changes can be undertaken.

3.) Advective Barrier Experiment

An investigation of the importance of short and intermediate term advective mixing of soil gas was initiated in October, 1989. To accomplish this, a 12 m by 12 m plastic tarp was installed on the soil surface directly over the north monitoring array (Figure 7). It was anticipated that the barrier would inhibit the short and intermediate term pressure driven mixing of soil gas with atmospheric air, but would still allow near-normal diffusive loss of radon through the plastic. Comparison of the radon response between the covered array and the uncovered array has provided information on the relative influences of advective and diffusive movement of radon in soil gas.

Figure 32 is a plot contrasting the radon response between the two arrays at 0.8 m depth, as well as barometric pressure, rainfall and soil moisture data. The radon concentrations and response to the intense rainfall events at the two arrays are almost identical prior to the barrier installation. After the barrier is in place however, (hour 900, Figure 32) the radon response begins to differ dramatically. While radon activities at the uncovered array gradually descend to near the pre-rainfall levels, radon concentrations under the barrier increase by almost 150% until hour 1300. This is due to a combination of the elevated soil saturation and the inhibition of soil ventilation by the barrier. It was planned that the barrier would be installed when the soil was in a dry state, but due to time constraints and the onset of an extremely rainy period of weather, the barrier was installed when the soil was quite wet (Figure 32). The high saturation level of the soil may have introduced an additional perturbation to the radon data. However, comparison of the radon

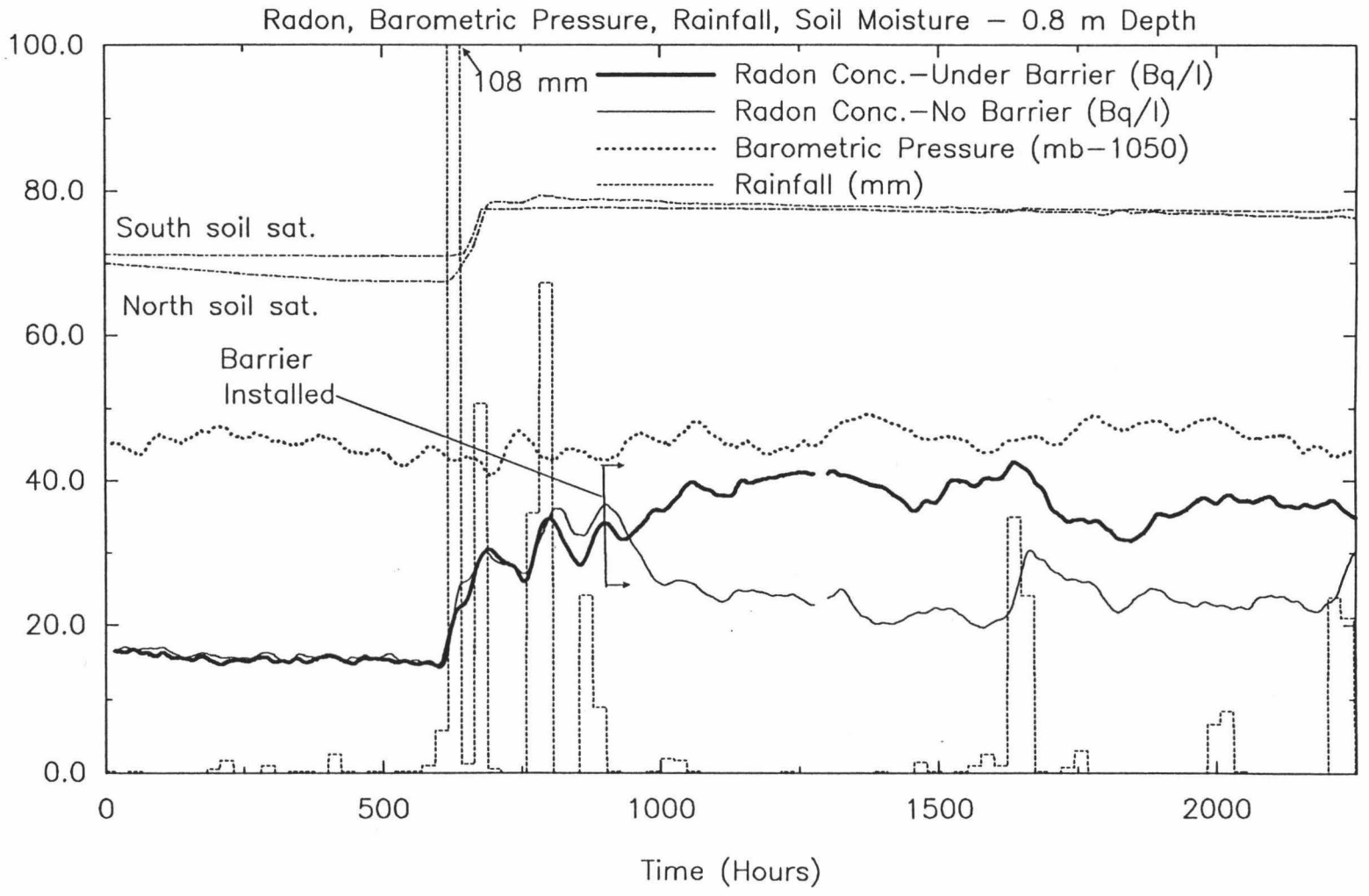

Figure 32. Radon, meteorologic and soil saturation time series showing comparison of radon activities at 0.8 m depth with and without advective barrier.

response between the covered and the control array allows identification of the effect of the barrier in limiting soil gas/atmospheric exchange.

Under semi-dry conditions, just prior to the large rainfall at hour 1600 in Figure 32, the radon concentrations at 0.8 m are about 100% higher under the barrier than at the control array. The radon response at the control and experimental array to the rainfall event at hour 1600 in Figure 32 are quite different. Radon activity at 0.8 m in the control array shows an increase of about 50% in response to the rainfall while radon activity in the test array at 0.8 m increases only about 10% (Figure 32). The small radon response to the rainfall event at the test array suggests that the barrier has a slight blocking effect on rainfall infiltration.

An interesting feature in Figure 32 is that radon activities in the test array seem to exhibit a strong, but somewhat delayed, response to the long-term, synoptic atmospheric pressure variations (hours 1000 to 2000, Figure 32). The mechanism responsible for this apparent effect is unknown, but it may indicate enhanced lateral transmission of long-term barometric pressure changes through the shallow soil due to the presence of the barrier. Further data need to be analyzed to determine if this is a feasible mechanism.

To determine if the barrier had a significant impact on the semi-diurnal radon variation attributed to the S-2 pressure wave, Fourier transforms of the radon data from 0.8 m and 1.3 m depth for both arrays were performed to detect the presence or absence of the 12 hour periodicity previously observed in the shallow radon data. Figure 33 illustrates this analysis. There is a strong 12 hour signal present in both the 0.8 m radon data as well as in the 1.3 m radon data from the uncovered array. However, as Figure 33 shows, the 12 hour signal is barely discernible above the noise level for the covered array at 0.8 m depth and completely absent at 1.3 m depth. This provides further evidence that the semi-diurnal S-2 pressure wave has a significant impact on the shallow soil radon activities and that advective mixing is taking place to a depth of at least 0.8 m.

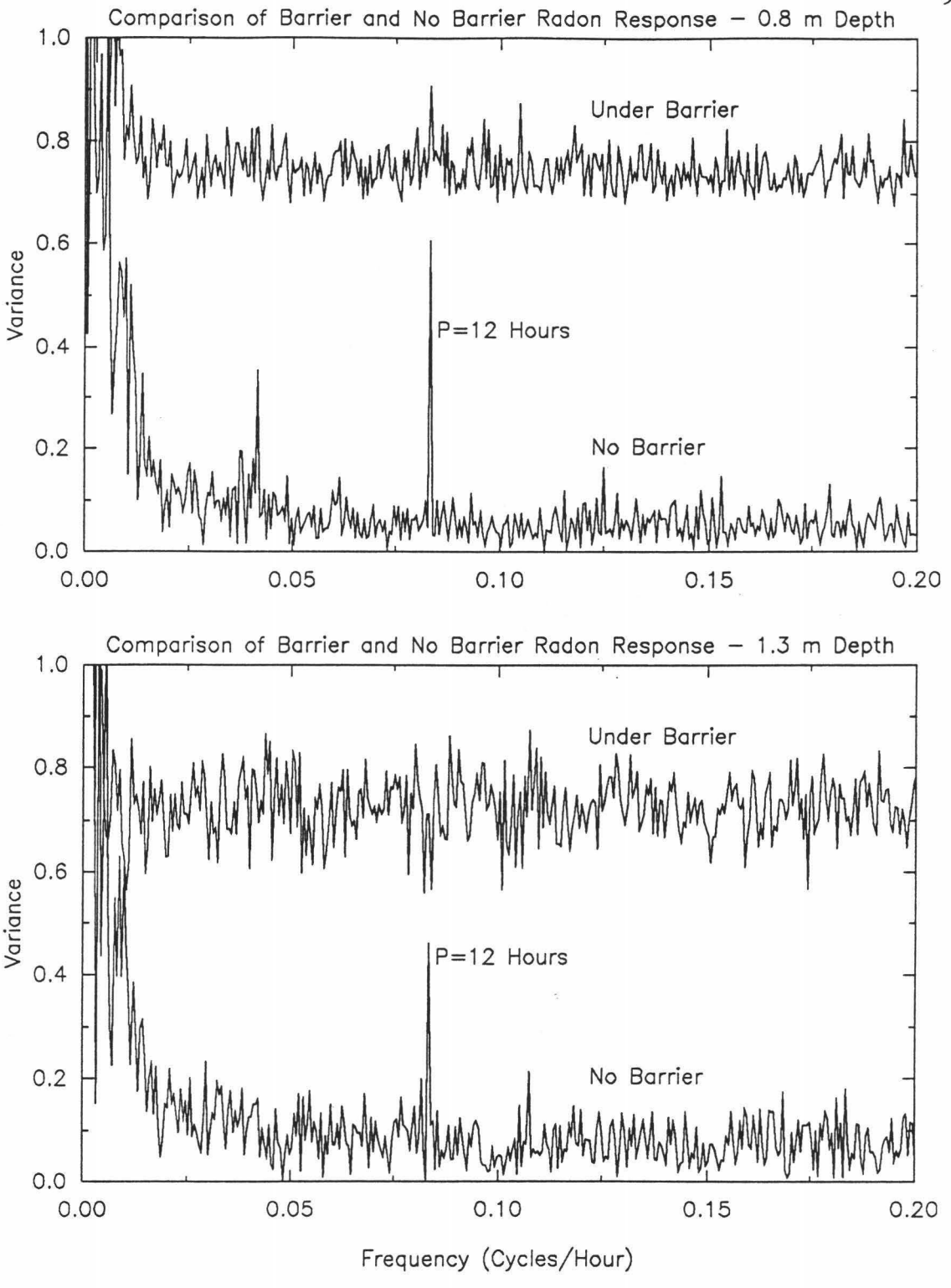

Figure 33. Fourier transforms of radon data for test and control arrays showing 12 h spectral peaks in data from control array and the absence of a response in the test array data.

Figures 34 and 35 are plots of the comparison between the radon response at 1.3 m and 2.3 m depths respectively for the covered and uncovered arrays. Radon concentration levels at the two depths between the control and experimental arrays are within 10% or less of each other indicating that, at least at this level of soil saturation, advective mixing of soil gas with atmospheric air does not occur at depths greater than ~1 m and that diffusion is the significant transport process at that depth. However, the apparent strong radon response under the barrier to synoptic pressure changes noted in the 0.8 m data (Figure 32) can also be seen in the 1.3 m radon data (Figure 34). Again, this may indicate that significant lateral advective movement of soil gas is occurring beneath the barrier. However, at present, this conclusion is considered to be speculative.

In general, the preliminary results of the advective barrier experiment reveal that the radon levels under the barrier range from 75 to 100% higher than radon activities in the control array at 0.8 m depth. This suggests that, assuming the diffusive flux from the control and the covered array is similar, advective flux of radon out of soil gas and the mixing of atmospheric air with soil gas is at least as significant as the diffusive transport of radon from the soil at depths to 1 m. Evidence is also presented for an inverse correlation between synoptic and diurnal pressure changes and radon activities at 0.8 m depth. However, additional data need to be collected to determine if the radon response at the control and experimental arrays differ significantly during periods when the soil is drier and advective transport is more pronounced.

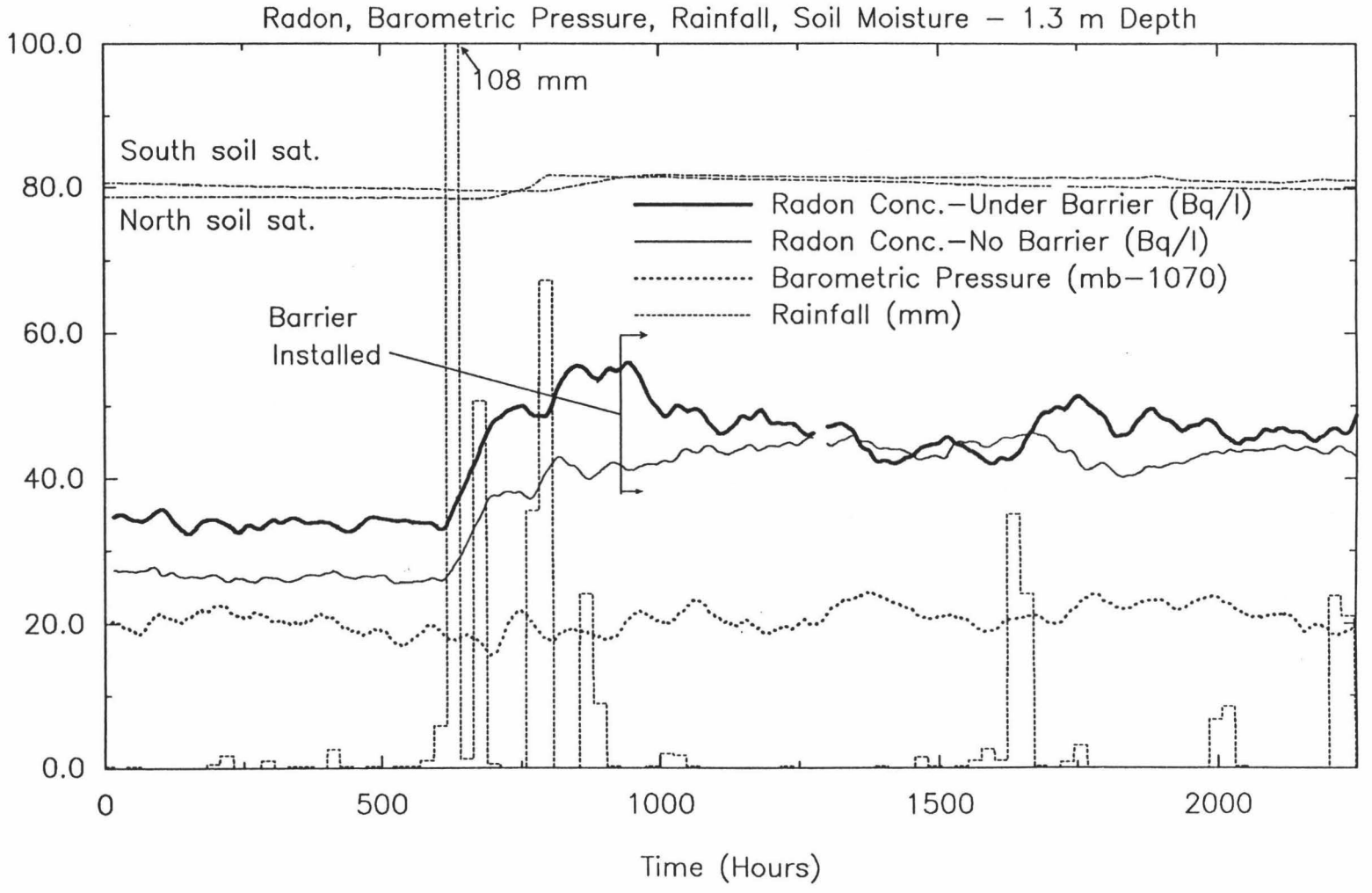

Figure 34. Radon, meteorologic and soil saturation time series showing comparison of radon activities at 1.3 m depth with and without advective barrier.

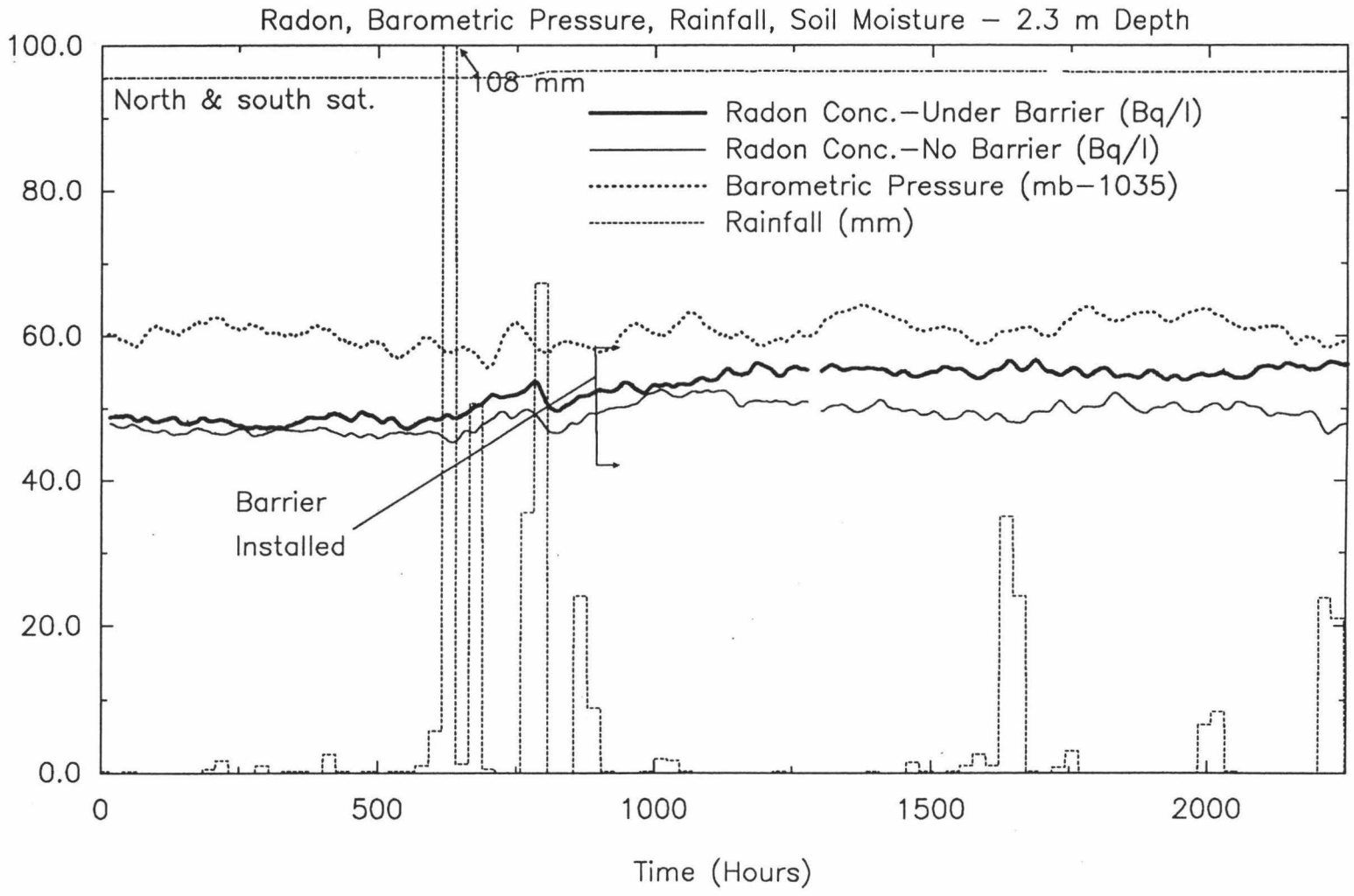

Figure 35. Radon, meteorologic and soil saturation time series showing comparison of radon activities at 2.3 m depth with and without advective barrier.

B. Modeling Results

Modeling of the data collected in the field monitoring study was undertaken using RN3D, in order to better characterize the processes which affect radon behavior in the soil and to provide a more accurate estimate of the true values of air permeability and diffusion coefficient at the field site. A sensitivity analysis was also performed to determine the relative importance of the various model input parameters on the silty clay soil type found at the Poamoho site. Holford et al. (1989) have previously performed a sensitivity analysis on a dry, sandy soil using RN3D.

1.) Model Calibration

Calibrating RN3D involved conducting model runs to determine if the observed radon response could be simulated by the model. This was done by entering measured and estimated soil parameters into the model in a realistic layer configuration and conducting steady state simulations ($t=t_0$). When the modeled radon concentration profile agreed satisfactorily with the observed radon profile (Figure 23), the resulting input parameters were used to conduct 1-D transient model runs ($t=t_0 + \Delta t$). When the resulting output duplicated the observed radon concentration time series, the model was considered calibrated. The resulting soil parameters were then used as input into 2-D model runs and used as the base-case parameters for the sensitivity analysis. A flow chart of the calibration process is shown in Figure 36.

a.) Layer Configuration

As discussed in Chapter 3, RN3D was modified to allow input of soil parameters which change with depth. The layer configuration used for the model runs was controlled by the physical characteristics of the site and by the depths of the measurement points. During the course of the field work it became apparent that a 0.3 m thick tilled layer of

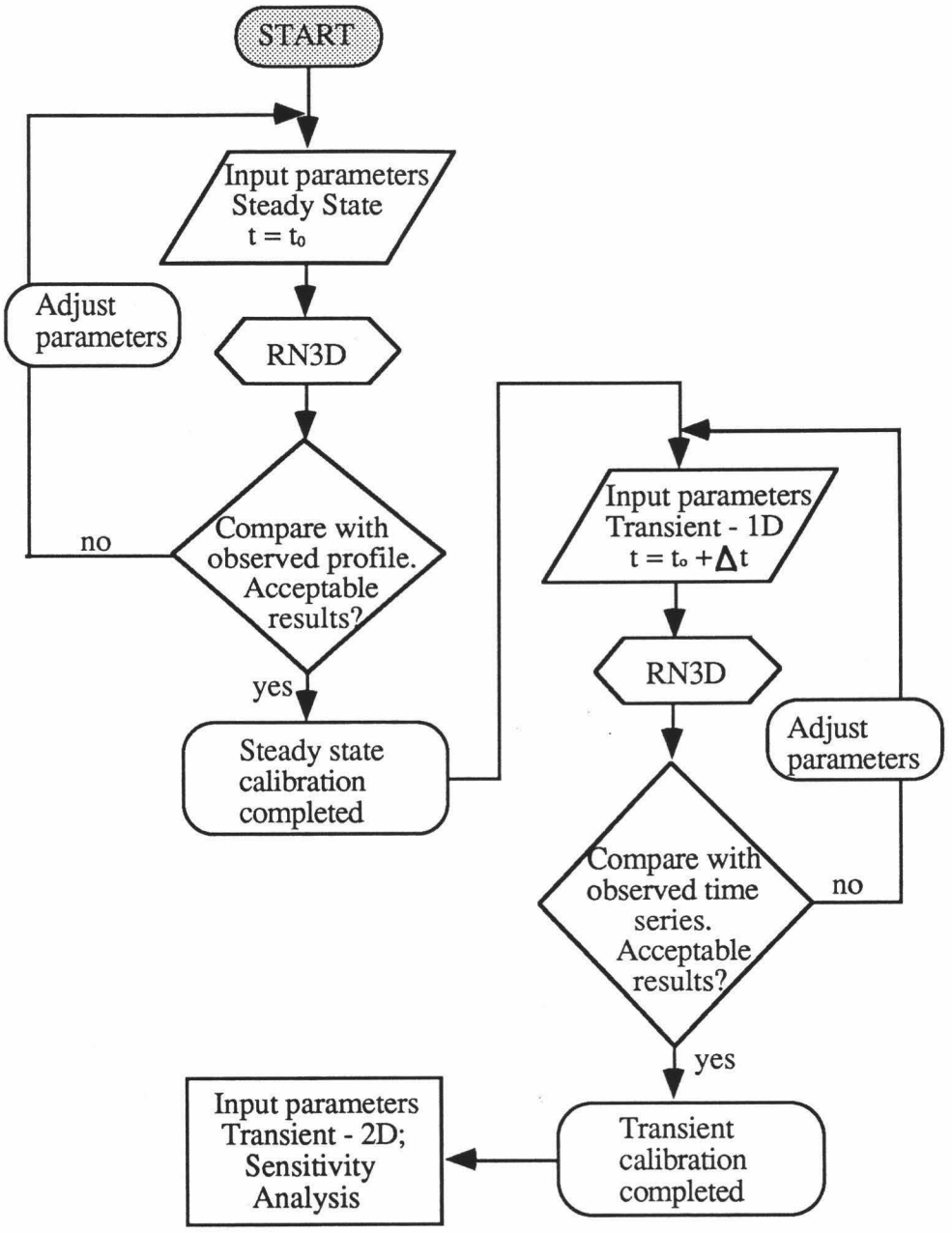

Figure 36. Flow chart of model calibration process showing steady state and transient simulations.

loose soil overlies a very compacted "hard pan" layer about 0.2 m thick that underlies the experimental plot. Deeper layers were chosen to center the measurement points within each layer. Figure 37 shows the arrangement of the layers utilized in the model runs as well as values for the model parameters which are not a function of soil moisture: soil bulk density, porosity and radium content. This layer configuration was used for all model runs. The depth to the water table was estimated to be 180 to 200 m (Mink and Lau, 1987).

b.) Predicted Air Permeability and Diffusion Coefficients

Two critical soil parameters, diffusion coefficient and air permeability, were initially estimated by fitting water retention data for the Poamoho soil given by Green et al. (1982) and Miller (1987), (Figure 59, Appendix A) to soil water characteristic models (Mualem, 1976; Van Genuchten, 1985). These models predict unsaturated hydraulic conductivities, relative unsaturated hydraulic conductivities and pressure heads versus soil moisture contents from observed soil water retention data. The predicted relative unsaturated conductivities were then converted into relative air permeabilities by the function (Brooks and Corey, 1966):

$$k_{ra} = (1 - k_{rw})(1 - \theta)^2 \qquad (5.5)$$

where, k_{ra} = relative air permeability = $k_{sat=s}/k_{dry\ soil}$
k_{rw} = relative water permeability = $k_{sat=s}/k_{saturated}$, (s=any given saturation)
θ = water content.

The air permeabilities at different moisture contents can be predicted if the air permeability is known at one moisture content or at dryness. Soil air permeabilities at saturations of 0.69 and 0.75 at 1 meter depth (Table 8, Appendix B), were measured as described in Chapter 4 and used to scale the air permeabilities predicted by the soil characteristic models. Figure 38 shows the relative air permeabilities and the actual air

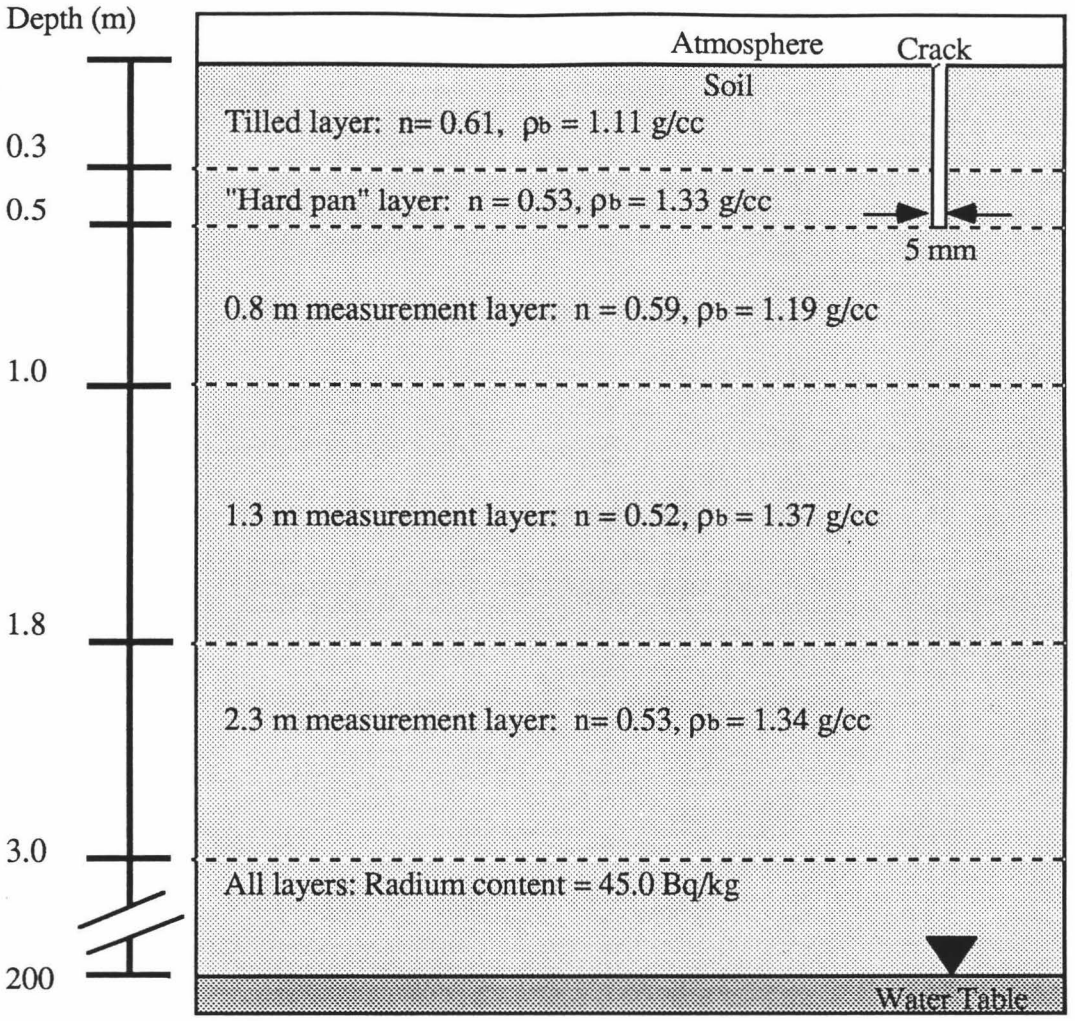

Figure 37. Schematic diagram of layer configuration for RN3D model runs showing porosity, bulk density and radium content. Typical soil crack dimensions also shown.

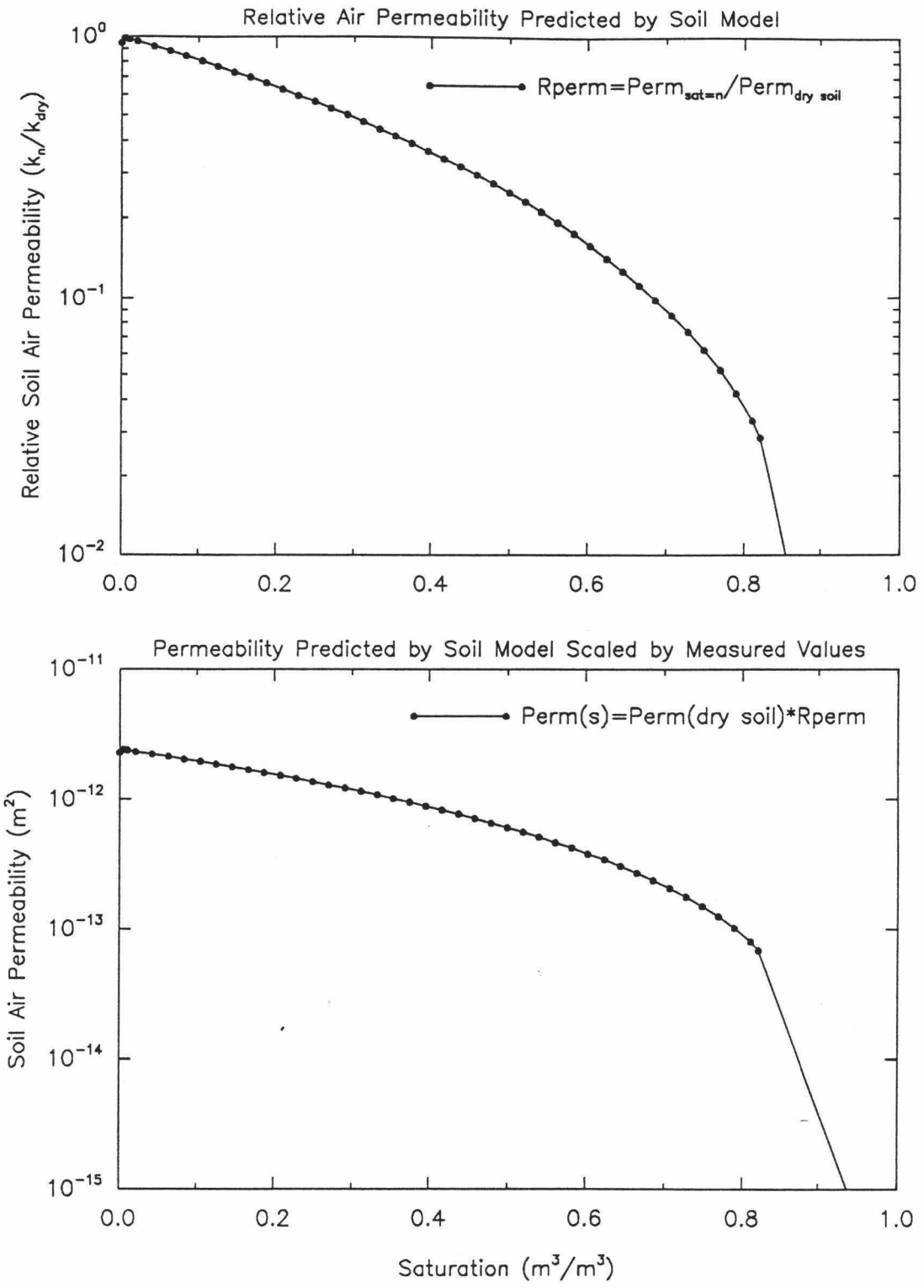

Figure 38. Relative air permeabilities and permeabilities versus soil saturations as predicted by the soil water characteristic model. Permeabilities scaled by field measured values.

permeabilities versus saturation for the Poamoho soil predicted by the soil water characteristic models.

To estimate diffusion coefficients at different saturation levels, two models were used. A model proposed by Arya and Paris, (1981) was used to generate a pore size distribution for the Poamoho soil from the observed moisture content versus pressure head curves. The Arya and Paris model assumes spherical soil particles and cylindrical soil pores. A 9-increment pore size distribution generated by the model was used to calculate a tortuosity and bulk diffusion coefficient for all moisture contents by a theoretical model developed by Nielson et al. (1984). The diffusion coefficient versus saturation curve predicted by this method is given in Figure 39 (top).

An empirical correlation proposed by Rogers et al. (1984) was also used to estimate diffusion coefficients. A data base of over 200 radon diffusion coefficient measurements was used to develop a simple correlation between diffusion in soil (D) and saturation (s) using soil porosity (n):

$$D = 0.07 \exp[-4(s - sn^2 + s^5)] \qquad (5.6)$$

Figure 39 (bottom) illustrates the diffusion coefficient versus saturation curves given by this empirical model for porosities of 0.5 and 0.6, the approximate upper and lower limit of the Poamoho soil.

As Figure 39 illustrates, diffusion coefficients predicted by the Nielson et al. (1984) model are lower than diffusion coefficients predicted by the empirical model of Rogers et al. (1984) by a factor of about 10. This is due to the pore-filling sequence used by Nielson et al. (1984). In their model, a water film of uniform thickness is assumed to be present in all pores. As saturation increases the water film causes a greater degree of saturation in the small pore increments than in the large pores. For a silty-clay soil type consisting primarily of very small pores, the available pore volume would be saturated very quickly resulting in

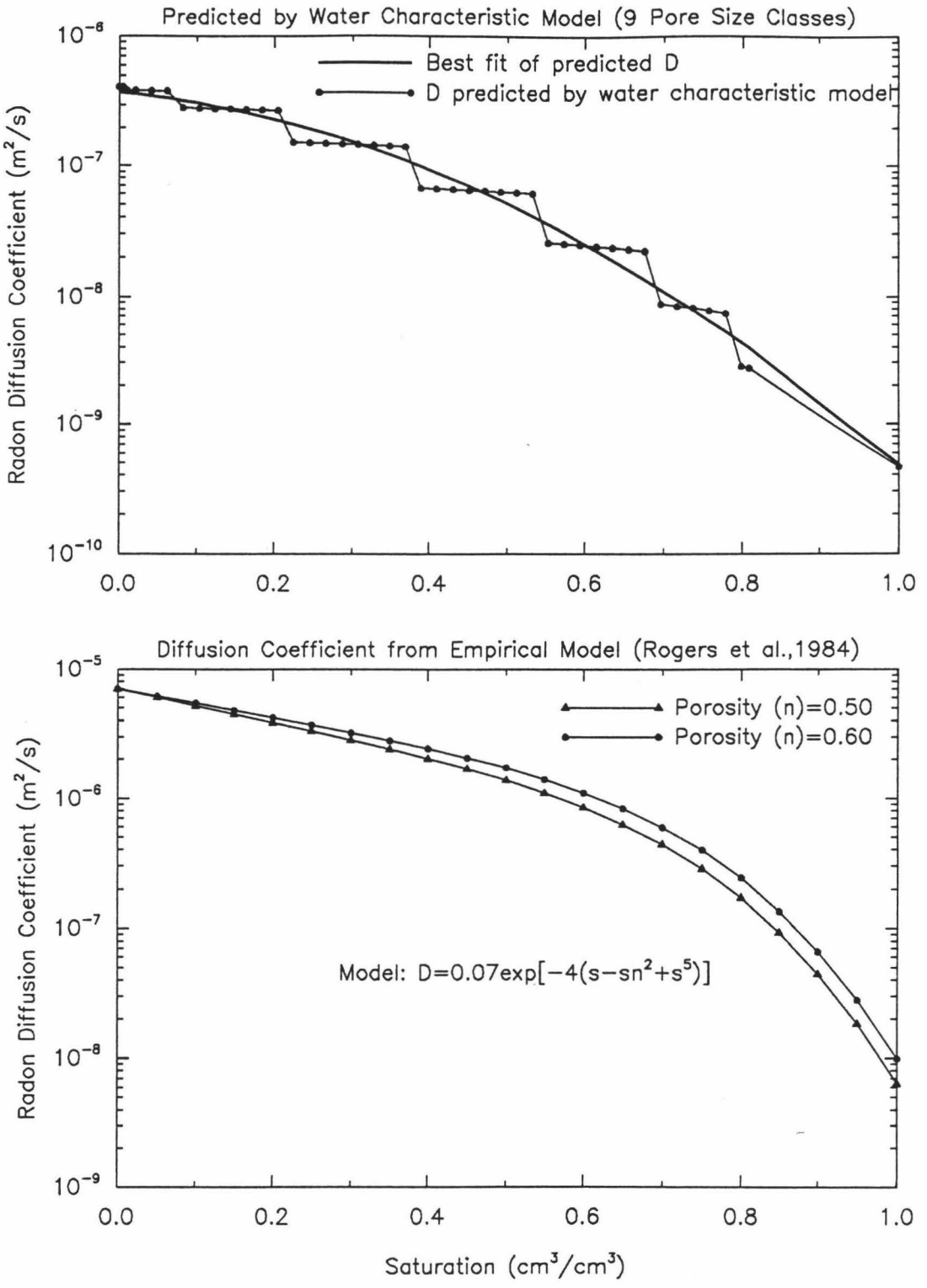

Figure 39. Diffusion coefficients versus soil saturations predicted by the soil characteristic model of Nielson et al. (1984) (top), and the empirical model of Rogers et al. (1984).

a lower diffusion coefficient. The model of Rogers et al. (1984) primarily considers the degree of saturation and the bulk porosity and results in a higher diffusion coefficient.

c.) Steady State Simulations

The initial calibration runs were conducted using a steady state condition ($t=t_0$) in an attempt to duplicate the observed average concentration profile (Figure 23). In 1-D steady state runs, the only means of radon flux from the soil is by diffusion. Therefore, only the diffusion coefficient was varied in each layer in the model runs with all other parameters held constant. Figure 40 illustrates three steady state model runs conducted with different diffusion coefficients for the various layers. The three model runs shown in Figure 40 show the effect of varying the diffusion coefficient from the lowest D (predicted by the soil characteristic model of Nielson et al. (1984)), to D predicted by the empirical model of Rogers et al. (1984) which gives a closer fit to the observed profile. The final run was performed with D adjusted to a slightly higher value to obtain the best possible fit of the observed concentration profile (Figure 40). This final diffusion coefficient was used as the initial input into the transient model runs.

d.) Transient, One Dimensional Simulations

One dimensional transient simulations were conducted to try to match the observed time series radon concentration data in order to gain a better understanding of the effect of varying diffusion coefficient and air permeability. As the model is driven by changes in atmospheric pressure, varying the soil air permeability will control the magnitude of the radon activity variations within the soil. Adjusting the diffusion coefficient affects the flux of radon out of the soil and thus, will control the absolute radon concentrations.

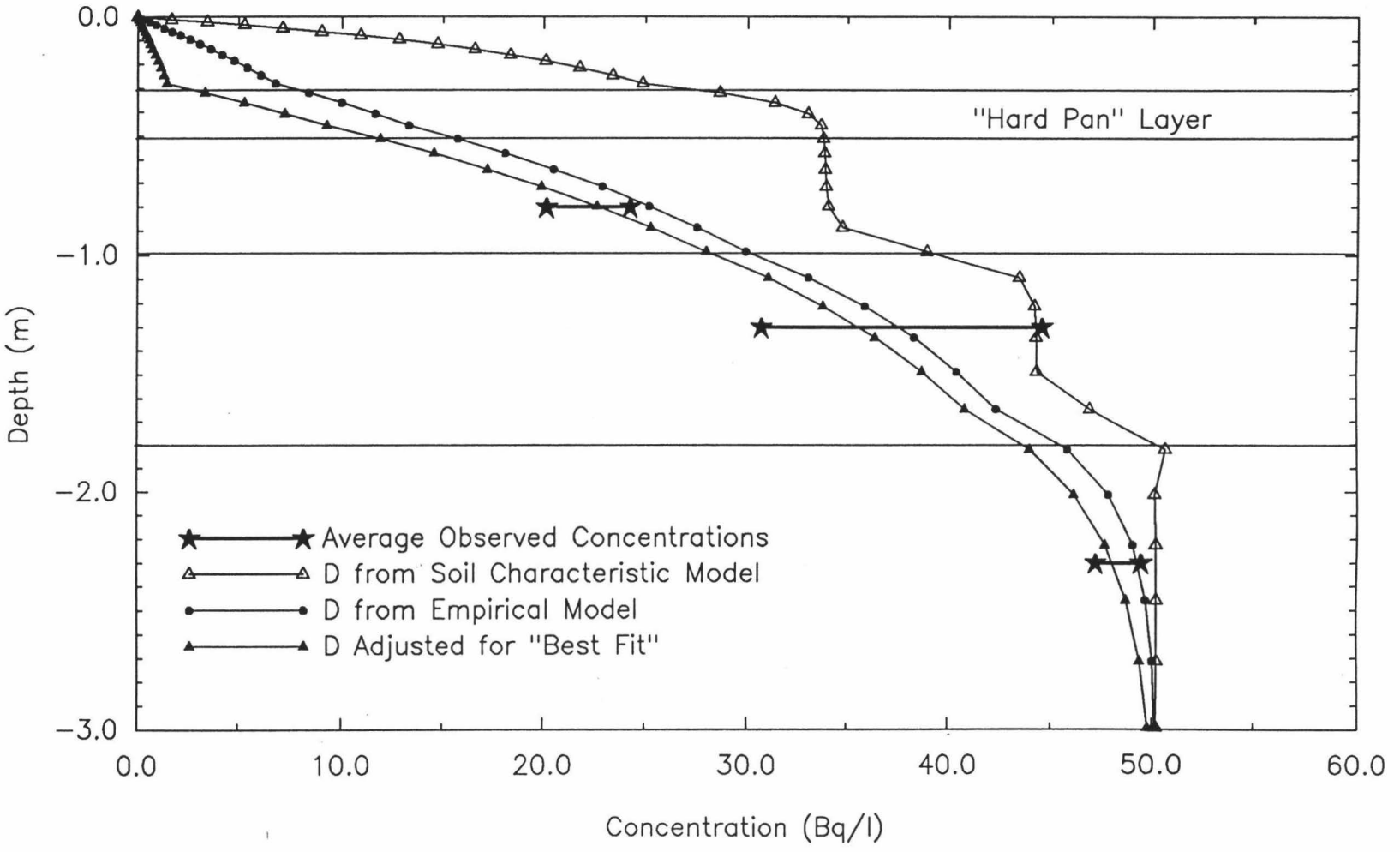

Figure 40. Simulated and observed radon concentration profiles. Three model runs with varying diffusion coefficients

All transient, 1-D model runs were conducted using the hourly barometric pressure observations as the top boundary condition. Figure 41 illustrates a generic 1-D transient model run with one hour time steps. Note how the barometric pressure changes, both short and long term, are mirrored by the simulated radon response, in agreement with the effects of atmospheric pressure changes on radon response observed in the field data.

The initial model runs were conducted with the saturation held constant, and thus diffusion coefficient and air permeability were held at a constant value for each layer throughout the run. The diffusion coefficients used for each layer were the final product of the best fit to the observed concentration profile from the steady state runs. The soil air permeabilities used were as predicted by the water characteristic model shown in Figure 38.

It quickly became apparent that, in order to match the observed variations in radon activities, the modeled air permeabilities needed to be increased by 3 to 4 orders of magnitude over those predicted by the water characteristic model (Figure 38) which had been scaled by the measured permeability values (Table 8, Appendix B). This finding suggests that the true gas permeability of the soil is significantly higher than was measured by the air permeameter technique used in this study (Figure 11). It is possible that the air permeameter does not adequately account for preferential flow and large scale soil features such as cracks and macropores which contribute to the true soil permeability. A second possibility is that the air flow and transport equations used in RN3D do not realistically characterize the subsurface gas movement in highly saturated, low permeability soils where preferential flow contributes substantially to the bulk soil permeability.

Figure 42 shows a time series of a model run and observed data conducted for a one month period with constant saturation and constant diffusion and permeability values. The minor rainfall events had negligible effect on soil moisture content and radon activities, hence, were not modeled. The radon concentrations and variations simulated by the model

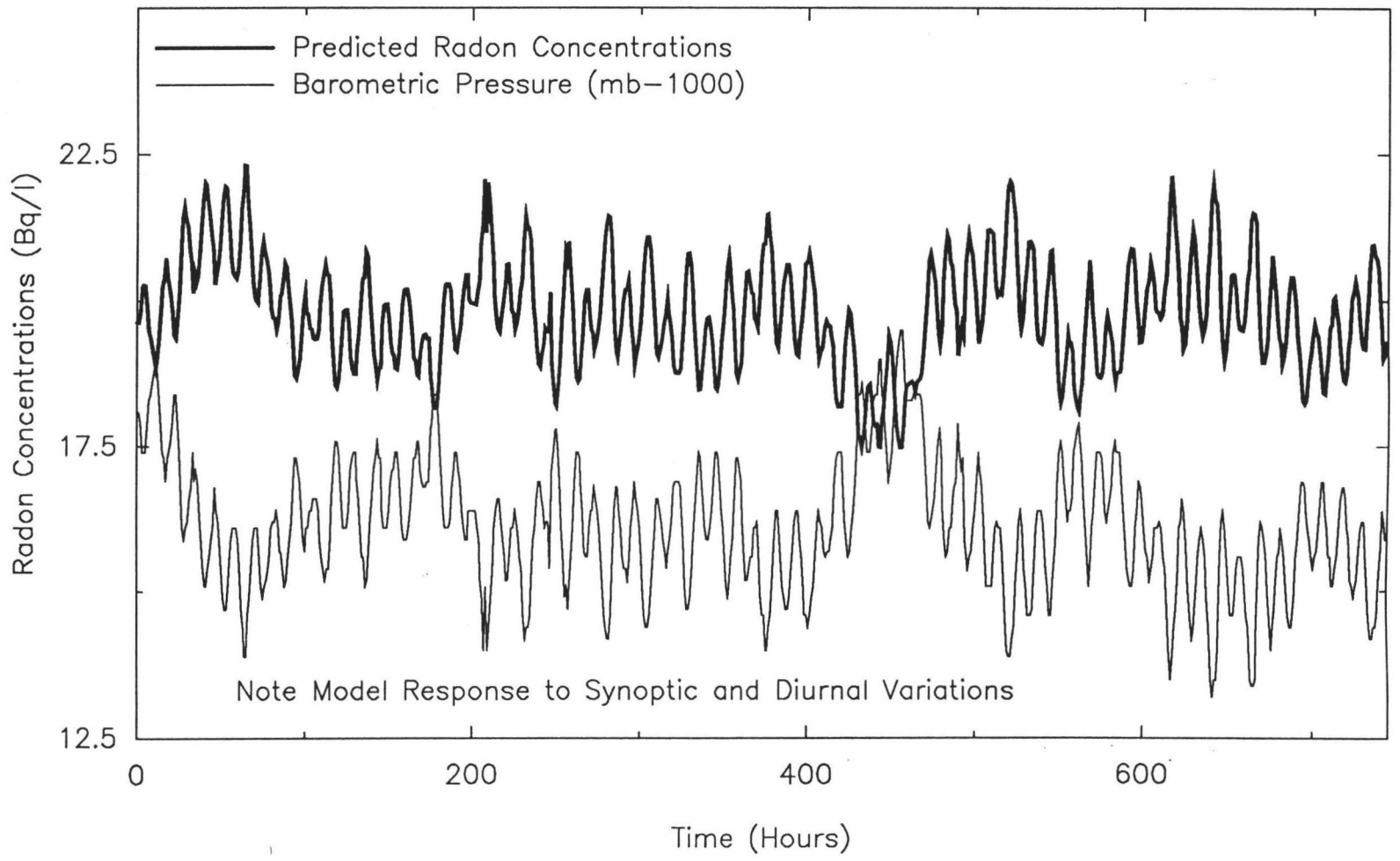

Figure 41. Transient 1-D model run with 1 hour time steps and constant soil parameters.

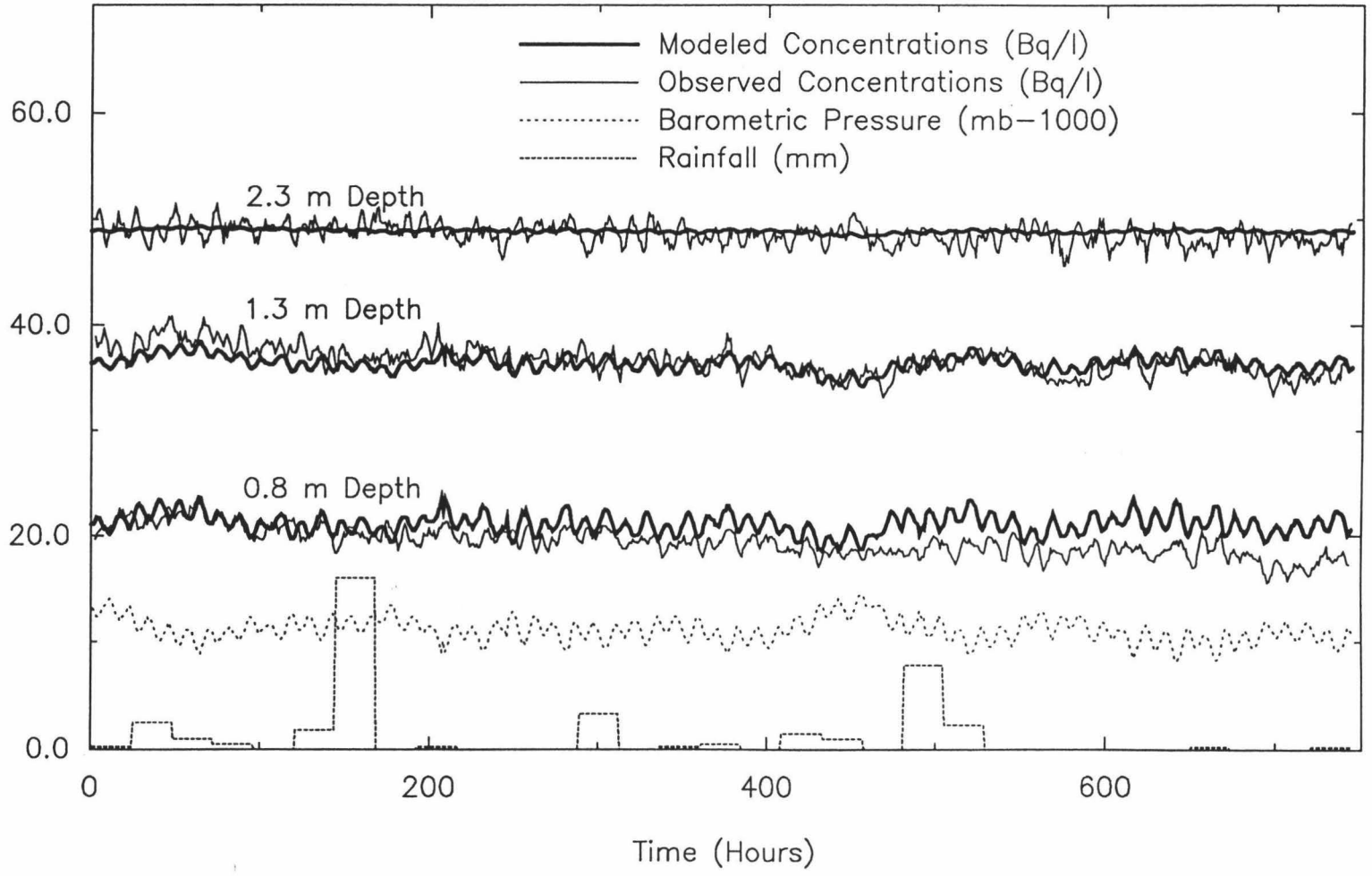

Figure 42. One dimensional simulated radon time series with constant soil parameters and observed radon time series showing model ability to track observed radon data.

track the observed data quite well for the 0.8 m and 1.3 m depths, indicating that the model is calibrated with respect to one dimensional diffusional radon flux and advective movement of radon in the soil. The small amount of variation in the simulated radon concentrations relative to the observed radon response at 2.3 m depth (Figure 42) is attributed to the very low permeability of the highly saturated (s~0.95) deeper layer. It is believed that the permeabilities used as model input are a more accurate estimate of the true air permeability of the Poamoho soil than the permeabilities measured by the method shown in Figure 11 and listed in Table 8 (Appendix B). This is due to the small scale of the measurement method which cannot account for preferential air flow in cracks and macropores.

Harmonic analysis was conducted on the modeled and observed radon data in Figure 42 to determine if the semi-diurnal signal seen in the field data is present in the simulated data. Fourier transforms of the simulated and observed radon data at depths of 0.8 m and 1.3 m are presented in Figures 43 and 44 respectively. As the model is driven by barometric pressure changes, it is not surprising that there is a very strong diurnal and semi-diurnal signal present in the simulated radon data. The observed radon data contain the 12 hour signal at 0.8 m, but no discernible signal at 1.3 m (Figures 43 and 44).

To simulate the effects of varying saturations on the simulated radon response, a moderate rainfall event was modeled. Figure 45 illustrates the ability of the model to simulate the observed radon response to varying soil moisture contents. The simulation in Figure 45 was conducted in three steps: 1) the run was started at steady state at a moderate saturation level; 2) at hour 475 a new run was started using as initial conditions the conditions at the final time step of the previous run and the saturation in the top layers was increased to about 95% and all water content-related parameters were decreased accordingly, causing radon levels in the shallow soil to increase; 3) at hour 575 a third run was initiated with saturation levels, and soil parameters, returned to more moderate values.

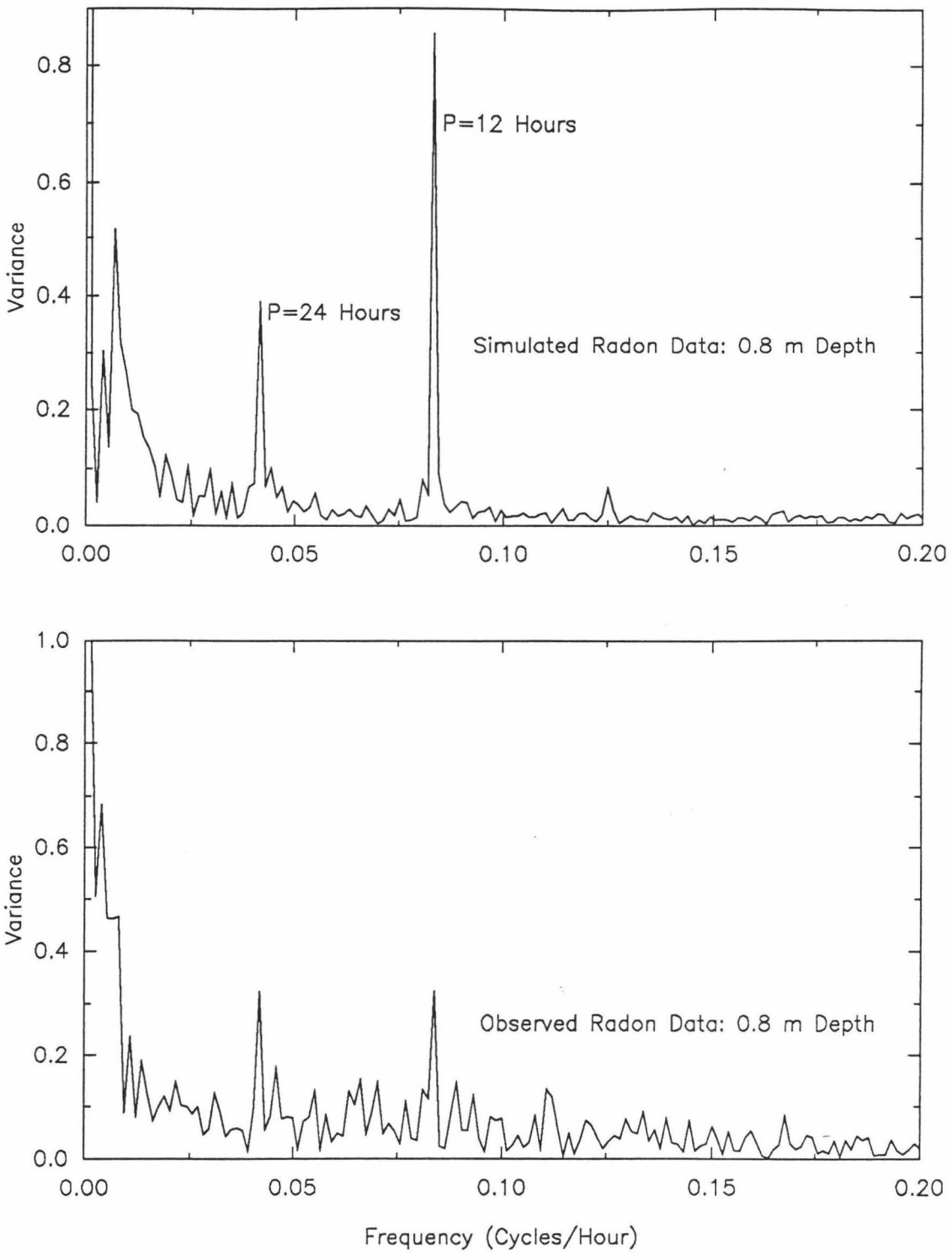

Figure 43. Fourier transforms of simulated and observed radon data at 0.8 m depth showing diurnal and semi-diurnal signal in both radon data sets.

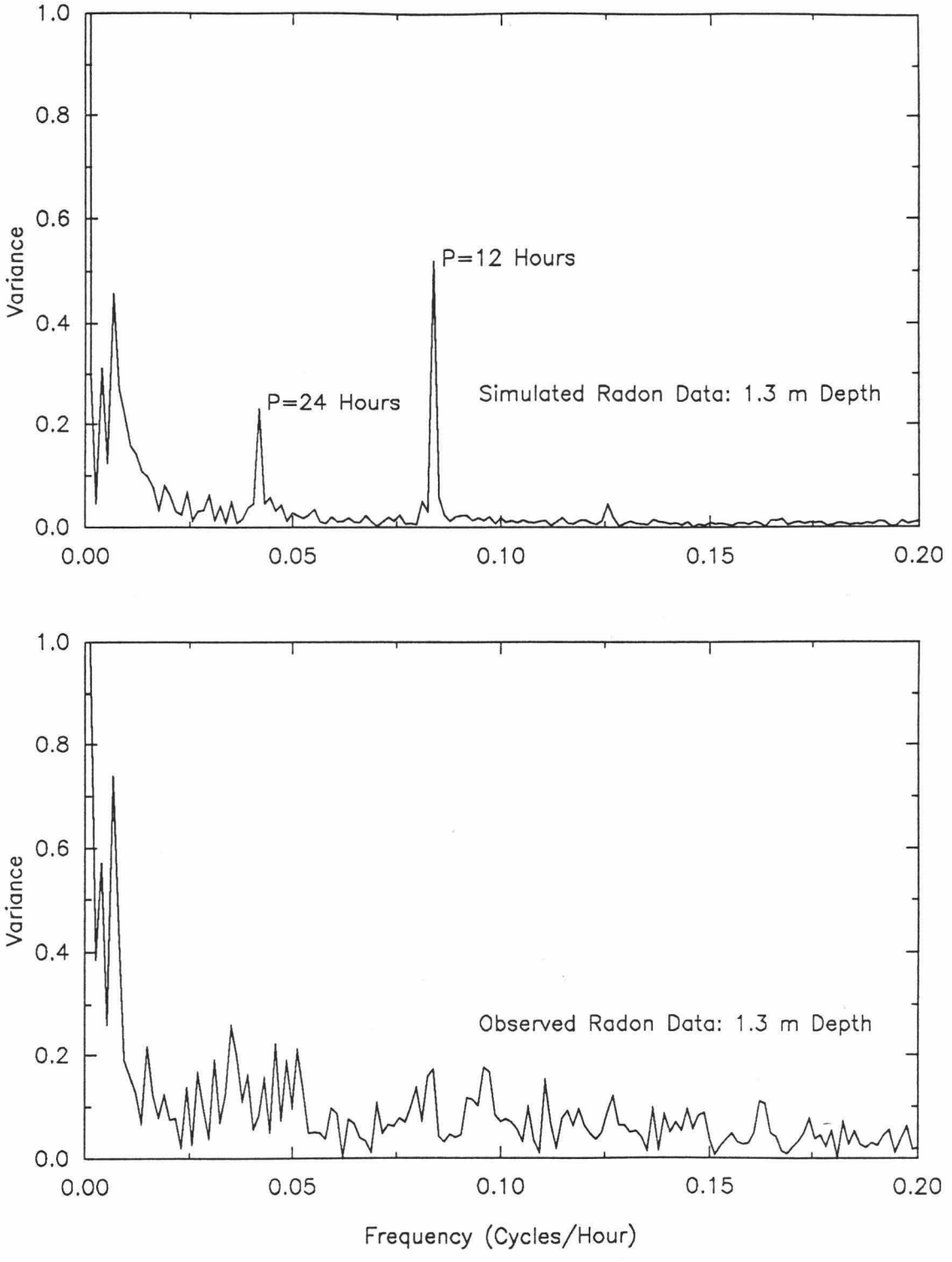

Figure 44. Fourier transforms of simulated and observed radon data at 1.3 m depth showing diurnal and semi-diurnal signal in simulated radon data only.

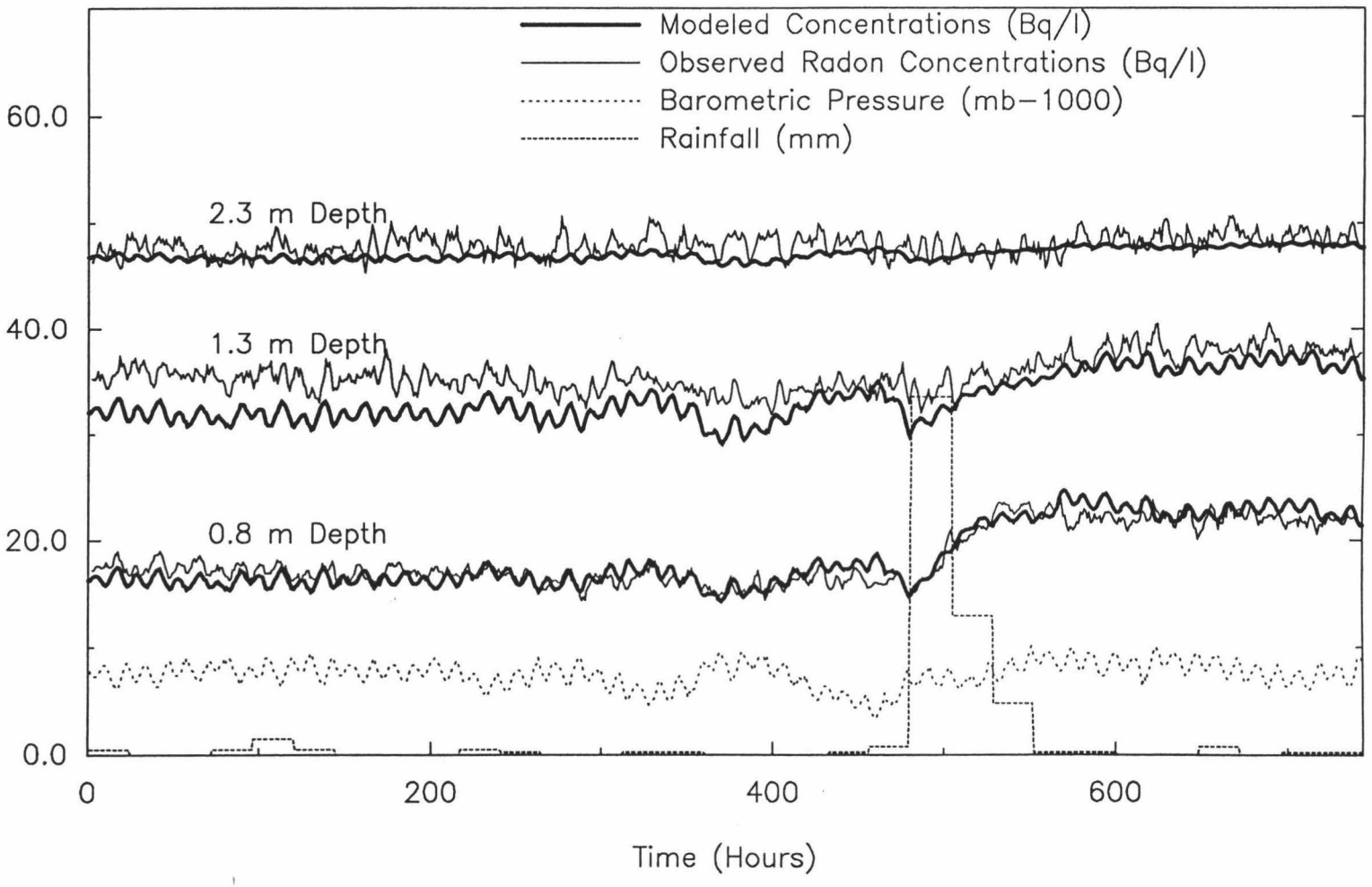

Figure 45. One dimensional simulated radon time series with varying soil parameters in response to rainfall event and observed radon time series showing model ability to track observed radon data.

At this point the model was considered calibrated in one dimension with respect to the effects of diffusion, air permeability and moisture content. The final values for the soil parameters at the conclusion of transient 1-D runs are given in Table 5. These values were used as initial base case values for the 2-D transient simulations.

Table 5

Final Soil Parameters From 1-D Simulations.

Depth (m)	Saturation	Intrinsic Air Permeability (k_{soil} - m^2)	Diffusion Coefficient (D_{soil} - m^2/s)	Emanation Coefficient
0 - 0.30	0.50	8.5×10^{-9}	8.0×10^{-6}	0.22
0.30 - 0.50	0.60	2.0×10^{-9}	1.0×10^{-6}	0.21
0.50 - 1.00	0.70	1.5×10^{-9}	8.0×10^{-7}	0.19
1.00 - 1.80	0.80	1.5×10^{-9}	7.0×10^{-7}	0.18
1.80 - 3.00	0.95	7.0×10^{-10}	5.0×10^{-7}	0.15

Radium content, all layers = 45.03 Bq/kg

e.) Transient, Two Dimensional Simulations

The soil parameters listed in Table 5 were used to initiate transient, 2-D simulations incorporating cracks in the model region. The examination of the effects of cracks on radon activities in the soil is essential because, as discussed previously, it is believed that subsurface discontinuities and preferential flow play a significant role in soil degassing and advective mixing, as well as increasing pathways for diffusional radon loss.

A typical finite element grid used for 2-D model runs is shown in Figure 46. Note that the grid is very fine near the soil surface, as well as in and near the crack. The fine grid is necessary in these areas because concentration and pressure gradients are high at the

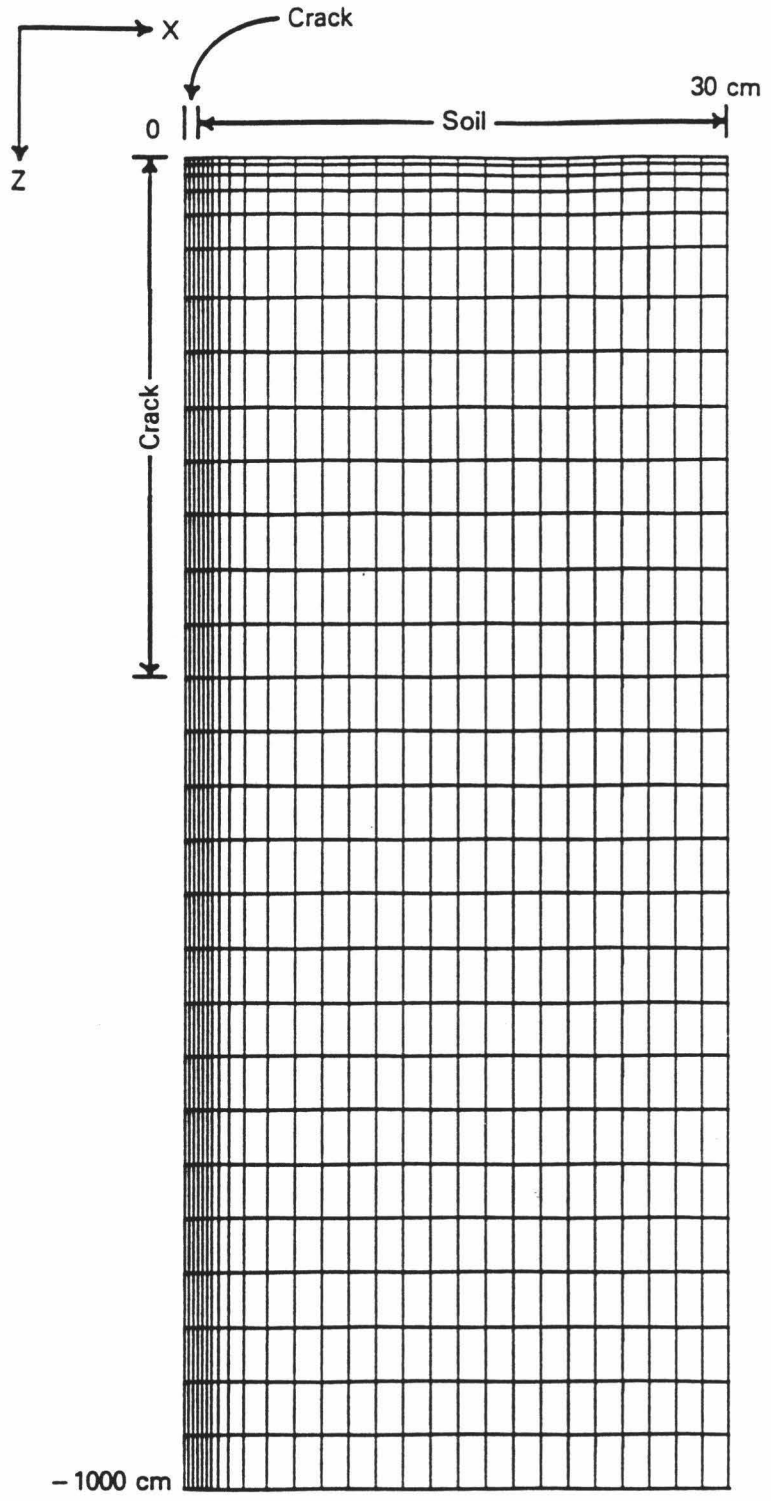

Figure 46. Typical finite element grid for 2-D model runs (Holford et al., 1989).

soil-air interfaces. The addition of a crack to the model region allows the simulation of advective radon flux in addition to diffusive radon flux. Due to the way in which the boundary conditions are defined for the 2-D model (Figure 4), advective radon flux is solely from the crack while diffusive radon flux continues to be from the soil surface. Figure 47 illustrates how total flux from a hypothetical, dry (sat=0), sandy soil modeled by Holford et al. (1989) responds to falling atmospheric pressure. The advective radon flux from the crack is much smaller than the diffusive radon flux from the soil surface because the crack is very small compared to the total soil surface.

Figure 48 shows the radon flux from a cracked soil with the characteristics given in Table 5 responding to decreasing atmospheric pressure: flux density increases as pressure decreases. Figure 48 also shows that the increase in flux is nonlinear for the first two hours but then becomes constant and proportional to the decrease in atmospheric pressure. Comparison of Figures 47 and 48 reveals that although the total flux from the highly saturated, silty clay soil type (Figure 47) is much less than the total flux from the very dry, sandy soil modeled by Holford et al. (1989), the relative portion of radon flux due to advective transport out of the crack is greater in the highly saturated soil than in the very dry soil. Although a comparison between a real soil and a hypothetical soil should not be emphasized too highly, this does seem to support the importance of cracks and discontinuities to advective transport of radon in a highly saturated, low permeability soil.

A cross-section of a 2-D simulation is presented in Figure 49 to show the effect of a changing atmospheric pressure with time on a soil region with the characteristics given in Table 5, and a 1 cm wide, 100 cm deep crack. The initial atmospheric pressure of 101500 Pa (1015.00 mb) is a common value for the field site. The soil gas pressures shown are responding to a drop in atmospheric pressure of -50 Pa/hr (-0.5 mb/hr), a typical semi-diurnal pressure change in Hawaii. Figure 49 shows that the subsurface pressure gradients slope towards the crack, but are strongest near the bottom of the crack.

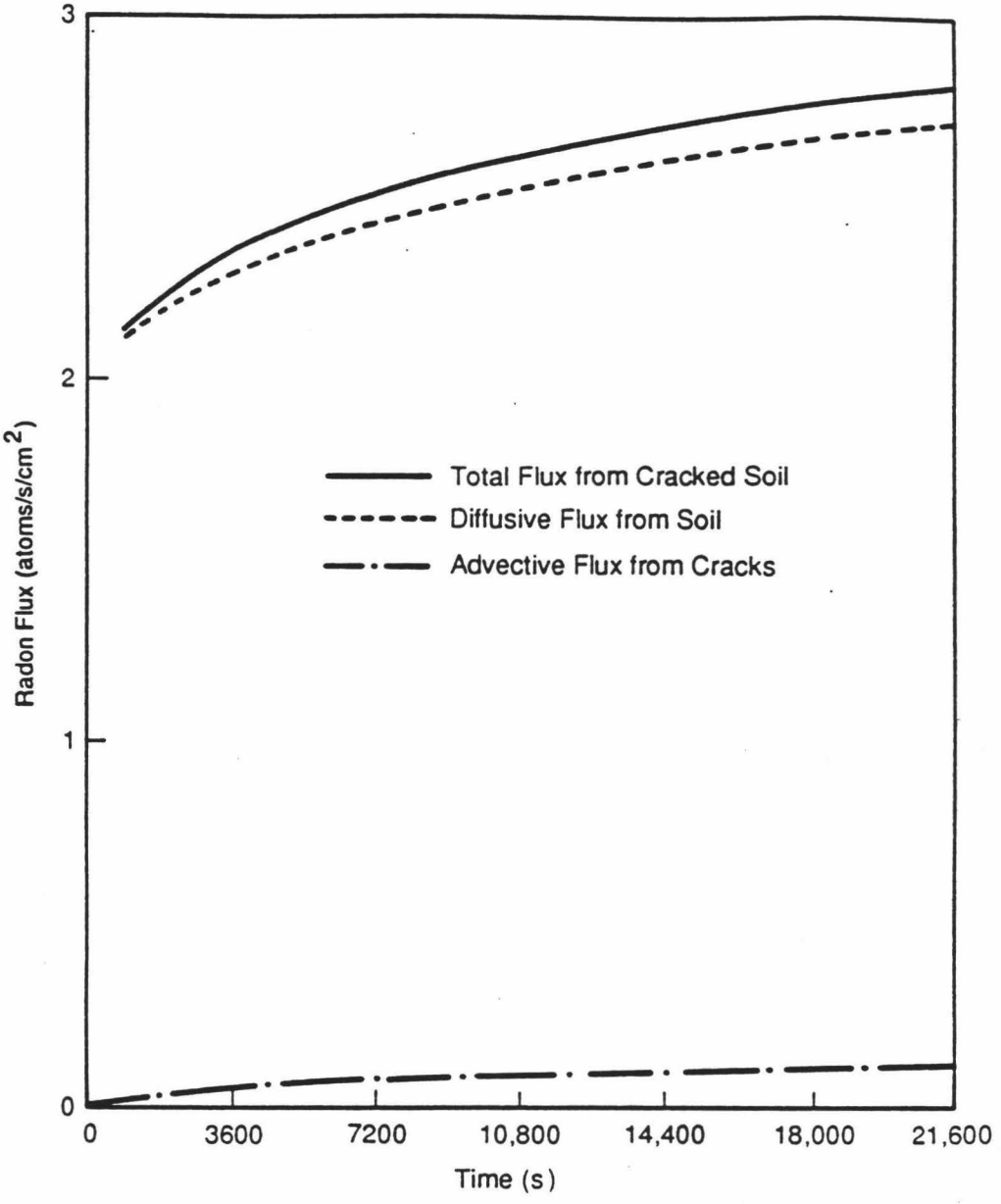

Figure 47. Effect of decreasing atmospheric pressure with time at a rate of -90 Pa/h on radon flux from a very dry (sat=0), sandy soil with cracks 400 cm deep, 0.06 cm wide and spaced 800 cm apart (Holford et al., 1989).

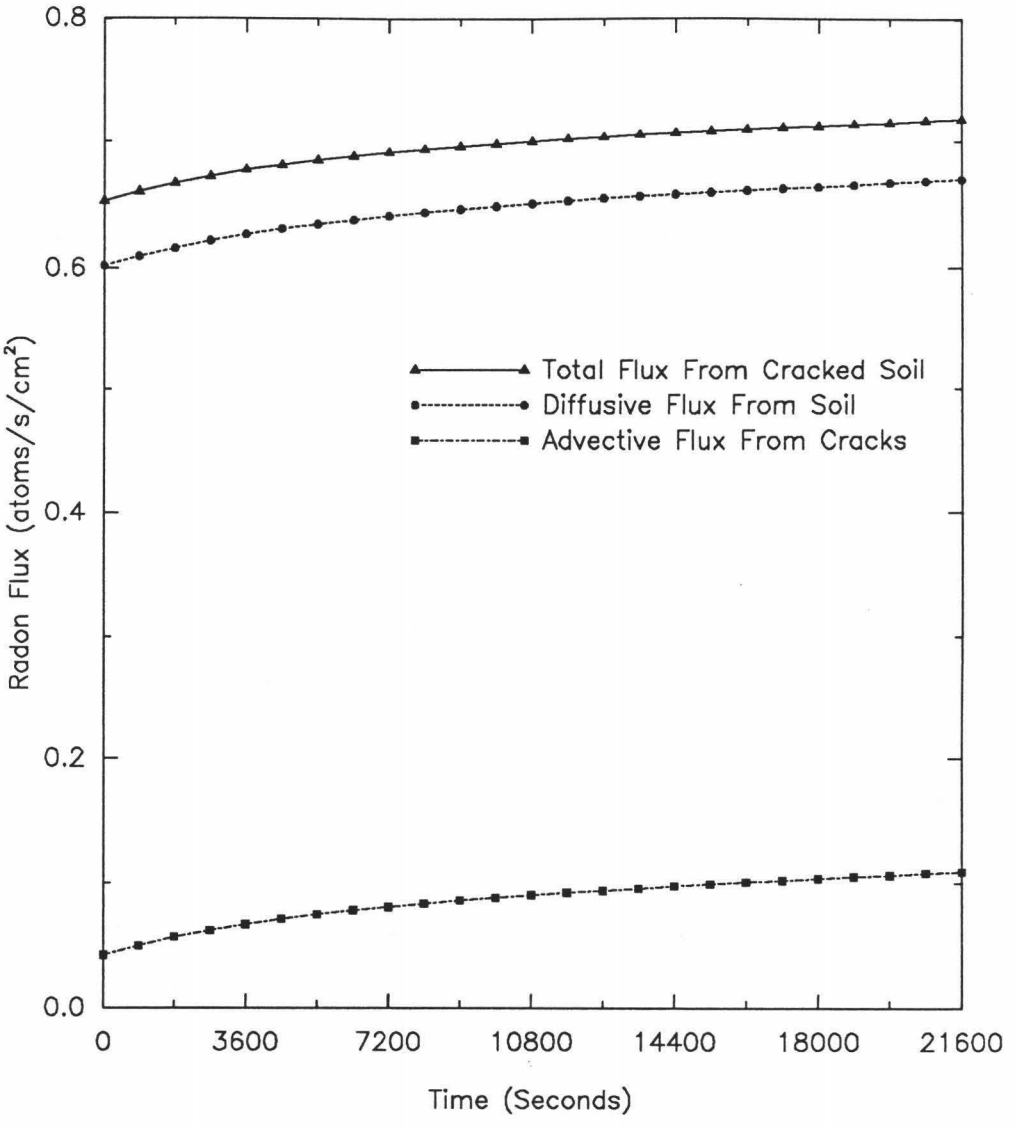

Figure 48. Effect of decreasing atmospheric pressure with time at a rate of -50 Pa/h on a soil with characteristics from Table 5 and cracks 50 cm deep, 1.0 cm wide and spaced 50 cm apart. Compare to Figure 47.

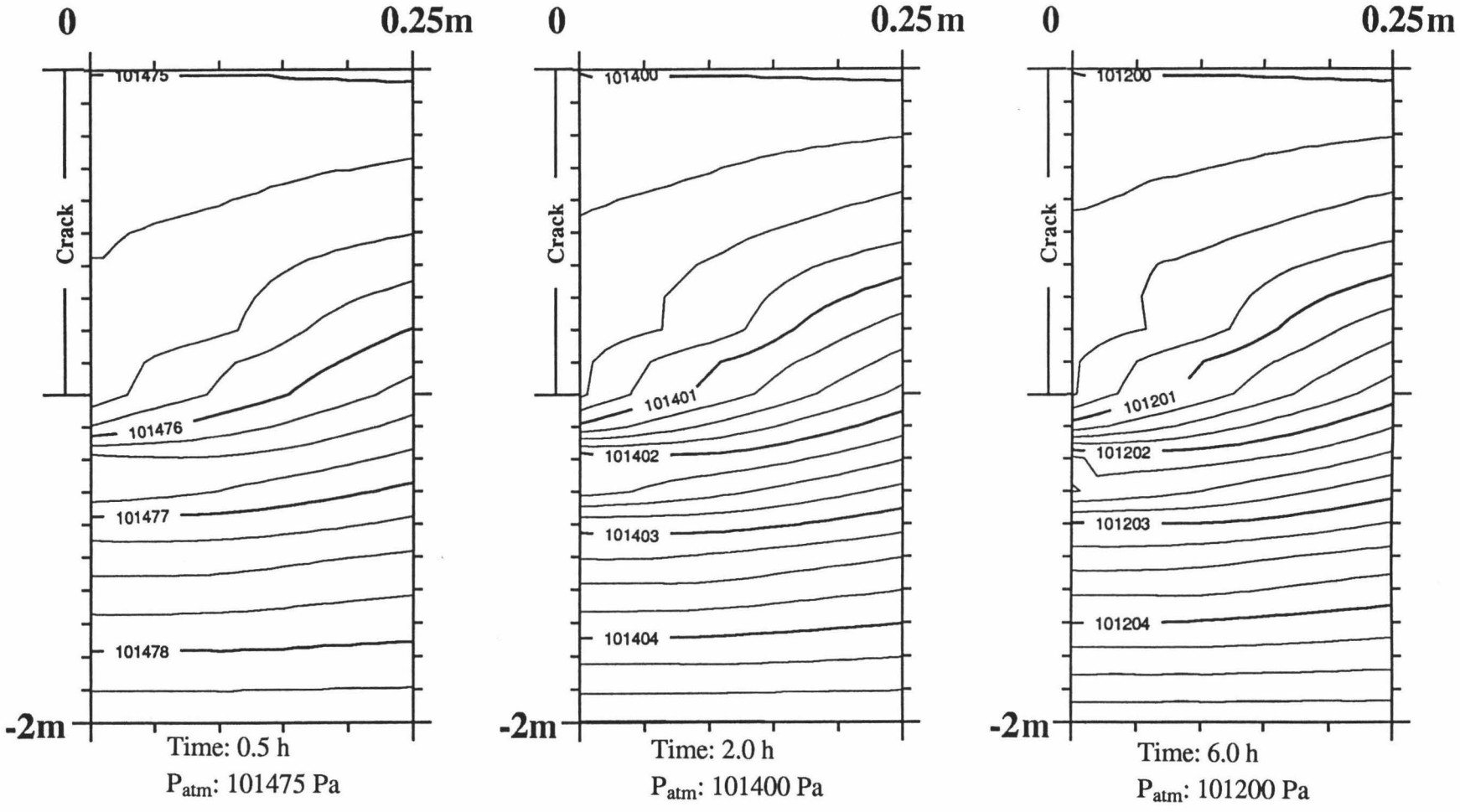

Figure 49. Two dimensional model run showing the effect of decreasing atmospheric pressure with time at a rate of -50 Pa/h on soil gas pressures (Pa) in a soil with characteristics from Table 5 and cracks 1.0 m deep, .01 m wide and spaced 1.0 m apart. Vertical scale is depth and horizontal scale is distance from center of crack.

Because of this pressure gradient, soil gas containing radon is drawn into the crack, where gas velocities are higher than those in the soil. Figure 50 illustrates that, due to the crack's higher permeability, radon concentrations in the crack increase with time, as higher concentrations are pulled up from deeper in the soil. It can also be seen that the radon concentrations in the crack increase more rapidly between 0.5 hrs and 2.0 hrs, than between 2.0 and 6.0 hrs (Figure 50), indicating that the pressure gradients and radon concentrations eventually reach some steady rate of increase, as illustrated in Figure 48. Figure 51 presents the radon response to a rise in atmospheric pressure of 50 Pa/hr (0.5 mb/hr) with the same soil conditions and crack size as Figure 50. Increasing surface pressures causes the flow of soil gas to reverse: air now flows into the crack and the soil. Radon concentrations in the crack now decrease, rapidly at first, but again reaching some steady rate, proportional to the increase in pressure (Figure 48).

2.) Sensitivity Analysis

In order to better understand how the important input parameters affect radon flux densities from the cracked soil model, a sensitivity analysis was performed. Crack dimensions (depth, width and spacing) were varied and the effect on flux densities were compared to fluxes from a one-dimensional, uncracked soil model. The soil properties, intrinsic permeability and diffusion coefficient, were also perturbed to examine the effect on the radon flux.

a.) Crack Dimensions

Cracks of different depths, widths and spacings were modeled to see how much the total radon flux could be enhanced in comparison to the flux predicted by a soil model without cracks. All other parameters are as shown in Table 5 and Figure 37. The results of the cracked soil model and uncracked soil model were compared after 6 hours of

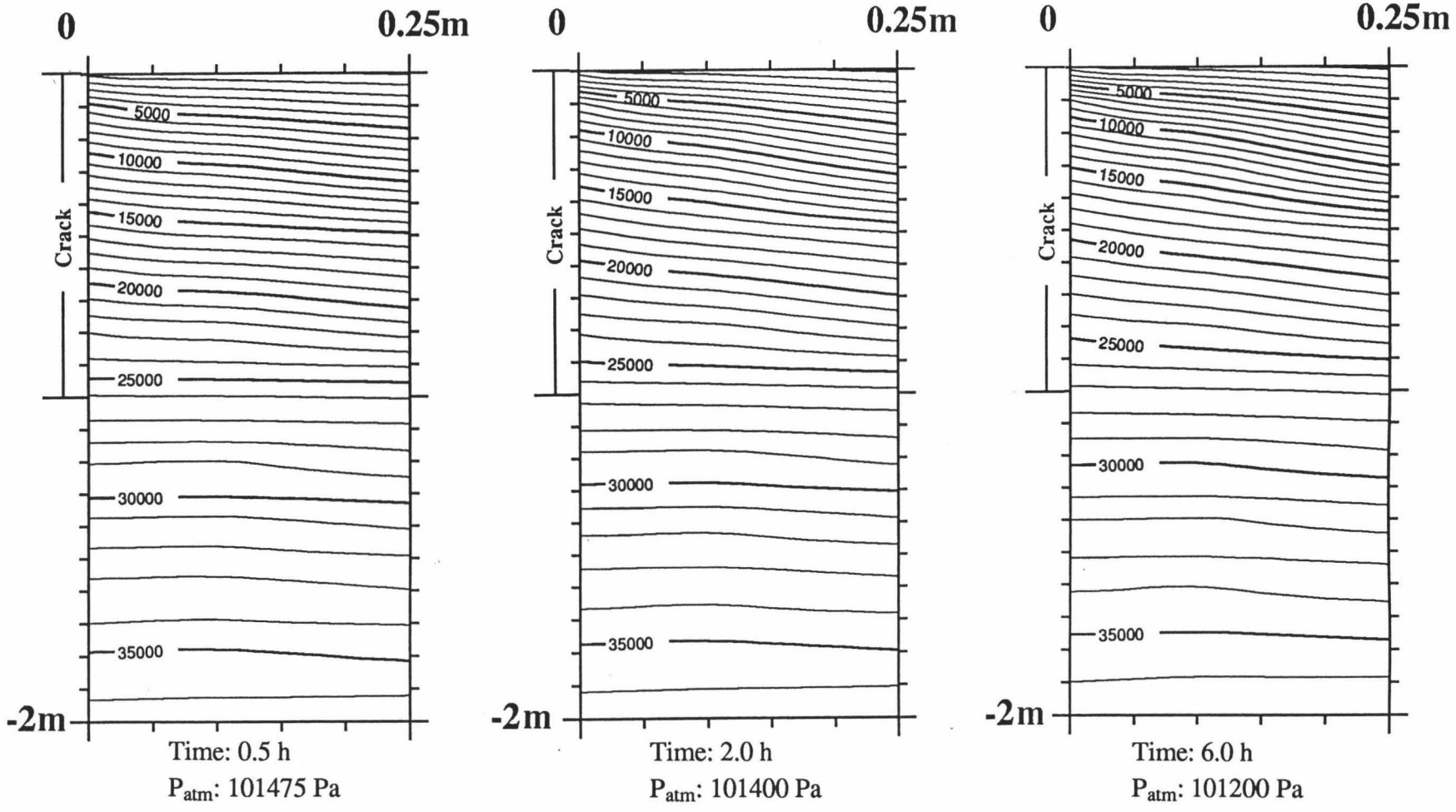

Figure 50. Two dimensional model run showing the effect of decreasing atmospheric pressure with time at a rate of -50 Pa/h on radon concentrations (Bq/m^3) in a soil with characteristics from Table 5 and cracks 1.0 m deep, .01 m wide and spaced 1.0 m apart. Vertical scale is depth and horizontal scale is distance from center of crack.

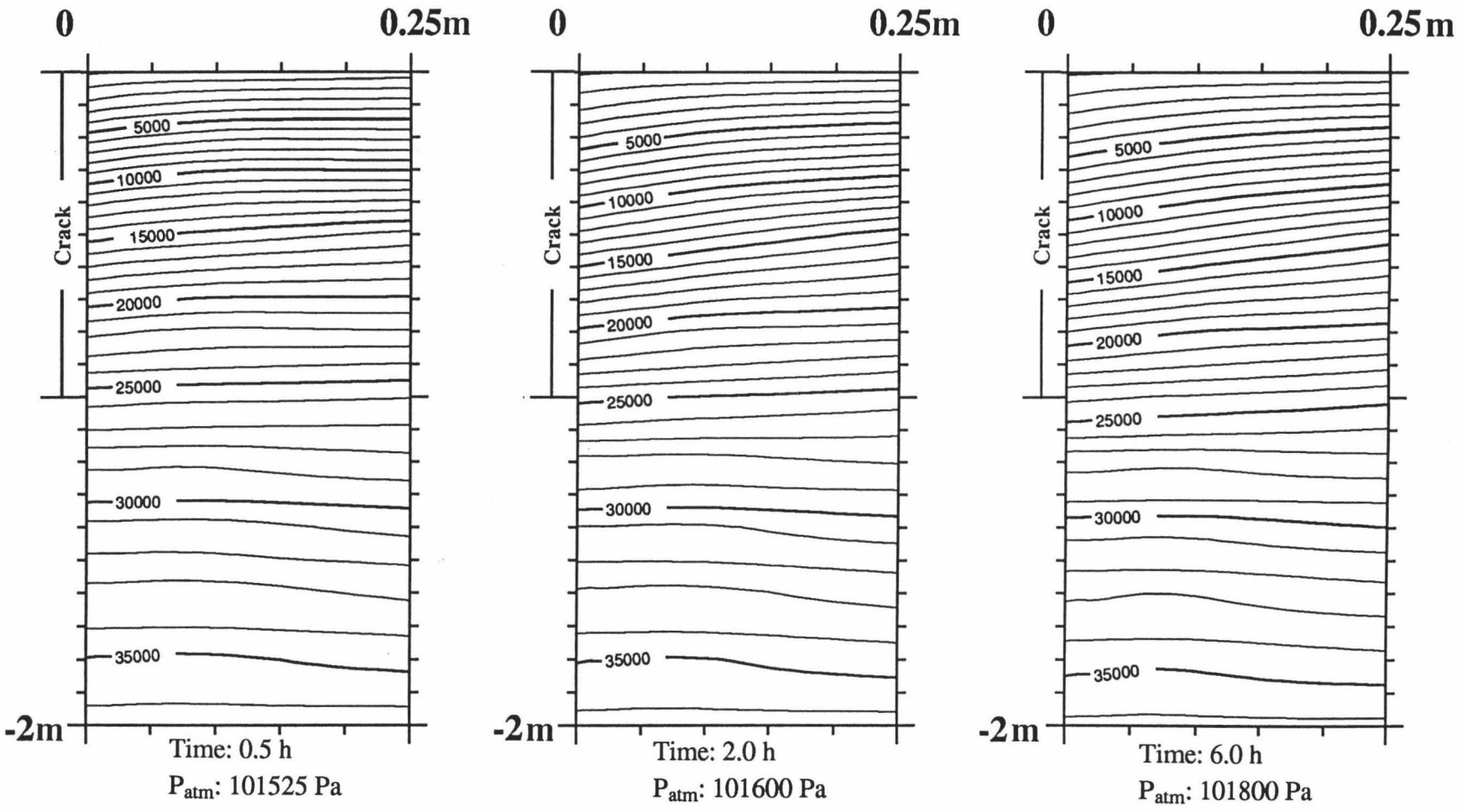

Figure 51. Two dimensional model run showing the effect of increasing atmospheric pressure with time at a rate of 50 Pa/h on radon concentrations (Bq/m3) in a soil with characteristics from Table 5 and cracks 1.0 m deep, .01 m wide and spaced 1.0 m apart. Vertical scale is depth and horizontal scale is distance from center of crack.

decreasing atmospheric pressure at a rate of -50 Pa/hr. The formula used to compare the flux predicted by the cracked soil model to the uncracked soil model is:

$$\text{Percent increase in flux} = \frac{F_c - F_u}{F_u} \times 100 \qquad (5.7)$$

where, F_c = radon flux predicted by cracked soil model ($Bq/s/m^2$, after 6 hr)
F_u = radon flux predicted by uncracked soil model ($Bq/s/m^2$, after 6 hr).

The effects of increasing crack depth, for cracks which are 0.5 cm wide and spaced 100 cm apart, are shown in Figure 52, where an increase in crack depth results in an increase in radon flux compared to the uncracked model. Cracks less than 50 cm deep do not enhance radon flux densities above the uncracked soil model, due to the small difference between the diffusion coefficient of the air in the crack (10^{-5} m^2) and the diffusion coefficient of the top soil layer (8×10^{-6} m^2). The large jump in radon flux densities between cracks 100 and 150 cm deep in Figure 52 is attributed to enhanced radon flux when crack depth becomes greater than crack spacing. As Figure 49 illustrated, the strongest pressure gradients are near the bottom of the crack, which is where the most radon will move into the crack. Hence, a deeper crack brings up higher radon concentrations from depth.

Figure 53 shows the effect of crack width and spacing on the percent increase in radon flux in comparison to an uncracked soil for a 200 cm deep crack. As crack width increases from 0.1 to 1.0 cm, so does radon flux, becoming more nonlinear as crack width increases (Figure 53). This effect can also be seen in Figure 54, where, for 200 cm deep cracks spaced 50 cm apart, the flux density increases very little for cracks as small as .075 to 0.1 cm. Cracks less than 0.075 cm wide, which can essentially be considered part of the soil, do not enhance fluxes above that predicted by the uncracked soil model.

Figure 53 showed the enhancement of radon flux for 200 cm deep cracks, at decreasing spacing intervals. Figure 55 illustrates a similar effect, but for cracks which are

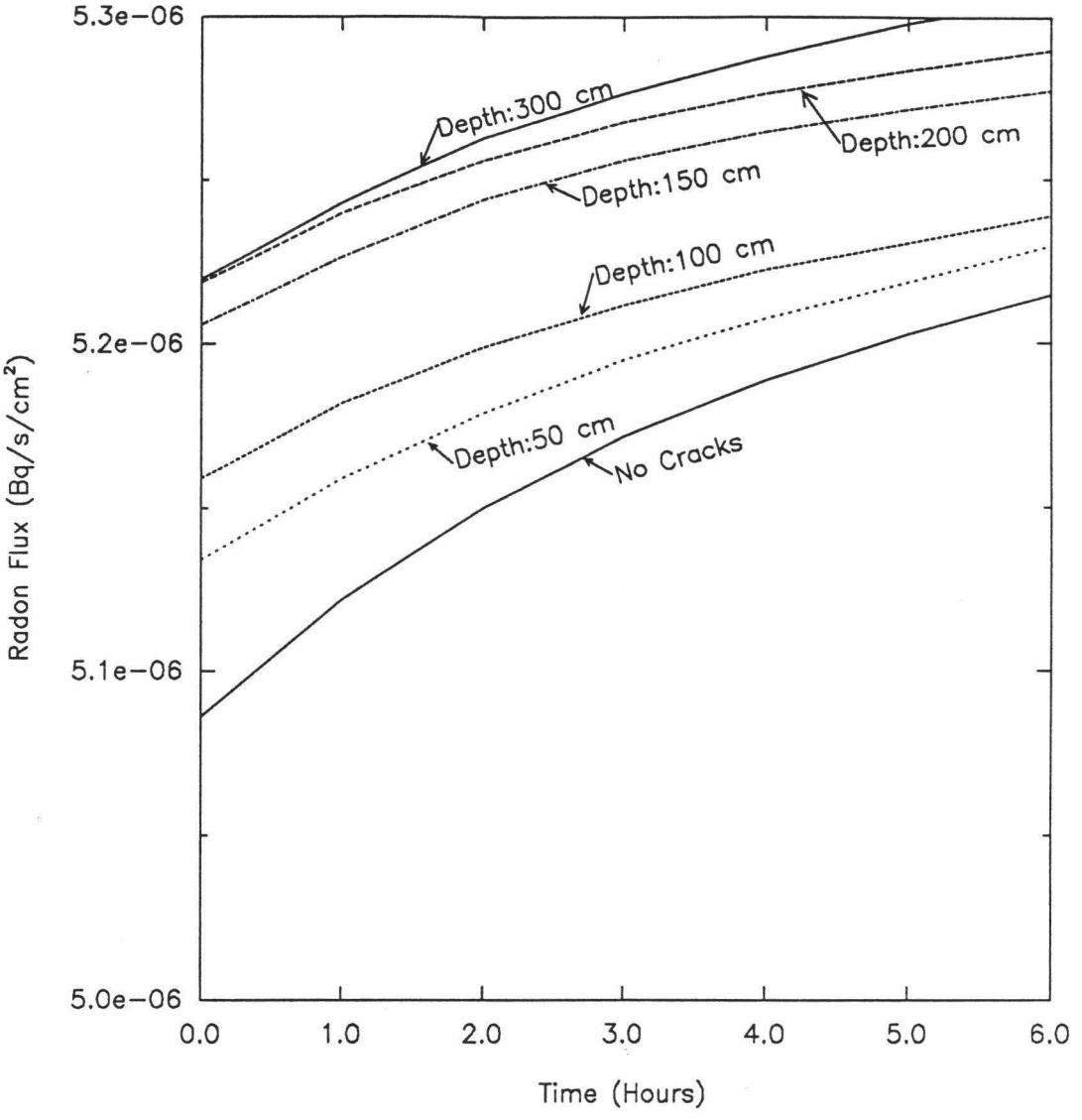

Figure 52. Effect of crack depth on radon flux from soil with cracks 0.5 cm wide and spaced 100 cm apart during 6 h of decreasing atmospheric pressure (-50 Pa/h).

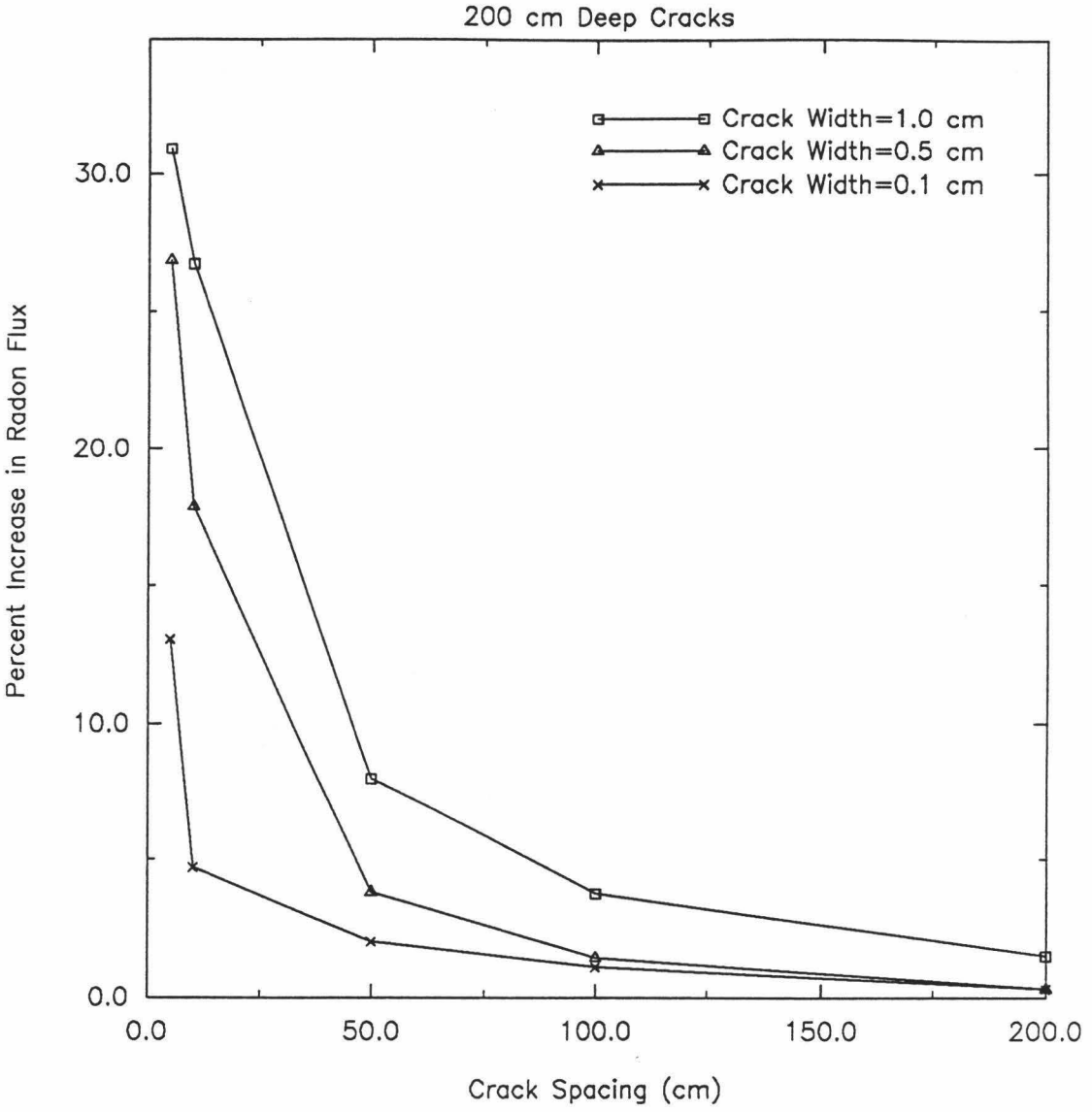

Figure 53. Effect of spacing and crack width on percent increase in radon flux between soil without cracks and soil with 200 cm deep cracks after 6 h of decreasing atmospheric pressure (-50 Pa/h).

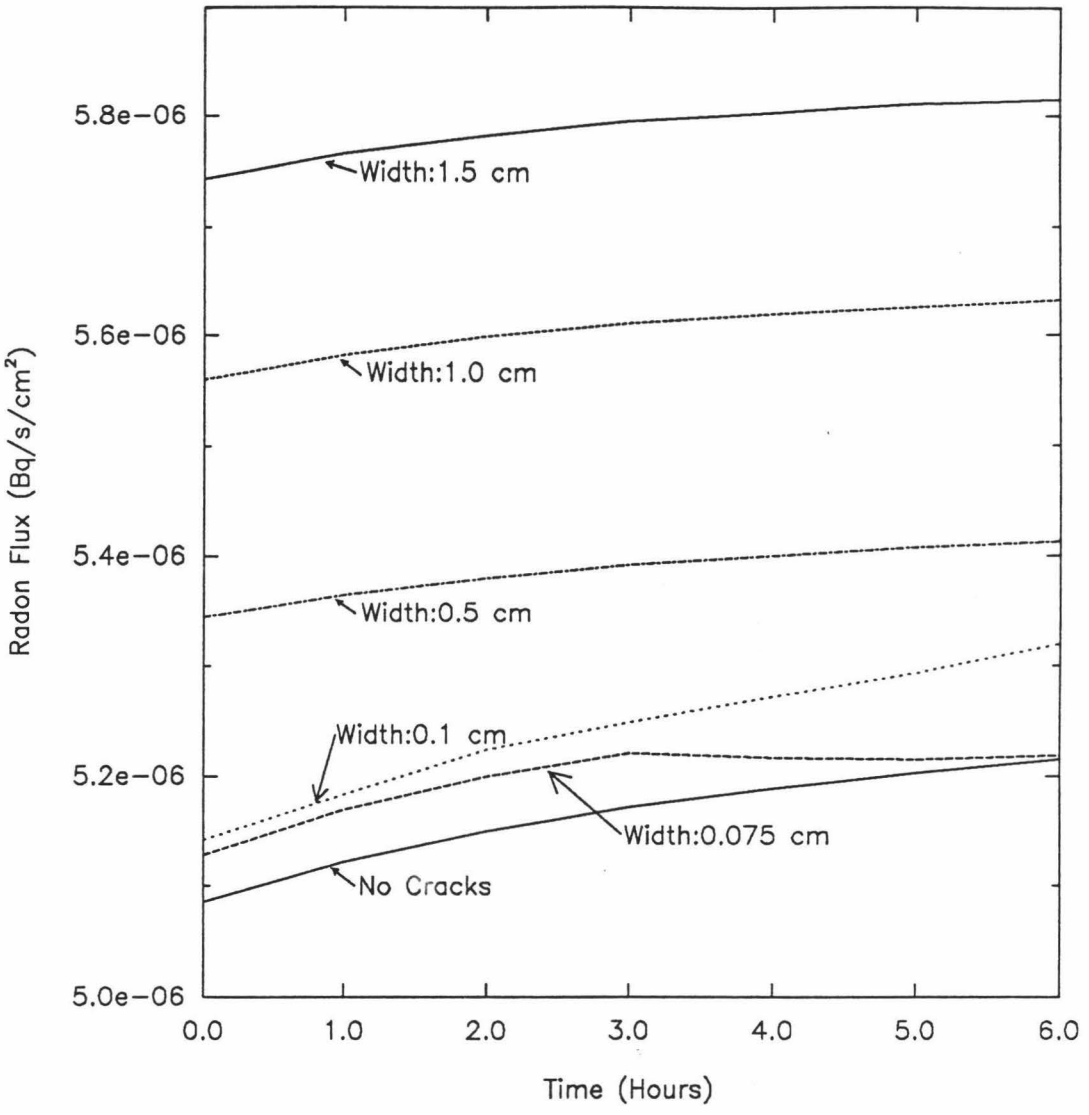

Figure 54. Effect of crack width on radon flux from soil with cracks 200 cm deep and spaced 50 cm apart during 6 h of decreasing atmospheric pressure (-50 Pa/h).

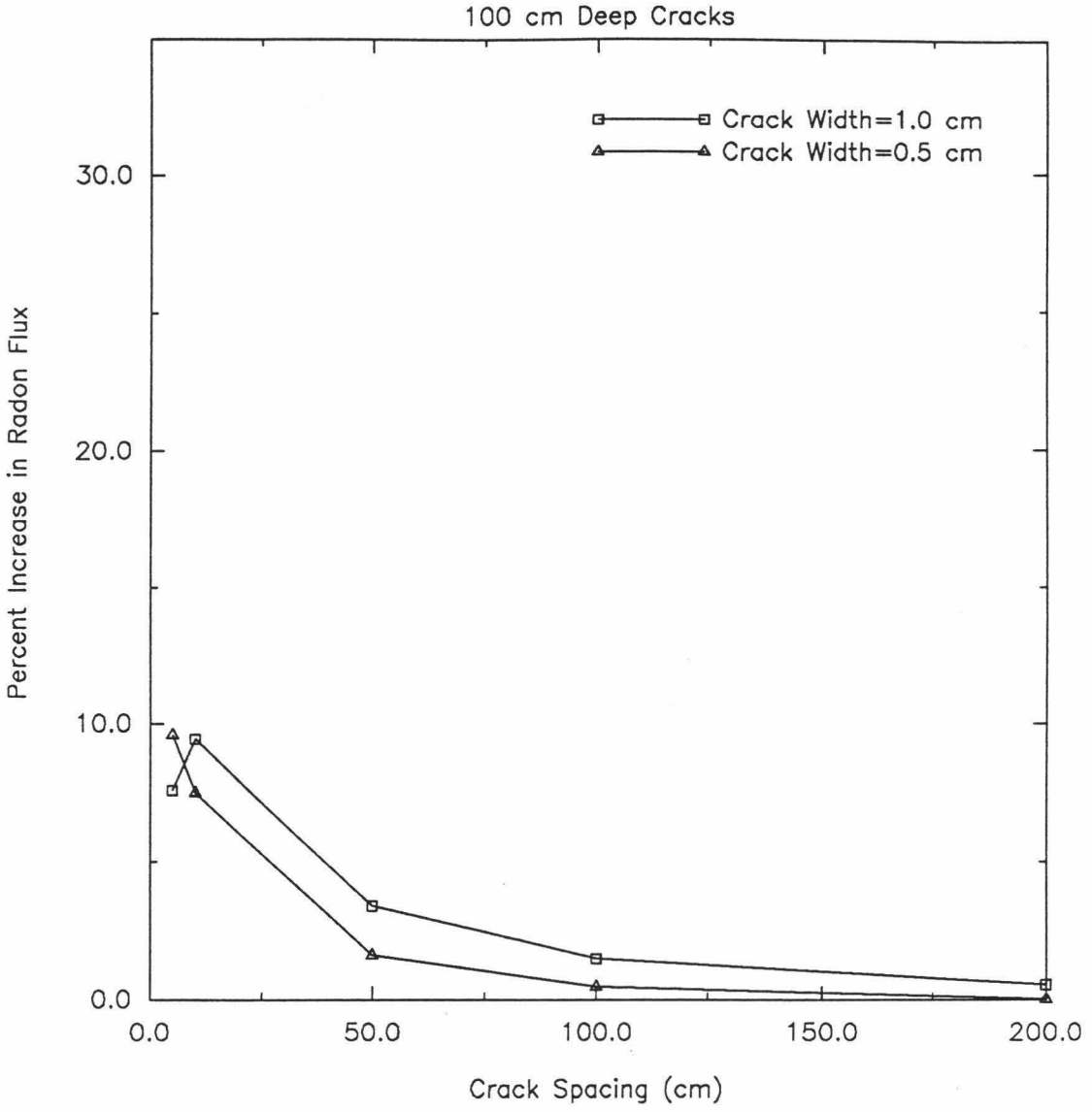

Figure 55. Effect of spacing and crack width on percent increase in radon flux between soil without cracks and soil with 100 cm deep cracks after 6 h of decreasing atmospheric pressure (-50 Pa/h).

100 cm deep. The percent increase in flux is substantially less than for the deeper case (Figure 53), but the trend is essentially the same: cracks spaced closer than 50 cm apart show the greatest flux enhancement over the uncracked case. The same trend is evident in Figure 56 as well, for cracks 1.5 cm wide and 150 cm deep, the flux enhancement is very small until the spacing between cracks is less than 50 cm.

The slight decrease in flux enhancement seen in 1.0 cm wide cracks spaced 10 cm apart (Figure 55) may be due to instability in the model. Holford et al. (1989) reported that, for a dry (sat=0), sandy soil, flux densities actually decreased when crack spacing became less than crack depth. This apparent anomaly was attributed to decreased pressure and concentration gradients in a soil with closely spaced cracks. The small gradients then oppose the effect of closer crack spacing in increasing radon flux. This effect, although not observed in this study except as mentioned in Figure 55, may indicate an instability in the RN3D solution to the flow and transport equations in certain situations as it is intuitively obvious that increasing the crack density of a soil should always enhance radon flux.

In general, the largest enhancement of radon flux during decreasing atmospheric pressure seems to occur when relatively deep cracks (200 cm) are spaced within at least 50 cm of each other. This seems reasonable because a deeper crack will intercept higher radon concentrations and the greater the number of cracks per unit area the greater will be the flux density. Increasing crack width results in a nonlinear increase in flux densities once the width is greater than about 0.1 cm.

b.) Soil Air Permeability

Soil air permeabilities (k_{soil}) for each layer were increased to values from 0.5 to 3 orders of magnitude higher than the levels given in Table 5 (base k_{soil} values) while soil diffusion coefficient and crack dimensions were held constant. As Figure 57 shows, radon flux increases slightly over the base case levels for increasing permeability soils during six

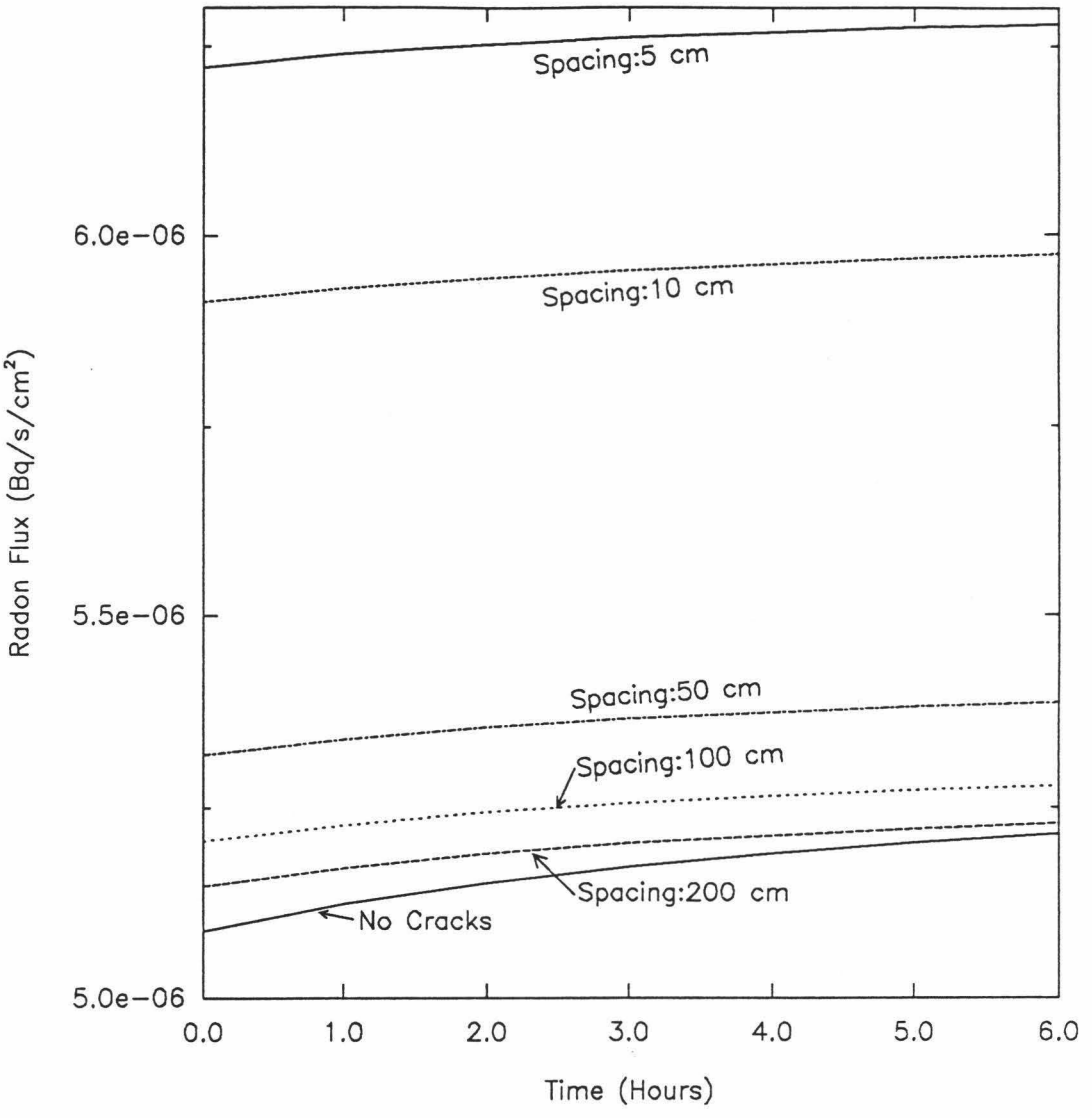

Figure 56. Effect of crack spacing on radon flux from soil with cracks 0.5 cm wide and 150 cm deep during 6 h of decreasing atmospheric pressure (-50 Pa/h).

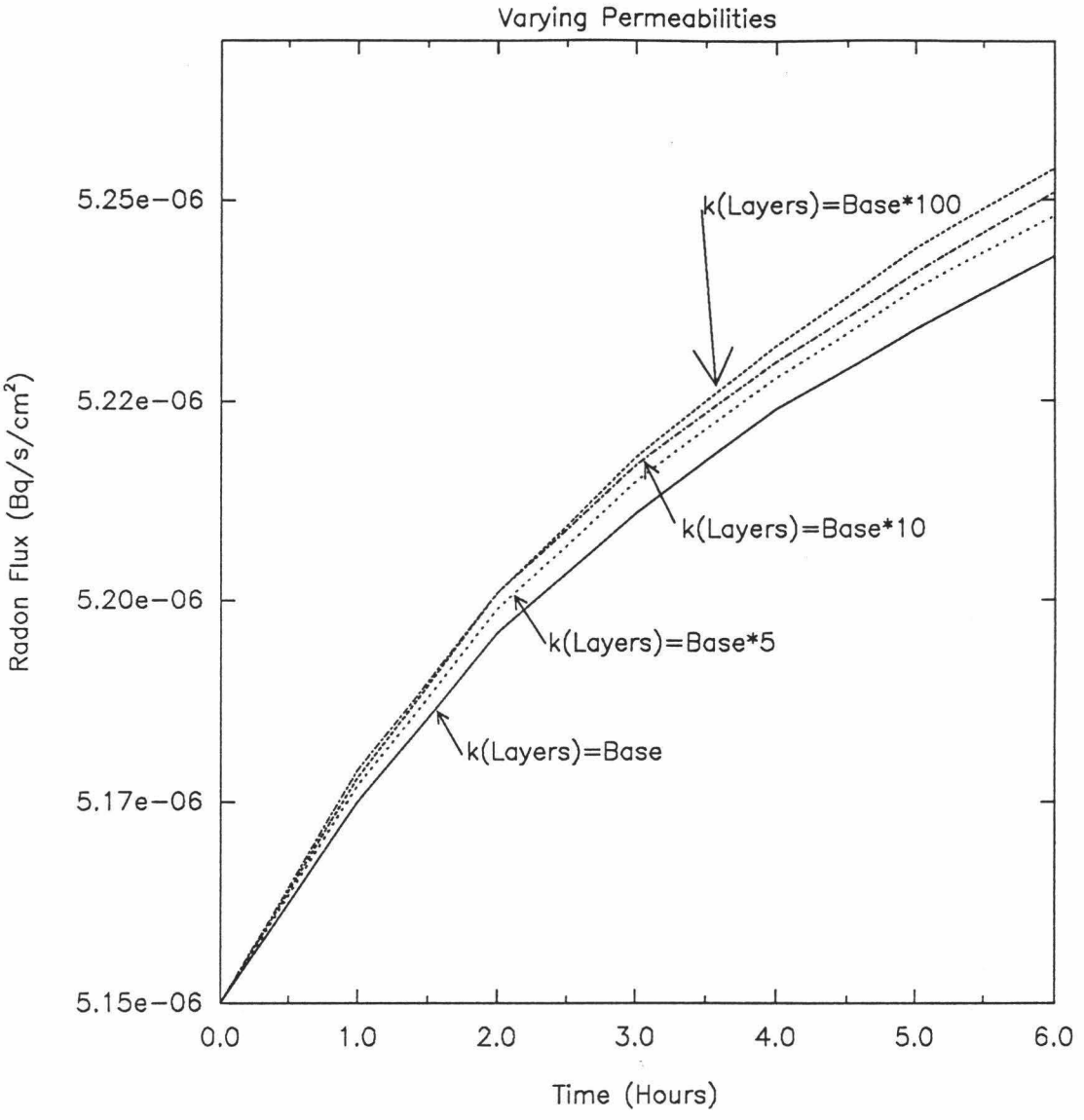

Figure 57. Effect of increasing soil air permeabilities above values in Table 5 (Base) on radon flux from soil with cracks 100 cm deep, 1 cm wide and spaced 200 cm apart during 6 h of decreasing atmospheric pressure (-50 Pa/h).

hours of decreasing atmospheric pressure. This is to be expected because soil gas velocities, and hence advective flux, are increased for higher permeability soils (Table 3). Interestingly, increasing the soil permeability above base*100 results in a very slight decrease (too small to be seen in Figure 57) in radon fluxes and further increase in permeability, (base*1000) results in a further small decrease in radon flux. Although air permeabilities greater than $k_{soil} = 10^{-7}$ m^2 are probably unrealistic for the soil at the Poamoho site (silty clay), the apparent decrease in radon flux with increasing permeability may indicate another instability in the RN3D solution to the governing equations as it seems clear that increasing soil air permeability must always result in enhanced transport of radon out of the soil under conditions of decreasing atmospheric pressure.

Holford et al. (1989) reported a similar effect in a sensitivity analysis performed on a dry (sat=0), sandy soil. The explanation given for the decreased radon flux with increasing permeability was: for low permeability soils, surface pressure changes are not propagated into the soil to any great extent, causing very high pressure gradients in the immediate vicinity of the crack and soil surface. Since gas velocities are directly proportional to pressure gradients (Darcys law), high gradients will produce high gas velocities and high fluxes. For a high permeability soil, pressure changes are propagated further into the soil, resulting in lower pressure gradients, lower gas velocities and relatively decreased fluxes.

For the soil type being investigated by this study, this would not seem to be a factor until permeabilities are increased to somewhat unrealistic levels, however further analysis of this apparent anomaly should be undertaken in drier, higher permeability soils to determine if this is a significant factor affecting radon fluxes in real-world situations, or if this is an artifact of model instability and unrealistic simplifying assumptions made in the development of the radon transport model.

c.) Soil Diffusion Coefficient

Soil diffusion coefficients (D_{soil}) were varied while soil permeabilities and crack dimensions were held constant. The base level diffusion coefficients for each layer are those given in Table 5. For the cracked soil model it can be seen in Figure 58 that, as expected, flux density is directly proportional to diffusion coefficient. An increase in diffusion coefficient results in increased ability of the soil to transport radon into the atmosphere and thus radon flux rises substantially. Conversely, decreasing diffusion coefficients causes the radon flux to decrease (Figure 58).

Comparing the increases in flux densities due to crack dimensions and spacing, permeability and diffusion coefficient, it is clear that the modeled radon fluxes are the most sensitive to the diffusion coefficient, followed by the physical characteristics of the cracks, and then by permeability. For both 1-D and 2-D simulations, radon flux is directly proportional to the diffusion coefficient. For 2-D simulations with cracks, the diffusion coefficient is still the dominant parameter but the spacing and density of the soil cracks can affect radon fluxes significantly. Soil permeability appears to have the smallest affect on radon flux.

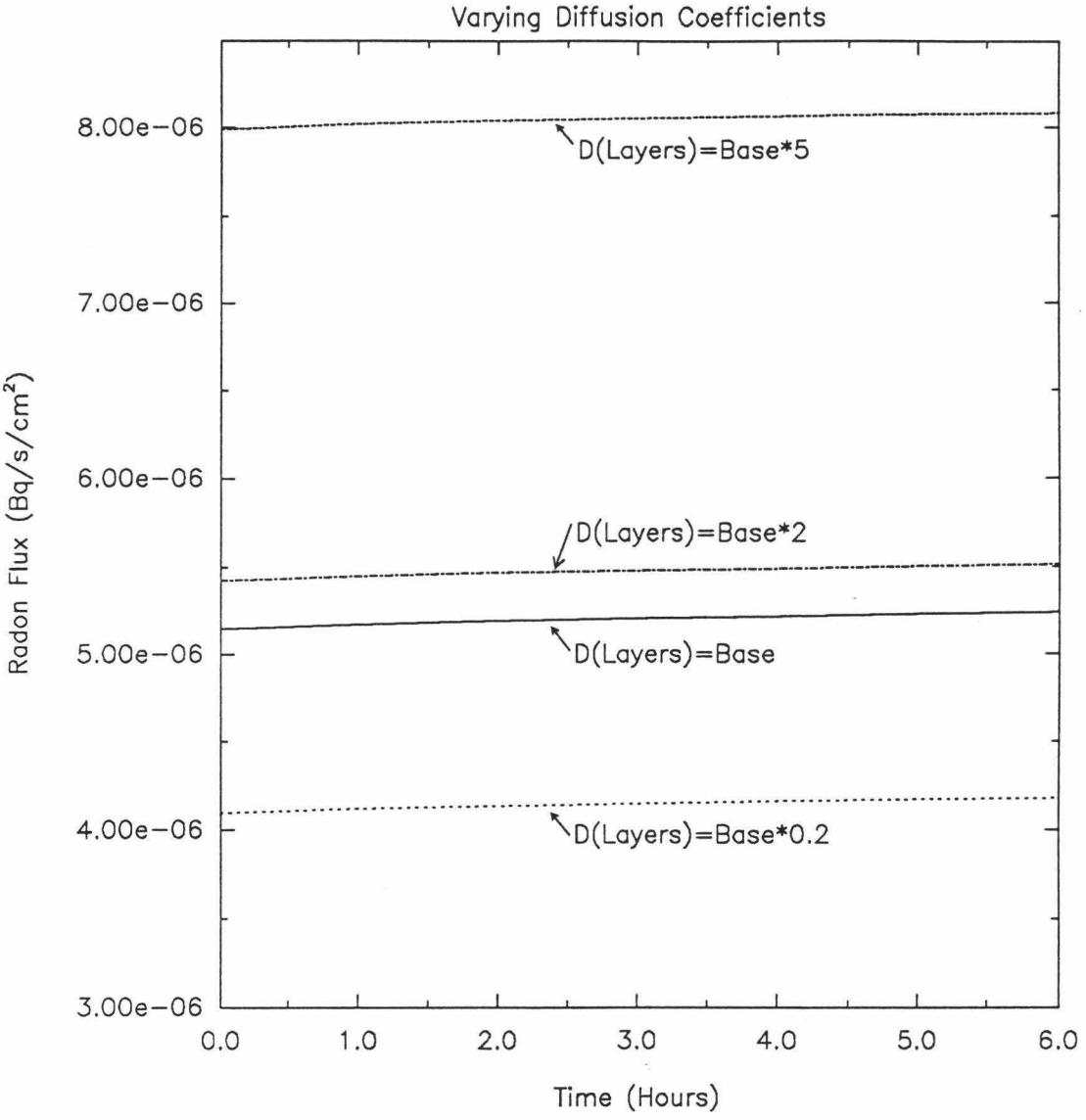

Figure 58. Effect of varying diffusion coefficients from values given in Table 5 (Base) on radon flux from soil with cracks 100 cm deep, 1 cm wide and spaced 200 cm apart during 6 h of decreasing atmospheric pressure (-50 Pa/h).

CHAPTER 6

CONCLUSIONS

The data obtained thus far from the radon and environmental monitoring study have provided a substantial database on radon response to a variety of natural and artificially induced conditions. The effects of soil moisture, atmospheric pressure changes, subsurface permeability discontinuities and the extent of advective mixing of soil gas with atmospheric air have been physically correlated with radon activities in soil gas. In addition, modeling of the radon activity data has revealed the relative importance of soil physical characteristics and how these characteristics interact with environmental processes to significantly alter radon activities and flux within and from the soil.

One of the most significant findings of the field monitoring program is that extreme care must be taken in the deployment of radon monitoring instrumentation to ensure that the disturbance to the soil profile and the presence of the instrument itself has not irretrievably perturbed the normal radon response. The work carried out in this study suggests that open channels in the soil can significantly enhance advective movement of soil gas, especially in a highly saturated, low permeability soil.

Although the presence of the radon monitoring probes used in this study clearly have an effect on radon response, particularly in the shallower soil, substantial evidence has been presented for the existence of pressure-driven movement of soil gas containing radon as well as advective mixing of atmospheric air with shallow soil gas. The dependence of radon concentrations on depth in this soil type (silty clay) implies that shallow soil advective mixing and diffusive loss of radon are the factors which control the overall concentrations of radon in the shallow soil (≤ 1.3 m) at this particular site. At deeper levels (> 2 m), radon concentrations are close to equilibrium and are controlled by the amount of radium precursor present and the emanation characteristics of this soil.

The response of radon activities to increased soil saturation resulting from rainfall events suggests that, for a highly saturated silty clay soil, soil moisture exerts the greatest impact on radon concentrations at the three depths which were monitored. Large radon activity increases accompanying moderate to intense rainfall events are believed to be due to blockage of the advective and diffusive pathways decreasing the advective and diffusive exchange of soil gas radon with atmospheric air leading to an increase in soil radon concentrations. Conversely, during extended periods of little or no precipitation, steady declines in radon activities were observed due to soil drying and desiccation that allowed increasing advective and diffusive loss of radon.

Bearing in mind that the emplacement of the alphameter instruments in the soil profile may be enhancing the apparent effects of pressure-driven variations in radon activities, the radon response to synoptic barometric pressure changes clearly shows a significant perturbation to depths of at least 1.3 m. In addition, the semi-diurnal, S-2 pressure wave has a clear, consistent effect on radon activities at 0.8 m depth, and a less persistent effect at 1.3 m. The effects on radon activities due to very high frequency, wind-driven pressure changes are inconclusive at this point. Additional data need to be collected and analyzed to determine the effect wind-driven turbulent pumping may have on radon activities and flux.

Results from the advective barrier experiment support the findings expressed above: the radon activities at 0.8 m and 1.3 m depth under the barrier, where advective mixing and flux are inhibited by the barrier, are distinctly higher than radon activities at the same depths in the control monitoring array. If it can be assumed that diffusional radon loss through the barrier is similar to the normal case, this provides strong evidence that the advective movement of soil gas due to the propagation of atmospheric pressure changes through the soil exerts a substantial control over shallow radon behavior.

The results of the radon monitoring program were used to evaluate and modify the radon transport code, RN3D. The model was successfully calibrated using the existing field data and has been shown to accurately predict the observed radon concentration profile as well as the observed pressure-driven and moisture-driven radon variations in soil gas. Analysis of the field monitoring data using RN3D has shown that the measured soil air permeability at the field site was too low to adequately account for the observed radon variations. This suggests that the measurement technique which was used to determine the soil air permeability does not account for large-scale soil features such as cracks, macropores and root channels which can significantly affect soil gas advective transport rates.

A sensitivity analysis of the model input parameters revealed that radon flux from soil is most strongly affected by the diffusion coefficient, which is a function of soil moisture content. The second factor impacting radon flux densities from soil is the depth, width and spacing of soil cracks. The modeling analysis showed that relatively shallow cracks such as would result from normal soil drying and desiccation may have a slight to moderate affect on radon flux, but that deeper cracks introduced by plant roots or man-made disturbances can substantially enhance radon flux density. The least important factor to the modeled radon fluxes is the gas permeability of the soil, which is also controlled by soil moisture content.

RN3D has been shown to be a useful tool for the prediction of subsurface radon activities and fluxes if adequate constraining data are available. Some instability in the model solutions may exist in certain cases and further analysis of the model and comparison of field data to modeled results are required to determine if RN3D can correctly characterize a variety of "real world" situations or if some of the simplifying assumptions made by the model need to be modified.

Appendix A. Soil Descriptions and Water Retention Data

Descriptions of soil profiles, laboratory analyses and water retention data for the Poamoho field plot are presented in Tables 6 and 7. Figure 59 illustrates the water characteristic curve for the Poamoho soil measured by Green et al. (1982) at a depth of 1 m or less. Figure 59 also shows the water characteristic curve measured by Miller (1987) on a characteristic Wahiawa series soil for a depth of approximately 2 m.

Table 6

Poamoho Soil Profile (Green et al., 1982)

Site:	W1
Soil:	Wahiawa silty clay, Tropeptic Eutrustox; clayey, kaolinitic, isohyperthermic family
Location:	O'ahu UH Poamoho Experimental Farm; Poamoho II site, about 15 m SW of Kaukonahua Rd. and 46 m NW of reservoir
Date:	5 July 1977
Description by:	S. Nakamura, Soil Conservation Service
Topography:	Gently sloping upland; 7% slope
Parent Material:	Residuum from basic igneous rock
Elevation:	213 m
Annual Rainfall:	1,016 mm
Drainage and Permeability:	Well drained; moderately rapid permeability (low end of moderately rapid)
Erosion:	None
Stoniness:	None
Vegetation:	Guineagrass, natal redtop, lantana, koa-hoale
Remarks:	Representative of Wahiawa series

Profile Description: (Colors for moist soil unless otherwise noted; all textures "apparent field textures")

Ap 0-30 cm - Very dusky red (2.5 YR 2/2) silty clay; weak, very fine granular structure; friable, very sticky and plastic; many pores; many roots; many very fine manganese concretions; clear, smooth boundary

B21 30-96 cm - Dark reddish brown (2.5 YR 2/4) silty clay; gritty due to earthy lumps; strong, fine and very fine subangular blocky structure; few roots; common very fine pores; common manganese concretions and stains; nearly continuous pressure faces; compact in place; diffuse smooth boundary

B22 96-112 cm - Dark reddish brown (2.5 YR 2/4) silty clay; moderate, fine and medium subangular blocky structure; friable, stocky and plastic; few roots, many very fine pores; common pressure faces; common manganese stains and concretions; firm in place

Table 7

Laboratory Data of Wahiawa Silty Clay (after Ikawa et al., 1985)

Soil Name: Wahiawa — Classification: Tropeptic Eutrustox, clayey, kaolinitic, isohyperthermic
Soil no.: S70Ha-7-2-(1-4) — Location: Poamoho Experiment Station

		Particle size analysis			Bulk	Water Content			Organic
Depth	Horizon	Sand	Silt	Clay	Density	.1-bar	.3-bar	15-bar	Carbon
--cm--		-----pct < 2mm-----			--g/cc--	----------pct----------			---pct---
0-25	Ap1	18.6	37.7	43.7	1.31			24.1	1.50
25-41	Ap2	20.9	37.8	41.3	1.15			25.6	1.22
41-86	B21	14.2	15.9	69.9	1.42			23.4	0.12
86-127	B22	5.3	21.2	73.5	1.37			25.1	0.28

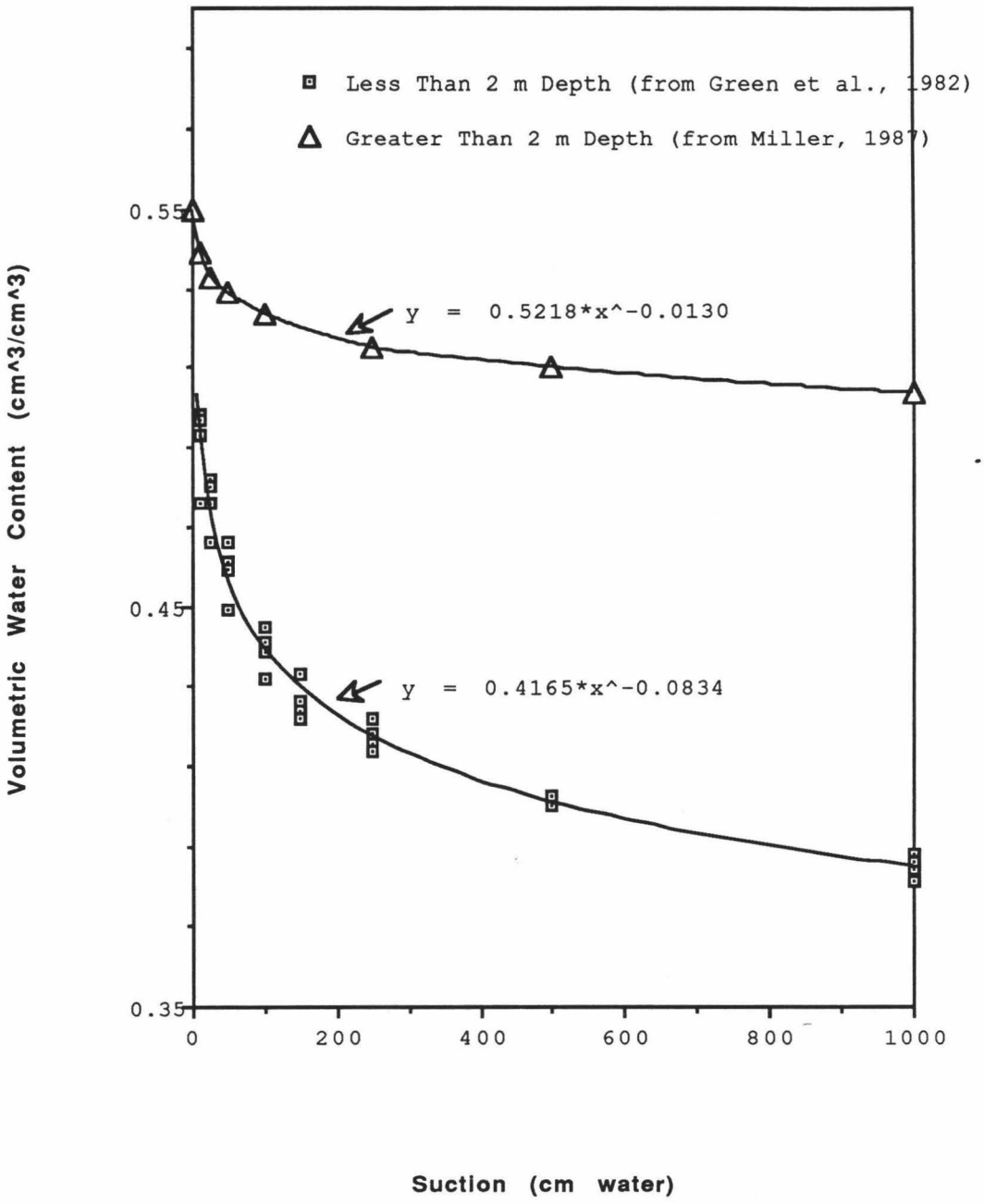

Figure 59. Water retention data from Poamoho soil (Green et al., 1982) and a similar Wahiawa series soil (Miller, 1987).

Appendix B. Measured Soil Properties

Values of soil air permeability and radium content measured at the Poamoho field site are presented in Tables 8 and 9. Table 10 gives values of bulk density and porosity measured from four soil cores taken at the Poamoho site. Figure 60 illustrates the emanation versus saturation curve measured on the four Poamoho soil cores.

Table 8

Soil Air Permeabilities Measured by Air Permeameter at Poamoho Site

Depth (m)	Saturation	Permeability (m^2)
1.0	0.69	1.18×10^{-13}
1.0	0.69	1.95×10^{-13}
1.0	0.73	4.95×10^{-14}
1.0	0.75	5.18×10^{-14}
1.0	0.75	9.71×10^{-14}
1.0	0.75	5.64×10^{-14}

Table 9

Poamoho Soil Radium Contents

Depth (m)	Radium Content (Bq/kg)	
	U.H.[a]	P.N.L.[b]
0.5	45.0	46.2
1.0	21.9	28.7
2.0	29.3	13.9

[a]Measured at University of Hawaii

[b]Measured at Pacific Northwest Laboratory

Table 10

Bulk Density and Porosity Measured From Soil Cores

Depth (m)	Bulk Density (kg/m^3)	Porosity (m^3/m^3)
0.5	1190.	0.590
0.5	1324.	0.544
0.5	1180.	0.593
0.5	1305.	0.550

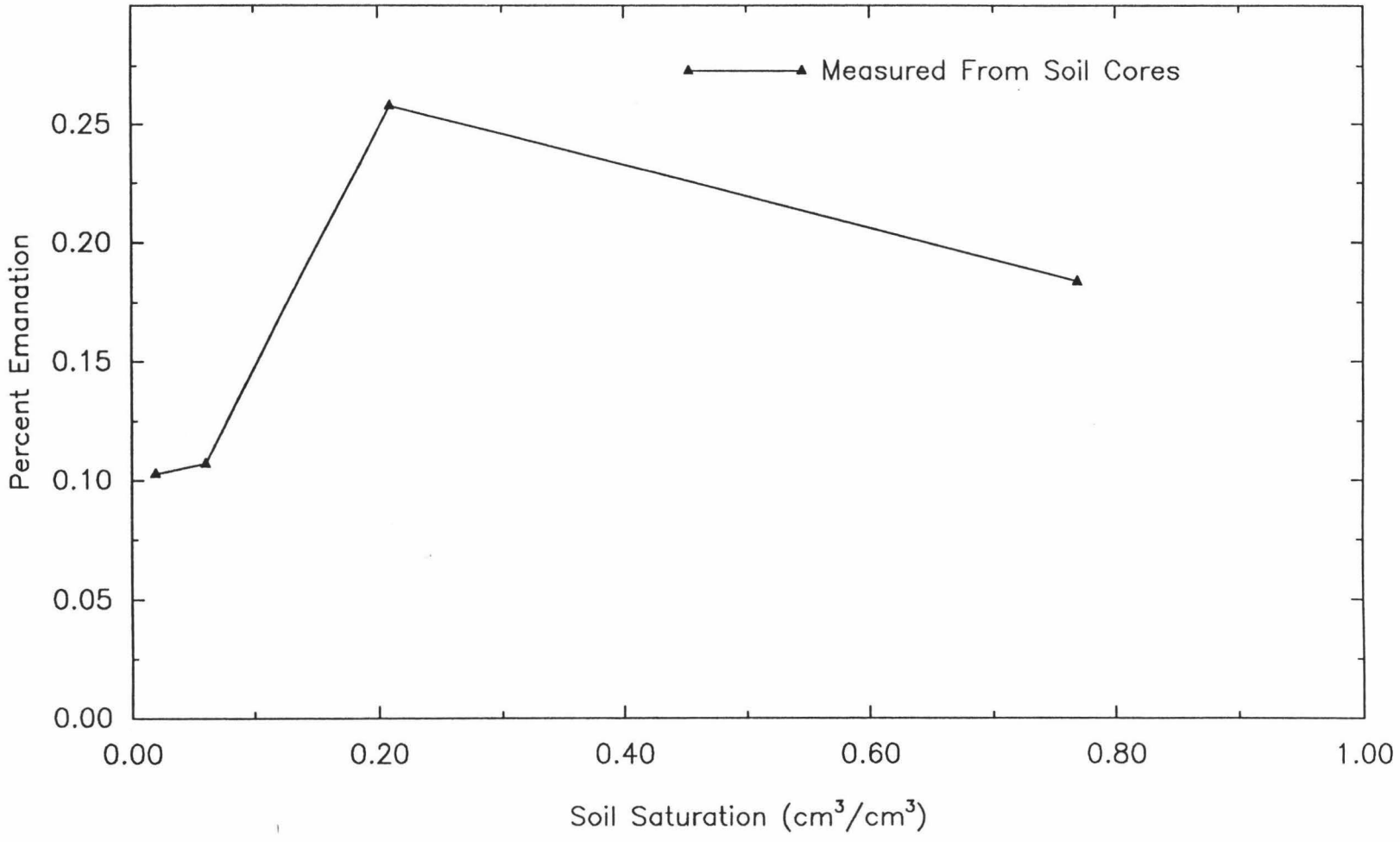

Figure 60. Emanation versus saturation for Poamoho soil at 0.5 m depth measured from soil cores.

Appendix C. Calibration of Alphameters and Soil Moisture Probes

Calibration of the radon alphameters was done as discussed in Chapter 4 in order to translate alpha decay counts per minute into absolute radon concentrations. Table 11 gives the calibration constants for the alphameters used in the current study. Table 12 gives empirical transformations used to convert readings given by the soil moisture probes into moisture readings which are in agreement with the field tensiometers.

Table 11

Calibration Constants for Alphameters

Alphameter Depth and Location	Calibration Constant (Bq/m^3) (1 CPM=Bq/m^3)
0.8 m - North Array	3513.
1.3 m - North Array	3526.
2.3 m - North Array	3694.
0.8 m - South Array	3382.
1.3 m - South Array	3531.
2.3 m - South Array	3562.

Table 12

Calibration Equations for Soil Moisture Probes

Probe Depth and Location	Transformation (X=Pressure Head Reading (cm))
0.8 m and 1.3 m; North and South Array	True Pressure Head = X/15
2.3 m; North and South Array	True Pressure Head = 25 + (X/15)

REFERENCES

Arya, L.M. and J.F. Paris, 1981. A physicoempirical model to predict the soil moisture characteristic from particle-size distribution and bulk density data *Soil Sci. Soc. Am. J.* 45: 1023-1030.

Atkinson, G.D., 1971. Forecasters guide to tropical meterology. Air Weather Service Tech. Rep. 240; USAF

Bear, J., 1979. Hydraulics of groundwater. McGraw-Hill, New York.

Brooks, R.H. and A.T. Corey, 1966. Properties of porous media affecting fluid flow. *ASCE Journal of the Irrigation and Drainage Division* 92(IR2): 61-68.

Chu, E., A. George, J. Liu and E. Ng, 1984. SPARSPAK: Waterloo sparse matrix package; Users guide for SPARSPAK-A. University of Waterloo Res. Rep. CS-84-36.

Cassel, D.K. and A. Klute, 1986. Water potential: tensiometry; Methods of Soil Analysis, Part 1. Physical and Mineralogical Methods. Agronomy Monograph no. 9, 563 - 596.

Clements, W. E. and M. H. Wilkening, 1974. Atmospheric pressure effects on radon-222 transport across the earth-air interface *J. Geophys. Res.* 79 (33): 5025-5029.

Cohen, B. L., 1985. Survey of one-year average Rn levels in Pittsburgh area homes *Health Physics* 49(6): 1053-1059.

Cohen, B. L., J. Rakowski, R. Nason, 1986. A simple compact apparatus for measuring diffusion properties of Rn through soils and other materials, (note) *Health Physics* 50(1): 133-137.

Collin, M. and A. Rasmuson, 1988. A comparison of gas diffusivity models for unsaturated porous media *Soil Sci. Soc. Am. J.* 52: 1559-1565.

Cotter, J.M. and D.M. Thomas, 1989. Ground gas radon response to meteorological perturbations *Eos, Transactions of the American Geophysical Union (Abstracts)* 70(15): 497

Cotter, J.M., D.J. Holford and D.M. Thomas, 1989. Modeling radon transport in soil gas *Eos, Transactions of the American Geophysical Union (Abstracts)* 70(43): 1099

Davis, J.C., 1986. Statistics and data analysis in geology. John Wiley and Sons, New York.

Duenas, C. and M. C. Fernandez, 1988. Temporal variations in soil gas radon: any possible relation to earthquakes? *Tectonophysics* 15: 137-145.

DSMA ATCON LTD, 1985. A computer study of soil gas movement into buildings. Rep no. 1389/1333. Dept. of Health and Welfare, Ottawa, Ontario, Canada.

Eaton, R. S. and A. G. Scott, 1984. Understanding radon transport into houses *Radiation Protection Dosimetry* 7: 251-253.

Fernandez, P., L. S. Quindos, J. Soto, E. Villar and D. Guedalia, 1983. A new method for measuring radon exhalation *J. Geophys Res.* 88(C2): 1519-1524.

Fisher, R.A., 1929. Tests of significance in harmonic analysis *Proc. Royal Soc. Ser. A* 125: 54-59.

Fleischer, R. L., 1983. Theory of alpha recoil effects on radon release and isotopic disequilibrium *Geochimica et Cosmochimica Acta* 47: 779-784.

Fleischer, R. L., and A. Mogro-Campero, 1978. Mapping of integrated radon emanation for detection of long-distance migration of gases within the earth: techniques and principles *J. Geophys. Res.* 83(7): 3539-3549.

Friedlander, G., J.W. Kennedy and J.M. Miller, 1964. Nuclear and radiochemistry. Wiley and Sons, New York, 2nd edition.

Fukuda, H., 1955. Air and vapor movement in soil due to wind gustiness *Soil Sci.* 79: 249.

Fukui, M., 1987. Soil water effects on concentration profiles and variations of ^{222}Rn in a vadose zone *Health Physics* 53(2): 181-186.

Gavenda, R.T., 1989. Soil genesis and landscape evolution in central Oahu, Hawaii; University of Hawaii PhD Dissertation.

Green, R. E., L. R. Ahuja, S. K. Chong and L. S. Lau, 1982. Water conduction in Hawaii oxic soils; Water Res. Research Center tech. rep. no. 143; University of Hawaii.

Guedalia, D., J. L. Laurent, J. Fontan, D. Blanc and A. Druilhet, 1970. A study of radon 220 emanation from soils *J. Geophys. Res.* 75(2): 357-369.

Haan, C.T., 1977. Statistical methods in hydrology. Iowa State University Press, Ames.

Hart, K.P., 1986. Radon exhalation from uranium tailings; University of New South Wales PhD Thesis.

Holford, D. J., G. W. Gee, P. C. Owczarski and H. D. Freeman, 1988. A finite element model of radon advection and diffusion in unsaturated cracked soils *Eos, Transactions of the American Geophysical Union (abstracts)* 69(44): 1216.

Holford, D. J., S.D. Schery, J.D. Wilson and F.M. Phillips, 1989. Radon transport in dry, cracked soil: Two-dimensional, finite element model; Pacific Northwest Laboratory, Richland, Washington. PNL-7116.

Ikawa, H., H. H. Sato, A. K. S. Chang, S. Nakamura, E. Robello, Jr. and S.P. Periaswamy, 1985. Soils of Hawaii agricultural experiment station, University of Hawaii: soil survey, laboratory data, and soil descriptions. BSP Tech. Rep. 4, HITAHR Res. Ext. Series 022.

Kalkwarf, D. R., K. K. Nielson, D. C. Rich and V. C. Rogers, 1982. Comparison of radon diffusion coefficients measured by transient-diffusion and steady-state laboratory methods; U.S. Nuclear Regulatory Commission NUREG/CR-2875.

Kovach, E. M., 1945. Meteorological influences upon the radon-content of soil-gas *Transactions, American Geophysical Union* 26: 241-248.

Kovach, E. M., 1946. Diurnal variations of the radon content of soil-gas *J. Geophys. Res.* 51: 45-55.

Kraner, H. W., Schroeder, G. L. and R. D. Evans., 1964. Measurements of the effects of atmospheric variables on radon-222 flux and soil-gas concentrations; in The Natural Radiation Environment, 191-214.

LeGrand, H. E., 1987. Radon and radium emanations from fractured crystalline rocks -a conceptual hydrogeological model *Ground Water* 25(1): 59-69.

Macdonald, G.A., A.T. Abbott and F.L. Peterson, 1983. Volcanoes in the sea. University of Hawaii press, Honolulu HI.

Mathieu, G. G., 1977. Rn^{222} - Ra^{226} Techniques of analysis; Appendix 1 in annual report to ERDA, Transport and Transfer Rates in the Waters of the Continental Shelf. Contract EY76-S-02-2185.

Megumi, K. and T. Mamuro, 1973. Radon and thoron exhalation from the ground *J. Geophys. Res.* 78(11): 1804-1808.

Miller M.E., 1987. Hydrogeologic characteristics of central Oahu subsoil and saprolite: implications for solute transport. University of Hawaii MS thesis.

Mink, J.F. and L.S. Lau, 1987. Aquifer indentification and classification for O'ahu: Groundwater protection strategy for Hawaii, University of Hawaii Press.

Miyahira, R.N., 1990. Simulated solute transport through the unsaturated zone of an urban environment near the Waiawa shaft, O'ahu, Hawai'i. University of Hawaii MS Thesis.

Mogro-Campero, A. and R. L. Fleischer, 1977. Subterrestrial fluid convection: a hypothesis for long distance migration of radon within the earth *Earth Planet. Sci. Lett.* 34: 3053-3057.

Morozova, N. G. and V. I. Mukhraneli, 1971. Soil emanation as a function of moisture content *Soviet Soil Sci.*: 583-588.

Mualem, Y., 1976. A new model for predicting the hydraulic conductivity of unsaturated porous media *Water Resour. Res.* 12: 513-522.

Nazaroff, W. W., B. A. Moed, R. G. Sextro, K.L. Revzan and A.V. Nero, 1986. Factors influencing soil as a source of indoor radon: A framework for geographically assesing radon source potentials; Report LBL-20645, Lawerence Berkeley Laboratory, Berkeley, CA.

Nazaroff, W. W. and A. V. Nero, Jr., 1988. Radon and its Decay Products in Indoor Air; W. W. Nazaroff and A. V. Nero, Jr. editors, John Wiley and Sons.

Nazaroff, W. W., B. A. Moed and R. G. Sextro, 1988. Soil as a source of indoor radon: generation, migration, and entry; in Radon and its Decay Products in Indoor Air, W. W. Nazaroff and A. V. Nero, Jr. editors, John Wiley and Sons.

Nero, Jr., A. V., 1988. Radon and its decay products in indoor air: an overview; in Radon and its Decay Products in Indoor Air, W. W. Nazaroff and A. V. Nero, Jr. editors, John Wiley and Sons.

Nero, A.V., M.B. Schwehr, W.W. Nazaroff and K.L. Revzan, 1986. Distribution of airborne radon-222 concentrations in U.S. homes *Science* 234: 992.

Nielson, K. K. and V. C. Rogers, 1984. A mathematical model for radon diffusion in earthen materials NUREG/CR-2765, PNL-4301.

Nielson, K. K., V. C. Rogers and G. W. Gee, 1984. Diffusion of radon through soils: a pore distribution model *Soil Sci. Soc. Am. J* 48: 482-487.

Owczarski P.C., D.J. Holford, H.D. Freeman and G.W. Gee, 1989. Effect of soil porosity, permeability and water content on radon flux from soil surfaces. American Geophysical Union Spring Meeting, Baltimore MD.

Pinder, G.F. and W.G. Gray, 1977. Finite element simulation in surface and subsurface hydrology. New York: Academic Press.

Raghavayya, M., A. H. Khan, N. Padmanabhan and G. K. Srivastava, 1981. Exhalation of Rn-222 from soil: some aspects of variations; in The Natural Radiation Environment, Proceedings of the 2nd Special Symposium in India, January 19-23, 1981. D. G. Voshra, U. C. Mishra, K. C. Pillai, S. Sadasivan, eds., 584-591.

Riemer, G.M. and L.C.S. Gunderson, 1989. A direct correlation among indoor Rn, soil gas Rn and geology in the reading prong near Boyertown, Pennsylvania *Health Physics (note)* 57(1): 155-160.

Rogers, V. C., R. F. Overmeyer, K. M. Putzig, C. M. Jensen, K. K. Nielson, B. W. Sermon, 1980. Characterization of uranium tailings cover materials for radon flux reduction. U.S. Nuclear Regulatory Commission NUREG/CR-1081.

Rogers, V. C., K. K. Nielson and D. R. Kalkwarf, 1984. Radon attenuation handbook for uranium mill tailings cover design; U. S. Nuclear Regulatory Commission NUREG/CR-3533.

Rogers, V.C., K.K. Nielson and G.B. Merrell, 1989. Radon generation, adsorption, absorption and transport in porous media. Rogers and Assoc. Engineering Corp. RAE-8810-1

Schery, S. D., D. H. Gaeddert and M. H. Wilkening, 1982. Transport of radon from fractured rock *J. Geophys. Res.* 87(64): 2969-2976.

Schery, S. D. and A. G. Petschek, 1983. Exhalation of radon and thoron: the question of the effect of thermal gradients in soil *Earth Planet. Sci. Lett.* 64: 56-60.

Schery, S. D., D. H. Gaeddert and M. H. Wilkening, 1984. Factors affecting exhalation of radon from a gravelly sandy loam *J. Geophys. Res.* 89(D5): 7299-7309.

Schery, S. D. and D. Siegel, 1986. The role of channels in the transport of radon from the soil *J. Geophys. Res.* 91(B12): 12,366-12374.

Sextro, R. G., B. A. Moed, W. W. Nazaroff, K. L. Revzan, and A. V. Nero, 1987. Investigations of soil as a source of indoor radon; in Radon and its Decay Products. P. K. Hopke ed. American Chemical Society.

Silker, W. B. and D. R. Kalkwarf, 1983. Radon diffusion in candidate soils for covering uranium mill tailings; U.S. Nuclear Regulatory Commission NUREG/CR-2924.

Singh, M., R. C. Ramola, N. P. Singh, S. Singh and H. S. Virk, 1988. Measurement of soil gas radon at Amritsar *Geophys. Res. Bull.* 26(1): 8-12.

Sogaard-Hansen, J. and A. Damkjaer, 1987. Determining ^{222}Rn diffusion lengths in soils and sediments *Health Physics* 53(5): 455-459.

Strong, K. P. and D. M. Levins, 1982. Effect of moisture content on radon emanation from uranium ore and tailings *Health Physics* 42(1): 27-32.

Tanner, A. B., 1964. Radon migration in the ground: A review; in The Natural Radiation Environment, Symposium Proceedings, Houston, Tex., Apr. 10-13, 1963, John A. S. Adams and Wayne M. Lowder, eds., p. 161-190, University of Chicago Press, Chicago.

Tanner, A.B., 1980. Radon migration in the ground: A supplementary review; in The Natural Radiation Environment III, T. F. Gesell and W. M. Lowder, eds., DOE Symp. Series, 1: 5-56.

Tanner, A. B., 1988a. A tentative protocol for measurement of radon availability from the ground *Northeastern Env. Sci.* 7(1): 58-62.

Tanner, A.B., 1988b. Measurement of radon availability from soil; in Marikos, M.A. and R.H. Hansman eds., Proceedings of the GEORAD Conference, St Louis, MO. Missouri Dept. Nat. Res., Div. Geology and Land Survey Spec. Pub. No. 4, 139-146.

Thomas, D. M. and J. Cotter, 1988. Radon as an in situ tracer for air/soil gas exchange *Eos, Transactions of the American Geophysical Union (abstracts)* 69(44): 1209.

Thomas, D. M. and J. Cotter, 1989. Environmental controls on radon mobility in the soil *Eos, Transactions of the American Geophysical Union (abstracts)* 70(43): 1099.

U.S. Geological Survey, 1983. Haleiwa topographic quadrangle map.

Van Genuchten, M Th., 1980. A closed form equation for predicting the hydraulic conductivity of unsaturated soils *Soil Sci. Soc. Am. J.* 44: 892-898.

Van Genuchten, M Th., 1985. RETC.F77: Program to analyze observed water retention and hydraulic conductivity data. U.S. Salinity Laboratory Special Report, Riverside, CA.

Woodcock, A. H. and I. Friedman, 1979. Mountain breathing--preliminary studies of air-land interaction on Mauna Kea, Hawaii; U.S. Geol. Surv. Prof. Pap. 1123-A, A1-A8.